UNIVERSITÀ DEGLI STUDI DI PARMA
DIPARTIMENTO DI INGEGNERIA DELL'INFORMAZIONE

Dottorato di Ricerca in Tecnologie dell'Informazione
XXVI Ciclo

Pouya Ahmadian

Development of Soft Computing Algorithms for the Analysis and Prediction of Motor Task from EEG data

DISSERTAZIONE PRESENTATA PER IL CONSEGUIMENTO
DEL TITOLO DI DOTTORE DI RICERCA

JANUARY 2014

UNIVERSITÀ DEGLI STUDI DI PARMA

Dottorato di Ricerca in Tecnologie dell'Informazione

XXVI Ciclo

Development of Soft Computing Algorithms for the Analysis and Prediction of Motor Task from EEG data

Coordinatore:

Chiar.mo Prof. Marco Locatelli

Tutori:

Chiar.mo Prof. Stefano Cagnoni

Ing. Luca Ascari, PhD

Dottorando:

Pouya Ahmadian

January 2014

This work has been funded by the European Commission under the MIBISOC project (Grant Agreement: 238819), within the action Marie Curie Initial Training Network of the 7FP.

To my supporting parents,
my wonderful husband
and my beautiful daughter, Tara.

Table of Contents

List of Figures

List of Tables

Introduction

I am a brain, Watson.
The rest of me is a mere appendix.

– Arthur Conan Doyle

In 1991, Leroy Burrell set a world record for the 100-meters dash with a spectacular time of 9.90 s, leaving the pre-race favorite Carl Lewis, who finished second with a time of 9.93 s, stunned. However, it was later realized that Burrell was not actually the faster runner. Instead, his reaction time to the gun shot that signed the beginning of the race was much shorter than Lewis's: a hair-trigger 117 ms against a relatively longer 166 ms. Without this difference, Lewis would have won easily. Why was Carl Lewis so much slower than Leroy Burrell at the start point that day?

Of course, nonathlete human beings also often prepare movements in anticipation of events in everyday life: while preparing to swat a fly, to press a car accelerator when a traffic light turns green, or to select the appropriate button while playing a video game. Sometimes we are slow in reacting and sometimes we move before we are completely ready. This inability to precisely time the onset of a movement can often be extremely frustrating.

What is the cause of this imprecision? Presumably, it is related with the operation of planning and executing movements. Voluntary movements are believed to be "prepared" before they are executed [1].

Important evidence for this belief of "preparation period" comes from behavioral tasks in which a delay period separates a stimulus instructing the goal of a reaching

movement from a subsequent "go" cue. Reaction time is the time elapsed from the go cue until movement onset in these delayed-reach tasks, and reaction time is shorter when delays are longer [2]. This suggests that a time-consuming preparatory process is given a head start by the delay period. How is this process reflected in neural activity, and why should the preparation take time?

The neural activity of the human brain starts between the 17th and 23rd week of prenatal development. Even since this early stage and, also, throughout life, electrical signals generated by the brain represent the brain function and the status of the whole body. The invention of electroencephalograms (EEG) for recording brain electrical activity has made it possible to have a deep and comprehensive understanding of brain functionality. EEGs were first recorded and named by Hans Berger in 1926. He first observed the large amplitude rhythm, of about 10 Hz, which was produced when awake and calm subjects closed their eyes. Since these rhythms were discovered first, he called them the "alpha" rhythms [3, 4].

During the course of time many other brain rhythms have been discovered which relate to various cognitive, motor, and other functions of the brain. However, although discovering dynamic brain electrical patterns is noteworthy, understanding their role in human behavior and cognition seems more important. Ever since Berger's early achievements, scientists have been trying to answer three main questions; how are EEG patterns generated with respect to a certain motor action or cognitive behavior, why are they oscillatory, and what is their content showing? Answering these questions required the investigation of brain activities in a simple yet fully controlled experiments. As the results, a number of academic and industrial research centers have tried and succeeded in establishing processing techniques and machines to help the neuroscientists in this job.

As a researcher, I tried to develop novel and effective schemes and signal processing algorithms and models to detect specific events within the brain which relate to simple voluntary movement tasks. My study has mostly focused on brain electrical activities happening before the movement during movement planning and movement preparation, and thus a considerable fraction of this dissertation is devoted to overviewing the brain status prior to voluntary tasks and the two algorithms I devel-

oped to analyses those EEG recordings. To have a more practical vision of how EEG data is used in real brain computer interfaces, the last chapter is devoted to the experience I had working with the famous P300-Speller paradigm which is developed to provide a mean of communication with locked-in patients.

Aims and objectives of the dissertation

The aim of this research has been to first, acquire a solid understanding of EEG and then contribute scientifically to advance the frontiers of this field. A prerequisite to achieve my defined goals was to understand the fundamentals of the neurophysiological processes that occur within the brain as much as possible. Another area that needed to be researched was the evidence related to movement preparation and planning. Moreover, observing EEG data in practical issues and how it is used to help humans with disability challenges seemed equally important. The objectives of this research are listed below:

- To understand the electroencephalogram and be able to interpret mental activities with special focus on the time interval associated with movement planning and movement preparation.

- Review of the current researches on analysis of EEG recordings prior to a movement or imagination of a movement and their effect on brain computer interfacing.

- Design of novel algorithms for extraction and detection of the electric potentials happening before any voluntary movement.

- Understanding of *on-line* analysis of EEG data and, hence, brain computer interfacing in action.

Outline of this dissertation

This thesis is structured as follows. In Chapter 1, the EEG recording procedure is briefly described. Then, the EEG advantages and disadvantages in comparison with other non-invasive data acquisition modalities for recording brain activities are provided. Some EEG features such as EEG rhythmic activities are also mentioned in Chapter 1. Moreover Event-Related Potentials (ERPs), their features and two particular example, i.e., Readiness Potential and P300, are described. This chapter ends with a brief discussion about the free downloadable EEG datasets which are categorized by the object of the study they were acquired for. This section means to be helpful for the beginners in EEG data analysis who do not have the means for recording EEG data themselves.

In Chapter 2, first, the concept of prediction in motor tasks, which is part of movement preparation and planning in humans, is introduced. Then, the changes in brain rhythm reported by neuroscientists just before the voluntary movement are listed. Then, it is demonstrated how these oscillations are used by engineers in different paradigms of brain computer interface researches to extract information about the next movement and therefore predict its various features. The studies are divided into three groups based on the main findings of authors: predicting the onset, the direction or the limb engaged in the next movement.

In Chapter 3, a new approach to the extraction of Readiness Potential in single trials of EEG data is proposed. This approach combines a well-known algorithm for blind source extraction of EEG data with a template matching technique. To test this approach, a suitable experimental protocol including the necessary software and hardware setup was designed. After data acquisition, the developed method was applied to the segmented EEG data and the results were showing to be promising. The drawback of the method is its computational cost which makes it inappropriate for on-line analysis.

In Chapter 4, another novel approach to the extraction of Readiness Potential in single trials of EEG data is introduced. This approach is based on a signal processing technique called “blind signal extraction”. To test this approach, another experiment

is designed which reflects a real-world situation. Both approaches are tested on the new acquired EEG data and are compared with each other. Finally, the superiority of the second approach is shown in comparison to the first one in terms of computational cost and false positive rate.

Since on-line analysis of EEG data and thus brain computer interfacing was also part of the main objectives of this thesis, Chapter 5 demonstrates an experience related to the P300 Speller paradigm. The experience regarded mainly the comparison of two paradigms from a subjective and an objective point of view. The first paradigm is a default module of the P300 Speller which uses a fixed number of trials to determine the letter which subject wants to communicate. In the improved paradigm, the number of trials is adaptive and therefore different from one letter to another. In this chapter, the superiority of the second approach is shown in comparison to the first one in different studies over 21 subjects.

And finally, in the last chapter, the thesis is concluded and some suggestions are made for further work.

Chapter 1

Overview of EEG and ERP

Biology gives you a brain.
Life turns it into a mind.

– Jeffrey Eugenides

In this chapter, the main concepts which are referred to in the next chapters are introduced. First, EEG is explained along with its recording procedure and specifications. Then, ERPs with particular regard to two of the main ERP components, namely Readiness Potential and P300, are briefly described. The chapter also shortly summarize the free online EEG datasets gathered from different experiments to offer a more practical overview of EEG data.

1.1 Electroencephalography

EEGs are bio-signals which are obtained by attaching a number of electrodes to the scalp to record the flowing currents during synaptic excitations of neurons in the cortex. When neurons are activated, the synaptic currents are produced within the dendrites. Like any electrical current, these currents generates a magnetic field measurable by electromyogram (EMG) machines and a secondary electrical field over the scalp measurable by EEG systems [5]. Since each electrode has a specific position

on the skull, a color map can be generated at any time sample, in which the color of pixel represents the signal amplitude in the corresponding skull position. This phenomenon is depicted in Figure 1.1. EEG has been found to be useful in diagnosing epilepsy, coma, encephalopathies, brain death, in monitoring the depth of anesthesia and in other clinical tasks. In addition to the conventional and clinical use of EEG, it is used for many other purposes such as brain-computer interfaces (BCI) which aim at improving the life style of people with physical challenges.

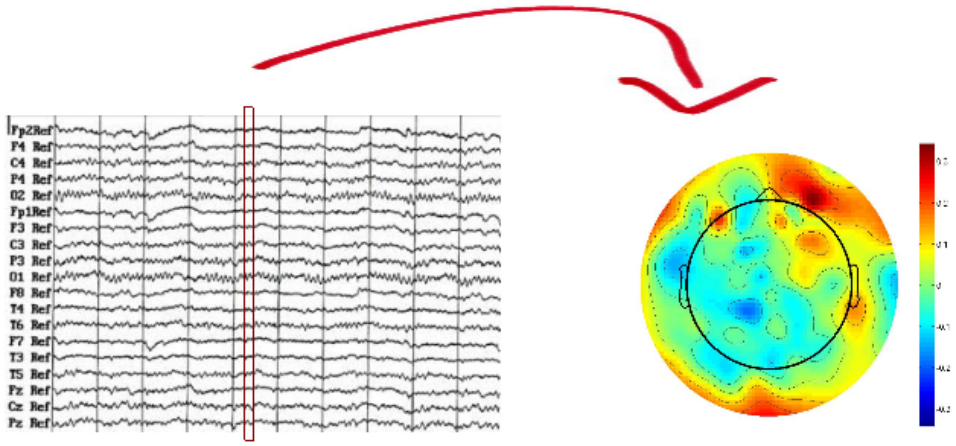

Figure 1.1: EEG signals show the flowing currents during synaptic excitations of neurons in the cortex.

1.1.1 EEG Recording

In conventional recording of EEG from the scalp, the electrodes are attached to the scalp using a conductive gel or paste. In most systems each electrode is connected to the machine through an individual wire. Usually, in most clinical and research applications, the international 10-20 system is used for specifying the electrode's name and place on the scalp. Therefore, by knowing the name of the electrode, one can understand its position on the scalp. The electrode locations or montage of a 75-electrode EEG recording system using the international 10-20 electrode positioning

and their labels are illustrated in Figure 1.2

The recorded EEG signals are usually filtered in the preprocessing stage to remove noise and other artifacts. Normally, the EEG is low-pass filtered with cutoff frequency of 0.5-1 Hz and is high-pass filtered with cutoff frequency of 35-70 Hz. The high-pass filter is useful for filtering out slow artifacts like movement artifact whereas low-pass filter is useful for filtering out the high-frequency artifacts like electromyographic (the electrical activity produced by skeletal muscles) interferences. Most of the times an additional notch filtering is applied in order to remove the artifacts which are generated by electrical power lines (60 Hz in the United States and 50 Hz in many other countries).

In general, EEG recordings can be divided into two categories; non-invasive EEG recordings obtained from electrodes attached to the scalp surface and invasive EEG recorded from electrodes implanted inside the cranium. Since implanted electrodes in invasive EEG are closer to the brain than scalp electrodes, they can record the brain signals with higher amplitudes and spatial scales ranging from a single neuron cell to distributed cell groups. Moreover, it is assumed that invasive EEG recording does not include the major artifacts that compromises the non-invasive EEG, such as eye blinks. However, invasive EEG suffers from some technical difficulties and have significant clinical risks; because recording electrodes are implanted in the cortex and are required to function well for a long time, there is a risk of infections and other damage to the brain [6, 7, 8]. Many studies have shown that, although non-invasive EEG is less accurate in comparison with invasive EEG, it still contains enough real-time information to be used as a source for different applications and even in real-time Brain Computer Interface (BCI) machines, used in tasks like word processing, Internet browsing or controlling two-dimensional movement [8, 9, 10]. Thus, in this thesis the main focus is on non-invasive EEG single.

One of the most common and infamous types of artifact is eye blink. EEG signals are usually contaminated by the eye blink artifact. A well known method to remove the eye blink artifact is independent component analysis (ICA) [11] which includes three simple steps. First, ICA is applied to the EEG signals with an un-mixing matrix to generate the forming components. Second, one of the resulting components, which

corresponds to the eye blink, is set to zero and third all the components are projected back to the electrode space using a mixing matrix. In this way a new set of EEG signals are generated which are not effected by the eye blink artifact.

Since the EEG unit of measure is volts, the electric potentials are usually measured with respect to a reference electrode whose potential is used as an arbitrary chosen zero level. There are different choices for the reference, which depend on the recording purpose and montage. Several different reference electrode placements can be found in the literature. Physical references can be used such as vertex (C_z), linked-ears, contralateral ear, C_7, and tip of the nose [3].

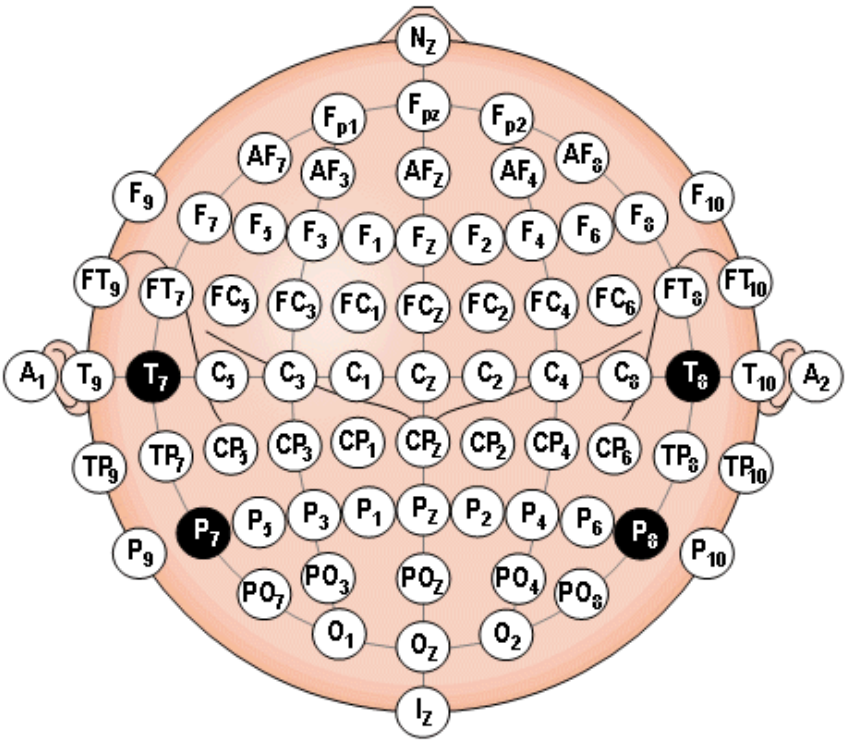

Figure 1.2: 75 electrode montage based on 10-20 system. Taken from [http://www.psych.nmsu.edu/ jkroger/lab/eegprinciples.htm]

1.1.2 EEG versus other Functional Brain Imaging

The human brain includes neurons and blood. Non-invasive recording from the human brain can rely on one of these elements to depict the brain function in real time, Figure 1.3 shows the overview of non-invasive recordings from human brain. Functional magnetic resonance imaging (fMRI) [12] and positron emission tomography (PET) [13] are two neuroimaging techniques based on the analysis of blood. The fMRI technique records the changes in blood and oxygen level and PET measures the changes in metabolic activity, both of which are indirect measures of the brain activity. However, they have higher spatial resolution and lower temporal resolution in comparison with electro-magnetic techniques such as the EEG.

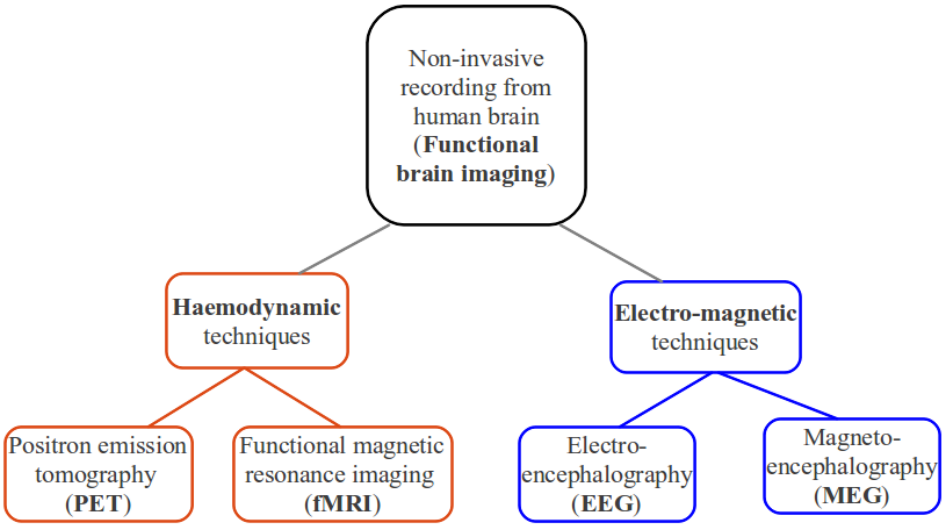

Figure 1.3: Non-invasive Functional Brain Imaging techniques can depend on neurons or blood in the brain

It is possible to record EEG data simultaneously with the fMRI [14, 15]. In this case a high temporal resolution data is acquired at the same time as a high spatial resolution data. However there are some difficulties in this multi-modal recording. One difficulty is that the data derived from each of the tools refer to different times

due to their various temporal resolution, therefore they do not necessarily relate to the same brain activity.

Magnetoencephalography (MEG)[16] and EEG are two neuroimaging techniques based directly on neuronal activity (Electro-magnetic technique). MEG is an imaging technique used to measure the magnetic fields produced by the electrical activity in the brain. The main advantage of MEG is that Magnetic fields are less distorted by the resistivity of the skull and scalp in comparison with electrical fields used in EEG. Therefore, MEG is less distorted by nonlinearity of the head tissues but is more noisy than EEG due to the complexity of the acquisition. The temporal resolution of EEG is higher than MEG.

It is also possible to record EEG data simultaneously with the MEG [17] so the recorded data can benefit from the higher temporal resolution of EEG.

The comparison between different non-invasive recordings from human brain is summarized in Table 1.1.

Table 1.1: Comparison of non-invasive Functional brain imaging

	PET	**fMRI**	**EEG**	**MEG**
Acquisition technique	Haemodynamic	Haemodynamic	Electro-magnetic	Electro-magnetic
Measure of neuronal activity	Indirect	Indirect	Direct	Direct
Equipment cost	Very expensive	Expensive	Rather cheap	Expensive
Temporal resolution	Poor (1-2 min)	Reasonable (4-5 s)	Excellent (<1 ms)	Excellent (<1 ms)
Spatial resolution	Good/Excellent (4 mm)	Excellent (2 mm)	Reasonable/Good (10 mm)	Good/Excellent (5 mm)

1.1.3 Brain Rhythms

the EEG is usually described with respect to its rhythmic activities which is characterized according to their frequency bands. It is noted that the EEG rhythmic activity in a certain frequency band has a certain scalp distribution and/or a certain biological importance. To extract the EEG rhythmic activity in a certain frequency band, usually spectral methods are applied. The six most important EEG rhythmic activities in different frequency bands are briefly described below and four of them are shown in Figure 1.4:

- Delta (δ) waves are rhythmic activities in the frequency range of 0-4 Hz which were introduced by Walter [18] in 1936 as a rhythmic activities below 8 Hz. However, later Walter and Dovey [19] established the rhythmic activities below 4 Hz as the delta waves. The delta rhythm contains the high amplitude waves. They are usually observed in babies, adults in sleep and during some sustained attention [20]. The location of delta waves are the frontal part of the adult brain and the posterior parts of the children brain. Delta rhythmic activities are prominent over the anterior regions of the brain in the deep stage of sleep [21].

- Theta (θ) waves are rhythmic activities in the frequency range of 4-7 Hz that were introduced by Walter and Dovey [19] in 1944. They are usually observed in children and in the state of drowsiness or arousal of the older children and adults. It also has been found to be associated with the inhibition of the elicited responses [20]. In [19], it has been shown that Theta activities are associated with emotional processes and it appears at the interruption of a pleasurable stimulus. Theta activities in the frequency range of 6-7 Hz over the frontal regions of the brain has been found to be related with mental activities [22, 23, 24].

- Alpha(α) waves are rhythmic activities in the frequency range of 8-12 Hz. They have been observed in the state of relaxing, closing eyes, and relative mental inactivities [25]. The posterior parts of the head are the main origin of the Alpha rhythms. The Alpha rhythms are expected to be blocked or attenu-

ated by attention, visual, and mental effort [25]. However, there are some reports that say that, in most cases, the Alpha rhythm is not attenuated or blocked by mental efforts such as solving arithmetics [26]. Other factors such as the difficulty of the task, the motivation of the subject to please the examiners play an important role on blocking of Alpha rhythms [21].

- Mu (μ) waves are rhythmic activities in the frequency range of 8-13 Hz. They are almost in the same frequency range as Alpha rhythm and thus are sometimes confused with them. However, they are different from Alpha rhythm in terms of topography and physiological significance [21]. Mu waves are observed over the sensorimotor cortex. They are significantly suppressed during controlateral motor acts [27, 28]. It has been shown that Mu rhythm is suppressed in somatic areas of the cortex when an epileptic patient is observing moving body parts [29].

- Beta (β) waves are rhythmic activities in the range of 12-30 Hz. They contain low-amplitude waves which are mostly evident in frontal and central parts of the brain. The distribution of the Beta rhythms is symmetrical and in both sides of the head. The Beta rhythm is most evident when the brain is active, busy or in the state of concentration. Like Mu rhythms, Beta rhythms can be attenuated by movement, especially controlateral movement, and even by thinking about executing a movement [21].

- Gamma (γ) waves are rhythmic activities in the frequency range of 25-100 Hz. The amplitude of Gamma rhythms is usually very low and their appearance is rare. The Gamma rhythmic activities around 40 Hz over the brain central regions have been observed along with movement onset [30] which is associated with Event Related Synchronization (ERS). ERS or power increase of a specific band refers to an phase change in form of event-related amplitude enhancement in that frequency band [31]. The ERS of Gamma waves is used in [32] to demonstrate the locus for right and left index finger movement, right toes, and bilateral area for finger movement.

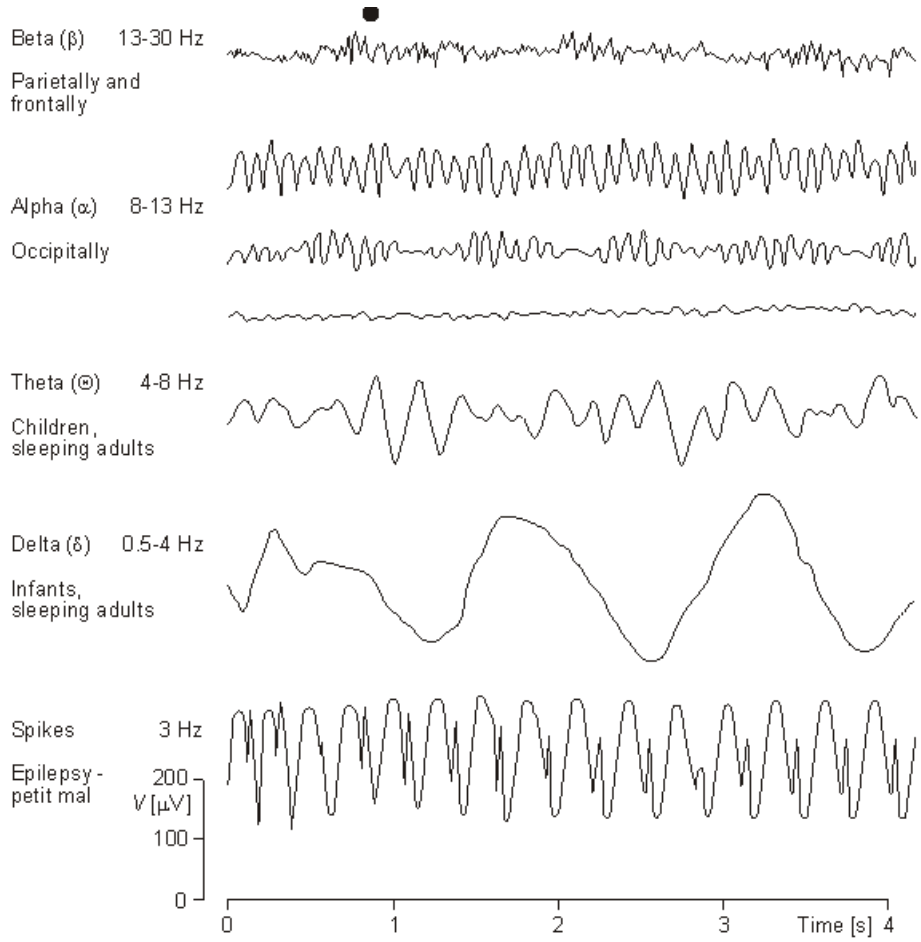

Figure 1.4: Wave morphology of rhythms with their frequency band and spatial distribution. Taken from [http://www.trueimpact.ca/introduction-to-electroencephalogram-eeg/].

1.2 Event-Related Potentials

Event-related potentials (ERPs) were first introduced in 1964, and are still used as a diagnostic tool in both psychiatry and neurology. Moreover, they have been widely used in brain-computer interfacing (BCI). ERPs are relatively well defined shape-

wise variations of the continuous EEG generated in reaction to an external stimulus and measure the electrical response of the cortex to sensory, affective, or cognitive events. Their most important features are listed below [3, 33, 34]:

- They are evoked by the cortex to when sensory, affective, or cognitive events occur and/or are temporally linked to these events.
- They are usually generated involuntarily and as a reflection of higher cognitive processing.
- ERPs are quite small in amplitude (about 1-30 μV) in comparison to the background EEG signals, thus they need the use of a signal-averaging procedure to be highlighted.
- The ERP signals are either positive or negative.
- ERP waveform can be characterized in three main domain; amplitude (index of the extent of neural activity), latency (the time point at which peak amplitude occurs), and distribution over scalp.

In the next section two ERPs referred to in this thesis, Readiness Potential (RP) and P300, are described.

1.2.1 Readiness Potential

Many of human everyday work and actions are considered voluntary. There are evidences from EEG data that show human brain is active even before the beginning of the voluntary movement. The first proof of this evidence was given by Kornhuber and Deecke in 1964 [35]. In their experiment, the subjects were asked to perform a repetitive movement (finger flexion) with their choice of speed while EEG and electromyogram (EMG) data were recorded simultaneously. Then, by averaging the EEG segment before the EMG onset, which indicated the start of movement as a trigger, a potential preceding human voluntary movement was discovered and published with the name Bereitschaftspotential (BP) or RP, shown in Figure 1.5.

RP is a negative cortical potential seen in motor cortex which can be observed 1.5 to 1 second before the onset of a self-paced or voluntary movement in EEG data. Moreover, RP is considered an ERP, because its onset is time-locked to an event such as a movement [35, 36, 37].

RP is proven to be evoked not only when a movement is performed by the subject, but also when execution of an action by others is observed or even when the movement is imagined [38, 39].

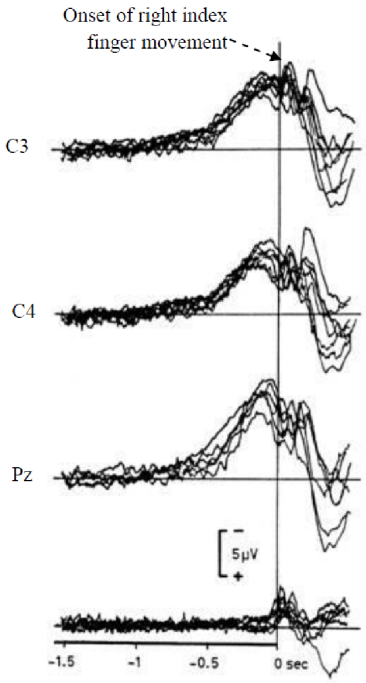

Figure 1.5: Readiness Potential preceding self-initiated movement (vertical line shows $t = 0s$). C3, C4 and Pz indicate the place of electrodes in conventional 10-20 EEG electrode positions. The plot at the bottom shows the difference between RP in C_3 and in C_4. Taken from [36].

1.2.2 P300

P300 potential is one of the main components of ERPs. It is a positive wave which occurs usually after an auditory, visual, or somatosensory stimulus and which peaks around 300 ms after the stimulus onset. The most common theory about what P300 represents is that P300 is related to memory and context updating [33]. Therefore, it is considered easy to evoke P300 potential. P300 often has a fairly large amplitude (5-20μV). Amplitude of P300 is described as the largest peak of ERP waveform within a time window around 300 ms. Latency of P300 is defined as the time from the stimulus onset to the timing of the largest positive peak of P300 (e.g. P300 amplitude) [40]. P300 amplitude is usually larger in parietal electrode sites [41].

P300 is typically evoked by the *oddball paradigm*. The oddball paradigm is a technique which series of regularly occurring stimuli that are usually auditory or visual are used to evoke the neural reactions to improbable, unpredictable but recognizable target events [42]. Different variants of the oddball tasks have been defined. In an oddball task which contains only one stimulus type, the infrequent or rare stimulus is the target. In a typical two-stimulus oddball a number of infrequent targets are presented in a background of frequent stimuli. In a typical three-stimulus oddball, a number of infrequent target are presented in a background of frequent stimuli and also a number of infrequent distractor stimuli.

In all types of oddball paradigms, the task of the subject is to respond to the target stimulus mostly by pressing a button or by counting the number of target stimuli such as P300 speller paradigm which will be described later in chapter 5. In single-stimulus and two-stimulus oddball, the response of the subject to the infrequent target stimulus does evake a P300 [40]. However in the three-stimulus oddball, the response of the subject to the infrequent target does evoke P3b and the infrequent distractor causes the P3a to be evoked [40].

P3a and P3b are two overlapping subcomponents of P300. The scalp distribution of P3a usually has maximum amplitude in the frontal/central regions of the brain while for P3b the scalp distribution is maximum in parietal regions, as shown in Figure 1.6. P3a and P3b can also be obtained by decomposing the P300 obtained in a single or two-stimulus oddball paradigm into its constituent subcomponents. This,

however, may not be necessary in BCI paradigms.

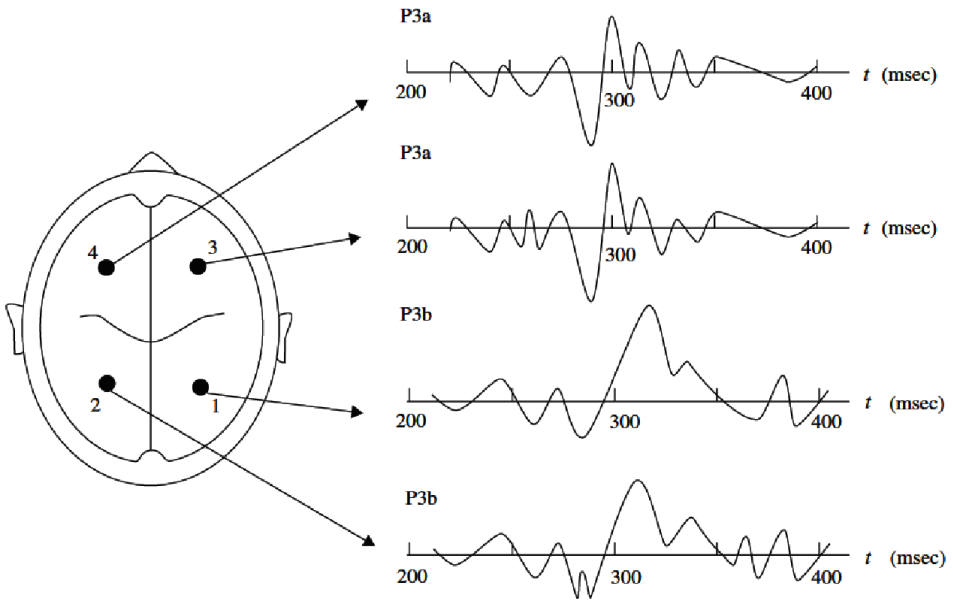

Figure 1.6: P300 and it's subcomponents with their scalp locations. Taken from [3].

1.3 Online free EEG databases

There are some EEG downloadable databases with different experiment setups used to acquire EEG data. Some of them are listed below and categorized by the main aim of the researches.

- For brain-computer interface (BCI) developers:

  www.bbci.de/activities: Currently the biggest and best-documented database for BCI experiments containing BCI Competitions dataset. Contains EEG's recorded while imagining various movements and therefore some important potentials such as P300. The descriptions and rankings for different BCI algorithms can also be found on the website.

mmspl.epfl.ch/page33712.html: EEG data of nine subjects (five severely disabled and four able-bodied subjects) where P300 potential is evoked and the Matlab code to simulate the results of the paper "An efficient P300-based brain-computer interface for disabled subjects"[43]

projectbci.googlepages.com: EEG motor activity of two subjects acquired while performing actual random movements of left or right hand with closed eyes.

- For sleep researches:

  www.physionet.org/physiobank/database/sleep-edf/: EEG data of eight subjects acquired while they were asleep.

  www.physionet.org/pn3/shhpsgdb/: Sleep EEG data from a heart study.

- Abnormal EEG from epileptic patients for medical researches:

  epileptologie-bonn.de/cms/front_content.php?idcat=193&lang=3: EEG data of healthy subjects and epileptic patients during seizures and seizure-free intervals.

  www.vis.caltech.edu/~rodri/data.htm: EEG, ERP and single-cell recordings data of epileptic patients and normal subjects.

- Other databases:

  kdd.ics.uci.edu/databases/eeg/eeg.html: A huge dataset containing 122 subsets of EEG recordings of control and alcoholic subjects. Each subject was asked to recall the picture of an object.

  sccn.ucsd.edu/~arno/fam2data/publicly_available_EEG_data.html: EEG data of 14 subjects (7 males) acquired while performing a categorization or picture recognition task.

  www.cs.colostate.edu/eeg/eegSoftware.htmlkeirndata: EEG recordings of 7 subjects performing simple tasks such as counting, math, rotation, letter-writing or just resting.

1.4 Summary

In this chapter a brief introduction about EEG and ERPs has been provided, which will be useful in the development of the rest of the thesis. The EEG recording procedure has been briefly described. Then, EEG is compared with other non-invasive functional brain imaging techniques such as fMRI, PET, MEG. In addition, an important characteristic of EEG which is its rhythmic activity has been explored. Finally, ERPs including RP and P300 have been briefly described. Moreover, some popular and useful free online EEG databases are listed at the end of the chapter, for practical issues.

Chapter 2

Predicting the next motor task from EEG

Prediction is not just one of the things your brain does.
It is the primary function of the neo-cortex, and the foundation of intelligence.

– Jeff Hawkins

2.1 Introduction

Generally, prediction refers to estimating the future states of a system. The concept of prediction in motor tasks was first introduced by Helmholtz in 1867 in an attempt to explain how humans localize objects. Later on, the concept of efference copies was described by Von Holst and Sperry in the fifties stating that motor commands create an internal copy which reflects the predicted movement and its resulting sensations [44, 45]. Since then, the idea that humans predict the consequences of their motor tasks has appeared as a prominent theory in all aspects of sensorimotor commands.

Through EEG data acquisition, the current state of the brain can be understood in real time. As mentioned also above, part of the current state is a prediction of the

next motor task. Therefore, by understanding and analyzing the brain rhythms and ERPs, the future motor commands can be predicted. This combination can lead to better rehabilitation tools for people with physical challenges. It might even have a potential to be used as supportive gadgets for healthy individuals.

Another concept to address is the meaning of "before the movement" or "pre-movement" activity. This phenomenon refers to the time when no muscle movement is detectable or irrelevant if it occurs, but the subject is completely aware of the action that he is going to perform in the near future; and it is also referred to as planning/preparation of the movements [46, 47]. In this time interval, which ranges from 500 ms to 2 s before movement onset, the cortex is preparing for action execution. As will be seen in Section 2.2, there is a noticeable change in brain waves that only happens before movement.

This chapter aims to investigate the combination of the concepts of EEG and prediction, to see, based on today's knowledge and previous experiments, if it is possible to predict the next motor movement using the current EEG recording. In the next section, the main changes in the EEG data observed just before the voluntary movement are described. Then, Section 2.2 tries to answer the question of how the knowledge of these changes can be used to extract information about the upcoming movement. In each case of this Section, the EEG setup and protocol used is addressed and the main foundation of the study is discussed. Finally, in the Discussion and Conclusion section the main ideas are summarized with the hope to draw more attention to the richness of pre-movement and pre-motor imagery EEG.

2.2 Changes in Brain rhythm reported just before the movement

This section describes the changes detectable in EEG before the onset of the movement or motor imagery. All the following phenomena have been reported both when the movement is actually executed and when it is imagined as a part of the motor preparation procedure. One or a combination of these changes are the main focus of the studies trying to extract features from pre-movement or pre-motor imagery period

discussed in the next section.

2.2.1 Bereitschaftspotential or Readiness Potential

As also mentioned in Section 1.2.1 BP or RP is a negative cortical potential which starts to develop around 1.5 to 1 s before the onset of a voluntary movement and is an ERP, since its onset is time-locked to an event such as movement [35, 37]. Here the two main components of RP are described. The first component, also called "early BP", is a slow-rising negative segment which begins about 1.5 s prior to the movement onset and is more prominent in the central-medial scalp. The other component, the "late BP", has a steeper slope and occurs around 400 ms prior to the movement onset, having maximum amplitude over the primary motor cortex (M1). RP is proven to be evoked not only when a movement is performed by the subject, but also when the execution of an action by others is observed or even when the movement is imagined [38, 48].

2.2.2 Event-Related Desynchronization

A short-lasting block/decrease of frequency power or event-related desynchronization (ERD) in the Alpha (Mu) band (about 8-12 Hz) and in the central Beta band (about 16-24 Hz) has been reported beginning about 2 s before self-paced movement or motor imageries [31, 49]. The Alpha band (Mu) ERD (about 8-12 Hz) begins 2.5 s before the movement onset, reaches its maximal desynchronization shortly after movement onset, and recovers to baseline level within a few seconds. The central Beta activity (about 16-24 Hz), on the other hand, displays a short-lasting ERD during initiation of movement followed by a synchronization (ERS) with a maximum after movement execution. These phenomena is depicted in Figure 2.1

2.2.3 Contingent Negative Variation

Contingent negative variation (CNV), shown in Figure 2.2 is a slow negative wave that develops in the interval between a "Warning" and a "Go" stimulus and shows anticipation for a forthcoming signal and preparation for execution of a response. In

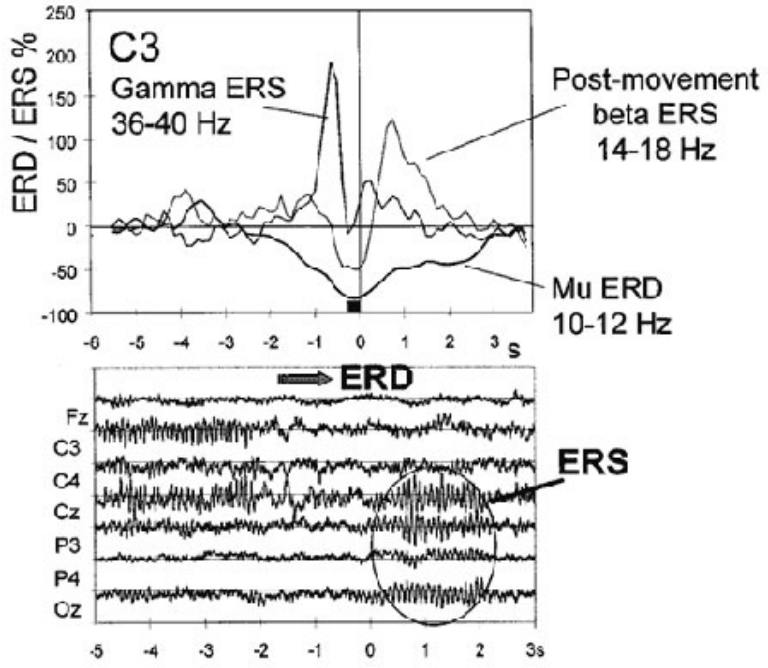

Figure 2.1: Above: Superimposed band power time courses computed for three different frequency bands (10-12 Hz, 14-18 Hz, and 36-40 Hz) from EEG trials recorded from electrode position C_3 during right index finger lifting. EEG data are triggered with respect to movement-offset (vertical line at t = 0 s). Note the onset of Mu ERD around 2.5 s prior to movement-offset, the maximum of Gamma ERS immediately prior to movement-onset and the maximum of the Beta ERS within the first second after movement-offset. Below: Examples of ongoing EEG recorded during right finger movement. Movement-onset at t = 0 s. Note the EEG desynchronization (ERD) at central electrode locations prior to movement-onset and the enhanced Alpha band activity over the posterior region (ERS) during movement. Taken from [49].

other words, CNV reflects the preparation for *signaled* movements and is an index for *expectation*. The earlier segment of the CNV has maximum amplitude over the frontal cortex and is generated in response to a “Warning” cue. The later or terminal

CNV (tCNV) begins around 1.5 s before the “Go” cue, it reflects preparation for motor response and has maximum amplitude over the motor cortex (M1) [50, 51].

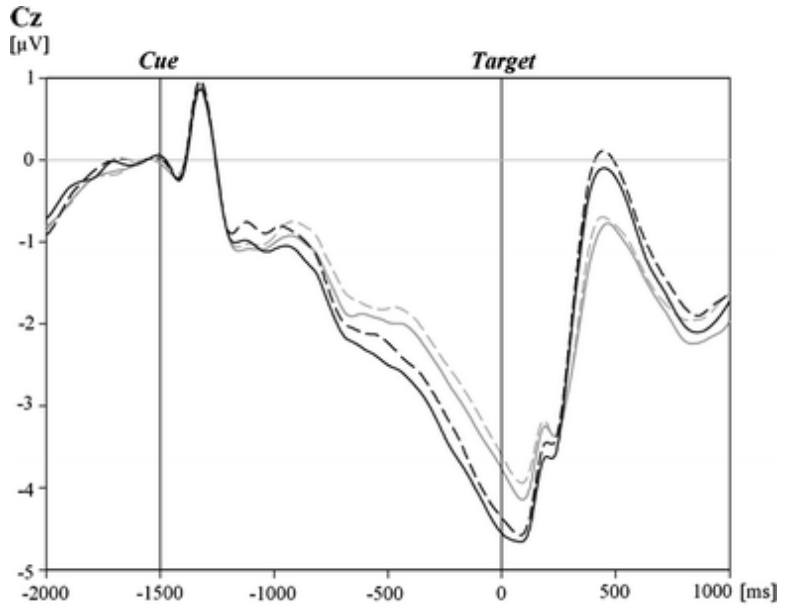

Figure 2.2: Contingent Negative Variation is a slow negative wave that develops in the interval between a “Warning” and a “Go” stimulus. Taken from [52].

2.3 Studies

This section describes the studies that extract information from the pre-movement or pre-imageries EEG data. Some studies show the effectiveness of data acquired in this period for real-time BCIs. Overview of systems used in these studies can be observed in Figure 2.3. Each study used a different EEG data acquisition protocol including the electrodes montage and signal enhancement which is also discussed, since it is directly related to the results reported. The studies are organized in three groups based on the aims and findings of the authors: predicting the onset of the next movement, the direction of next movement and also the limb engaged in the next movement.

These studies prove that with the right EEG setting and signal processing techniques, significant information can be extracted about the movement yet to come (please see Table 2.1 for the summary and details).

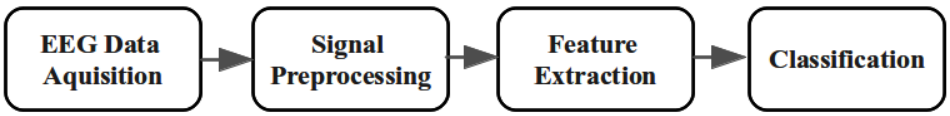

Figure 2.3: Overview of systems designed for the analysis of EEG data acquired prior to the movement or imagination of movement.

2.3.1 Predicting the intention of movement

Studies carried out in [53, 54, 55, 56] try to answer the question whether or not the subject wants to move in the short future. They do not try to determine the kind or the direction of movement but to detect the upcoming of any movement. In these studies, the movement onset is not used as a prior in the detection method in order to simulate the full meaning of prediction.

In [53] the authors implemented a user specific template matching structure as part of a method to detect movement planning. Here the focus was more on detecting the movement rather than predicting it. To build the template, a RP waveform recorded via just one electrode placed between C3 and A1 in the 10-20 International System was used. For each subject 12 movements during 3 or 4 sessions, each containing 6 right and left hand movements, were used to build the subject's template. A classifier was implemented to compare the template with EEG raw data and detect the movement in the test trails. This classifier was tested over five subjects and could predict movements with average accuracy of 70% and a low false positive rate.

Authors in [54] focused on prediction. In their experiment, subjects were asked to perform three sessions in each of which the only task was to perform a right-

hand wrist extension movement whenever they wanted, without any cue (self-paced movement). EEG data from the first two sessions were used for training and applied to the third session to test the predictions. The work was based on detection of the ERD or power decrease in Alpha and Beta bands in single trials. The study reported an average true positive rate of $75 \pm 10\%$ of total predictions, on average about 0.62 s before the movement onset.

In [55], the authors were able to detect the onset of the movement as early as 187 ms before the movement with an average accuracy of 82.5% over 15 subjects. Using 10 electrodes focused on the motor cortex, the subjects were asked to perform an ankle dorsiflexion movement with speed of their choice without any cue. Each subject performed 5 runs, 2 for the training and the rest for the testing phase. Since the detection method was based on movement-related cortical potentials such as RP, the data were band-pass filtered between 0.05 Hz and 10 Hz and then, using a spatial filter, a template was extracted from the training data sets. The detection decision was based on the likelihood ratio computed between spatially filtered channels of the test data sets and the template in a sliding window 2 seconds wide with 200 ms shifting.

In [56], the authors showed that it is possible to predict the movement 500 ms prior to its occurrence. Using 64 electrodes and 12 subjects they designed a protocol where the subjects were asked to move their hand at least 2 seconds after hearing an auditory cue. For data analysis, since they aimed to focus on RPs, the data were first filtered with band-pass filter (0.1-1 Hz) and then 6 electrodes corresponding to the central motor cortex were selected. As for the classifier, linear discriminant analysis (LDA) was used. In the training phase data acquired 500 ms before the movement was used in comparison to data acquired 500 ms before the cue. For the testing phase, a shifting window 500 ms wide was moved every 10 ms starting from 2500 ms before movement onset until 1000 ms after movement onset. Their results showed maximum average true positive rate of 81% peaking 140 ms before movement onset across subjects.

2.3.2 Predicting the direction of the movement

In [57, 58, 59] it was shown that it is possible to determine the direction of the moving limb prior to movement onset. In [57], the authors analyzed 3 s of data before movement onset. The subjects were asked to move a manipulandum placed in their hands towards the direction indicated by a cue on the screen. For EEG analysis, spatio-temporal features were extracted via continuous wavelet transform (CWT). Then, they performed a wrapper method based on support vector machines (SVM) for feature selection and classification and reported an average accuracy of 81.5% during testing for two different directions.

In the study reported in [58], the subjects were asked to reach and touch the corner of the screen indicated by a directional cue. The delay between the direction cue and go cue was randomized between 750 ms and 1500 ms. Only the EEG data of the first 500 ms of the delay period were analyzed by three classifiers: a four-class classifier for reaching the target, and two binary classifiers of left versus right reaches and top versus bottom reaches. The results of the binary classifiers showed that distinguishing left from right targets is more effective than discriminating top from bottom targets.

In a follow up work in [59] the authors showed that EEG signals obtained from the posterior parietal cortex before the movement onset carry information about the direction of the intended movement. A delayed movement protocol was designed where the movement consisted of tracking the target with gaze, reaching for it with one hand without eye movement, or doing both actions. It had to be performed 700 ms after the subject was made aware of the task direction by a cue; this was the period which was then used for data analysis. For EEG analysis, they used independent component analysis (ICA) performed by the Extended Infomax algorithm. Two lateralized temporal-parietal components were identified in each subject's EEG data time locked to the onset of the movement cue. For a better understanding of direction coding, the parietal ICs were back-projected onto the scalp and visualized. The result produced a clear contralateral negativity and positivity with respect to the intended movement direction (see Figure 2.4). Moreover, using SVM, the authors obtained an average accuracy of 80.25% for single-trial classification of right versus left.

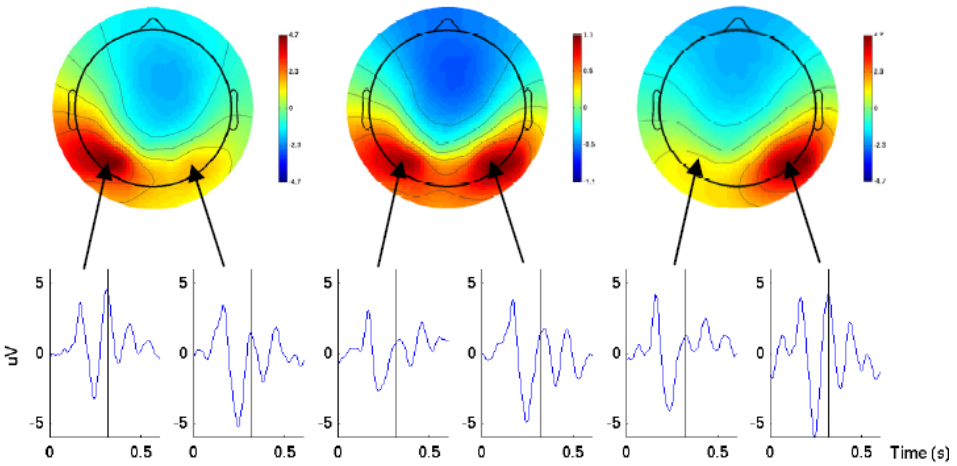

Figure 2.4: Scalp maps and ERP waveforms of the back-projected parietal ICs for one subject in three conditions (left, center and, right) 320 ms after the direction cue. The ERP waveforms were acquired from the two lateral parietal electrodes with the highest amplitude projection of cortex. Taken from [59].

2.3.3 Predicting the type of the movement

This section deals with the studies which try to determine the type of the movement or the body part that will move in a short future. In the previous section the movement was carried out by one limb and the direction of the movement was in question. However, some studies go beyond that to see whether it is possible to predict the future moving limb.

One of the earliest work in this area is the work reported in [60]. In this work, using the RP features, authors manage to discriminate between left and right-hand finger pre-movement in keyboard typing on average 100-230 ms before the key was pressed. The actual time at which the key was pressed was determined by electromyography (EMG). The subject task was to press the computer keyboard with the index or little fingers of both hands in a self-paced manner, resulting in an average speed of 1 key every 2.1 s. Based on this research, BCI competition 2003, data set IV, self paced taping, was released [61]. Using one subject executing the same task, 416 epochs of

500 ms EEG were provided, each ending 130 ms before an actual key press. The epochs were randomly shuffled and split into 316 labeled epochs for the training set and an 100 unlabeled epochs for the test set. Obviously, the goal of the competition was to submit the estimated labels for the test set with the smallest number of misclassifications. Needless to say, this data set attracted a lot of researchers to find a solution for the problem of predicting the next moving limb. A total of 15 groups submitted their results for this data set, 4 of which had a performance close to chance level (the error rate was higher than 43%) [62]. The best submission was given by Zhang and colleagues [63] with an error rate of 16%. The use of this data set did not stop after the end of the competition and the release of the results; since this dataset is still available for download, it has become a benchmark and has been used by other research groups, such as [64].

In [65], the authors used the concept of bit transfer to evaluate the speed and accuracy of their method in discriminating between left and right-hand finger movements in keyboard typing. The subjects were asked to press one of four keys, using the fingers of the right or left hand, in a self-chosen order and timing. For data analysis, after preprocessing the data, a classifier based on Fisher's Discriminant was applied to the means and covariance matrices calculated from the training data. Their results showed that not only could the discrimination between different limb movements be detected as early as 120 ms before their onset but that this was also achieved in motor sequences as fast as 2 taps per second.

In another study reported in [66], the authors used the EEG signals preceding movement and motor imagery to predict which of the movements/motor imageries of different body parts (right hand, left hand, tongue, and right foot) was about to occur. The subjects were informed about the type of the movement by a cue and performed it at least 2 s after being informed by another "Go" cue. The time window of 1.5 s before the "Go" cue was used in the analysis of data which correspond to ERD/ERS and CNV oscillation. The results showed that the preceding movement and motor imagery ERD/ERS can be used to predict which of the four movements/imageries is about to occur. Prediction accuracy depended on the signal quality. However, the highest average testing accuracies reported for the two-movement/imagery categories

were related to right-foot and left-hand responses. The study also tried to identify CNV and ERD/ERSs on motor areas in single trials and concluded that, compared to CNV, the ERD/ERS is the most specific pre-movement/pre-motor imagery signal with respect to the movement/imagery that is about to be performed.

2.4 Discussion

In the studies above there is a close link between one or more brain rhythms and ERPs and the preprocessing step. In particular, the choice of the filter and of the placement of the electrodes depends on the brain features on which the method is based. For instance, [56] and [65], which were based on RP, used a band-pass filter with upper cutoff frequency of less than 4 Hz and electrodes attached to the motor cortex. Consequently, more studies to further investigate the pre-movement period can improve the BCIs and, thus, the prediction of the next motor task.

CNV potential has not been the main focus of the studies, although some studies have used a cue-based delayed protocol which can trigger this potential and thus affect the results reported [56, 58, 59]. The one study that actually focused on detecting this potential states that it was not identified as the main pre-movement/pre-motor imagery feature in most of the subjects [66].

This chapter is not a completely exhaustive revision on the capability of EEG in predicting the next motor task. It mainly aimed at providing examples of the progress in the field as well as stimulating ideas for new research proposals.

2.5 Summary

In conclusion, the EEG data gathered before the forthcoming movement which corresponds to motor preparation and planning period of the brain show significant prediction potentials. The evidence from both Neuroscience and Engineering research supports this hypothesis, even though this field has not been vastly explored. Further studies in both fields on this short pre-movement time can extend exploration of the frontiers of motor preparation and decrease the response time of BCIs. To know be-

Table 2.1: Studies on Pre-movement or Pre-imagery motor task categorized by the main findings

Ref	Subjs #	EEG montage	Acquisition protocol	Brain feature	Prominent preprocessing	Classifier	Key findings
Prediction Of Onset Of Movement							
[53]	5	1 Electrode between C3 and A1	Finger movement after visual cues	RP	Building specific RP template for each subject during 3 or 4 training sessions	Thresholding based on error and correlation	Detected the movement with an average accuracy of 70% and a low false positive rate
[54]	7	27 Electrodes	Hand wrist extension movement without cues	ERD	Spatial filter using Surface Laplacian derivation, band-pass filter (8-30 Hz) and number of electrodes reduced to 14	Mahalanobis linear distance	Prediction of movement with an average true positive rate of $75 \pm 10\%$ of total predictions about 0.62 s before the movement onset
[55]	15	10 Electrodes focused on motor cortex	Ankle dorsiflexion movement without cues	RP	Band-pass filtering (0.05-10 Hz), extracted a template from the training data set using a spatial filter and sliding a window of 2 s wide with 200 ms shifts	Neyman Pearson lemma	Predicted the movement with an average true positive rate of 82.5% around 187 ms before movement onset
[56]	12	64 Electrodes	Hand movement at least 2 s after sound cues	RP	Band-pass filtering 0.1-1 Hz, number of electrode reduced to 6 electrodes placed over the motor cortex and sliding a window of 500 ms wide with 10 ms shifts from 2500 ms before movement onset to 1000 ms after	Linear Discriminant analysis	Predicted the movement with maximum average true positive rate of 81% around 140 ms before movement onset

Continued on next page

Table 2.1 – *Studies on Pre-movement or Pre-imagery motor task*

Ref	Subjs #	EEG montage	Acquisition protocol	Brain feature	Prominent preprocessing	Classifier	Key findings
Prediction Of Direction Of The Movement							
[57]	4	28 Electrodes	Move the manipulandum placed in their hands towards the direction cue	RP and ERD/ERSs	Artifact removal, low-pass filtering at 50 Hz, number of electrodes reduced to 1 ($C3$), and extracting spatio-temporal features via CWT	Wrapper based on SVM	Average accuracy of 81.5% on the test dataset for two different directions
[58]	2	64 Electrodes	Delayed reaching and touching of screen corner pointed by a directional cue	Not stated explicitly: RP, ERD, CNV	Artifact rejection, first 500 ms of the delay period used for analysis and extracted 8 vectors of different features	Multinomial logistic regression classifier	Distinguishing left from right targets is more effective than discriminating top from bottom targets
[59]	4	128 Electrodes	Delayed movement protocol; gazing towards the direction cue, reaching for it with one hand, or both activities	Not stated explicitly: RP, ERD, CNV	Segmented 700 ms after direction cue, baseline correction, removal of noisy electrodes, and spatial filtering with ICA using Extended Informax algorithm	SVM classifier using an RBF kernel	Pre-movement EEG signals carry information about the direction of the intended movement, classification of go-left and go-right planning with average accuracy of 80.25 ± 2.22
Prediction Of Type Of The Movement							

Continued on next page

Table 2.1 – *Studies on Pre-movement or Pre-imagery motor task*

Ref	**Subjs #**	**EEG montage**	**Acquisition protocol**	**Brain feature**	**Prominent preprocessing**	**Classifier**	**Key findings**
[60]	1	27 Electrodes	Pressing the computer keyboard with fingers of both hands at an average speed of 1 key every 2 s	RP	Artifact rejection, low-pass filtering at 5 Hz, sub-sampling it at 20 Hz and, number of electrodes reduced to 21	Learning machines, e.g. SVM	Discrimination between left and right-hand finger pre-movement on average 100-230 ms before key pressed with 96% classification accuracy
[65]	8	32, 64, or 128 Electrodes	Self-paced pressing one of four keys, using the fingers of the right or left-hand	RP	Band-pass with Fourier transform between 0.4 and 3.5 Hz, sub-sampling at 20 Hz, and number of electrodes reduced to 23 over motor cortex	Classifier based on Fisher's Discriminant	Discrimination between left and right-hand finger pre-movement as early as 120 ms before the movement onset and as fast as 2 taps per second
[66]	8	29 Electrodes over sensorimotor areas	Delayed protocol; to perform or imagine right-hand, left-hand, tongue, or right-foot move after a "Go" cue.	CNV and ERD/ERSs	Artifact rejection, spatial filtering via ICA and, temporal filtering via DWT	Naive Bayesian classifier	Predicting which of the four movements/imageries is about to occur is possible and it is manifested stronger in the ERD/ERS in comparison with CNV

"Subjs #" indicates the number of subjects participated in the experiment.

forehand whether the subject is willing to move, in what direction, or using which limb can make it possible to determine the next course of actions in rehabilitation procedures more effectively. It can also decrease the response time of BCIs and let them appear more natural to their users. In some applications, such as driving, it may even have a more crucial role. Study reported in [67] showed that it is possible to predict an upcoming emergency brake up to 130 ms earlier than pedal response. At driving speed of 100 $\frac{km}{h}$, this time reduces the braking distance by 3.66 m, which can be very effective in terms of survival. They also showed that levels of predictive accuracy using EEG worked faster than EMG, suggesting the superiority of using EEG in such a context.

Chapter 3

Blind Source Separation Technique for Detection of RP

A signal is comprehended if it serves to make us notice the object or situation it bespeaks.
A symbol is understood when we conceive the idea it presents.

– Susanne K. Langer

3.1 Introduction

In the previous chapter some of the researches that focus on extracting information from pre-movement or pre-imaginary EEG data were reviewed. As can be observed in Table 2.1, a significant amount of these researches used RP as the brain feature in their study. This suggests the importance of detecting RP in single trials. Unfortunately, there has been no research where the main emphasis is on detection of this potential. Although in studies such as [53, 54, 55, 56] the features of RP are used in their experiments, none of them focused on the extraction or detection of this wave and, thus, no results were published on this concept.

In this chapter, the first attempt at detection of RP in single trials is illustrated. To

do so, first, an experimental setup including the necessary software and hardware to evoke the RP in EEG of subjects has to be designed. The experiments involved trials of delayed movement where subjects raised their hands and pressed a button and trials of delayed observations where a short movie of grasping an object was played. After data acquisition the EEG data was first segmented based on the start of hand movement or the start of the short movie . Then, without further preprocessing, the SOBI was applied to the data and the results obtained or components extracted were analyzed manually. Interestingly, in each trial of movement or observation a source or wave was detected which showed many RP temporal and spatial characteristics. Although there were good reasons to hypothesize that this wave corresponds to the RP, further investigation was necessary to confirm it. However, assuming that the wave was a RP a method was created to detect the waveform automatically. In this method a template is designed based on Gamma distribution which simulates the shape of RP. Then, by means of template matching and applying a threshold, the wave is detected in the trials. As can be seen in the result section, the method is shown to be resilient in four subjects.

3.2 Second-Order Blind Identification (SOBI)

EEG signal is assumed to be formed by a number of independent components or sources. This assumption justifies the use of Independent Component Analysis (ICA) in EEG signal processing. One major application of ICA is in Blind Source Separation (BSS) algorithms. In these methods the mixture signals are decomposed to their constituent components using only the information observed at the sensors or electrodes [3]. A review of different ICA algorithms used for EEG can be found in [68]. A good example of BSS algorithms used in EEG signal processing is second-order blind identification (SOBI) which diagonalizes multiple time-delayed correlation matrices of the observation data to extract the sources that have different spatial distributions and stable power spectra [68, 69].

After applying different algorithms such as JADE [70] and FastICA [71], and

careful observation of their resulting components, the conclusion was that one of the components produced by SOBI[3, 72] best matched the features of RP and therefore, SOBI was used as the core for the automatic BSS-based method to detect the RP.

3.2.1 SOBI for EEG signal Analysis

SOBI has been used in EEG and MEG signal processing for source reconstruction both in temporal and spatial domains [73, 74, 75, 76, 77, 78, 79]. In all of these articles SOBI was shown to be able to recover the components that are meaningful from a physiological and neuroanatomical point of view. Here we briefly review some papers that used SOBI for analysis. SOBI was proved to have better performance for MEG classification of Alzheimer's disease patients compared with other BSS algorithms such as AMUSE, FastICA, and extended Infomax [76]. In [77] SOBI was shown to be able to successfully extract the EEG artifact components and it was used as part of a procedure to automatically correct the ocular artifacts. Validation of components extracted by SOBI from 128 channel EEG data was done in [78]. In this work, SOBI could accurately extract both known *noise sources* such as artificially generated noise sources added to a specific sensors and naturally occurring 60 Hz noise and highly constrained and well-characterized *neuronal sources* activated by median nerve stimulation from high-density EEG data. SOBI was also used as part of a method for classification of ERPs awakened by a sequence of randomly mixed left, right, and bilateral median nerve stimulations [79]. In [79], SOBI was shown to be applicable for preprocessing of EEG data recorded with 128 channels and extracting neural features from the left and right primary somatosensory (SI) cortices. Then, by feeding the SOBI extracted features to a Back-Propagation Neural Network as the classifier, the accuracy of 83.3 % $\pm$ 5.6% among four subjects was measured.

3.2.2 SOBI Algorithm

SOBI decomposes n-channel EEG data to n components or sources. Each SOBI generated component has a time course and a corresponding scalp projection which determines the effect of that specific component on all n electrodes. That is to show

which electrodes are nearer to the component or where in the scalp the component is originated.

Let's assume $\mathbf{X}(t)$ includes n continuous time series from n EEG channels and thus $\mathbf{x}_i(t)$ represents EEG data recorded by ith sensor. Since human scalp performs like a conductor, the sources coming from the brain are summed together and any of $\mathbf{x}(t)$ can be assumed as a linear mixture of m ($n \geq m$) unknown brain sources $\mathbf{s}(t)$, mixed through an unknown $n \times m$ mixing matrix $\mathbf{A}$. That is,

$$\mathbf{x}(t) = \mathbf{A}\mathbf{s}(t) + \mathbf{v}(t) \tag{3.1}$$

Where $\mathbf{v}(t)$ is a $n \times 1$ white-noise vector independent of the source signals, $\mathbf{x}(t) = [x_1(t), ..., x_n(t)]^T$, $\mathbf{s}(t) = [s_1(t), ..., s_m(t)]^T$ and superscript T represents the transpose operator. SOBI uses $\mathbf{X}$ to form the $m \times n$ un-mixing matrix $\mathbf{W}$ that approximates $\mathbf{A}^{-1}$ but is subject to permutation and scaling of its columns. Thus, assuming a noiseless situation, the estimated sources $\hat{\mathbf{S}}$, are given by

$$\hat{\mathbf{S}} = \mathbf{W}\mathbf{X} \tag{3.2}$$

$\hat{\mathbf{S}}$ shows the time course of the components. To calculate matrix $\mathbf{W}^{-1}$, SOBI considers the time coherence of signals. SOBI tries to find $\mathbf{W}$ by minimizing the squared sum of cross-correlations between one component at time t and another component at time $t + \tau$. SOBI applies this calculation across multiple time delays and across all pairs of components. Since this cross-correlation is sensitive to temporal features of time based signal, temporal information of EEG data is enough for source separation. For more information on SOBI algorithm see [3] or [72].

3.3 EEG Data Acquisition

Four healthy subjects, 2 males and 2 females, volunteered in conducting the experiment. All subjects were right-handed and aged between 24 and 30 years. None of the subjects had any history of neurological or psychological disorders.

3.3.1 Experiment Hardware and Software Setup

The acquisition framework used E-Prime and EGI's NetStation software to acquire EEG data from a 128-channel Sensor Net (Electrical Geodesic, Eugene, USA) helmet. To have better a view of the 128-channel Sensor Net, see Figure 3.1. In this Figure, top and side view of the net is demonstrated while the net is adjusted on the subject's head. The E-Prime software was used for experimental paradigm and stimuli delivery. The main feature of this setup was the possibility of marking on-line the beginning of the hand movement. This could be done thanks to the use of an external device, called HModule, which is shown in Figure 3.2. It is based on the Henesis WiModule [80], which has already been used for human motion acquisition in [81]. One of its main characteristics is that it contains a high-performance three-axis accelerometer, which permits detection of the beginning of the movement. At the same time, it allows recording the movements by saving the accelerometer data. The accelerometer used has a precision of ± 1 mg with a range of ± 6 g. The sampling frequency was set to 160 Hz, which means that a new sample from the accelerometer is acquired every 6.25 ms.

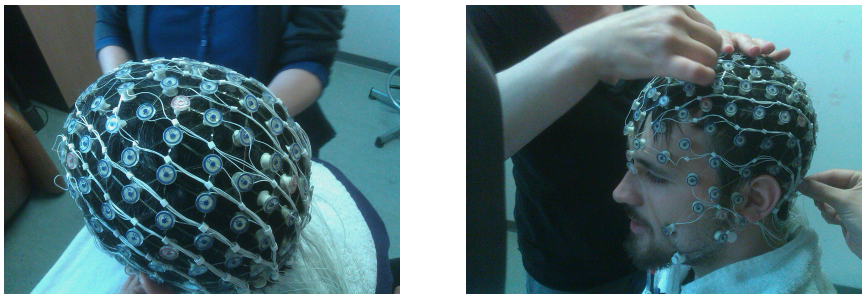

(a) (b)

Figure 3.1: 128-channel Sensor Net; (a) top view of the net, and (b) side view of the net while adjusting on subject's head

As can be appreciated in Figure 3.2(a), the HModule is small and wearable, which makes it ideal for being used in the experiments attached to the moving hand of subjects. An algorithm based on thresholding and the Exponential Moving Average

(EMA) has been implemented. Using this technique in time series leads to smoothing out the short-term fluctuations and to highlight longer-term trends. For each sample of the accelerometer, the energy is calculated considering the data related to the three axes. Afterwards, the energy is filtered, giving more weight to the latest data. This filtered value is the one compared with the set threshold. When a small hand movement is done (e.g. just when the subject starts to rise his/her hand), the given threshold is exceeded and the HModule triggers an event sending a signal to E-Prime to mark the EEG data. Choosing the correct threshold is of the utmost importance since if it is too low, any minimal movement done by the subject would be caught while, if it is too high, the beginning of the movement would not be marked properly, but later in the data sequence. Several experiments were carried out by different subjects in order to choose the correct threshold for the given movement, "raising the hand and pressing a button on a pad".

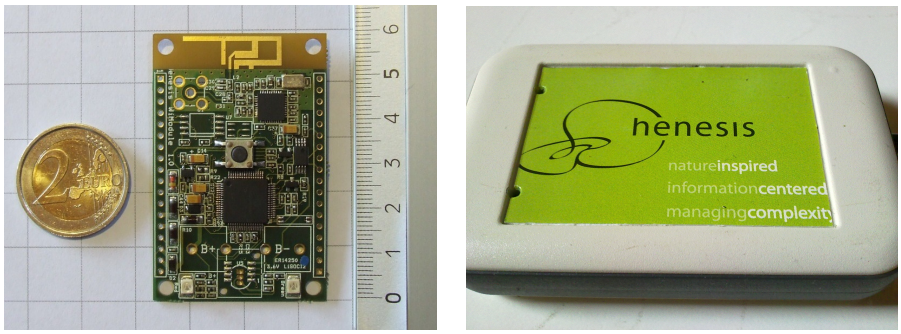

(a) (b)

Figure 3.2: HModule: External device design to mark the beginning of the hand movement on EEG data; (a) electronic board, and (b) packaging

The whole experiment's duration was about 10 to 11 minutes (the time variation is due to the fact that subjects were free to move their hand whenever they wanted after seeing the 'Go' signal) and consisted of 80 trials, each about 5 seconds long. Also, it took about 20 to 30 minutes to prepare each subject and adjust the sensor net on his/her head. Therefore, the whole experiment time was not more than 45 minutes per subject. The EEG data was recorded with a sampling frequency of 250 Hz.

3.3.2 Experiment Paradigm Simulation

The overview of each trial is shown in Figure 3.3. At the beginning of each trial there was a 2 seconds' time for baseline then, by individual cues on the screen which stayed on for 0.5 seconds, the subject was informed of the upcoming event. 2 seconds after the disappearance of the informative cue two different experimental conditions were randomly presented. In one case the cue instructed the subjects to prepare a movement waiting for the 'Go' signal for its execution (movement condition). In the other condition (Observation) the cue instructed the subjects to stay still waiting for a video presentation. Thus, the event could be one out of the following two:

- performing an action, i.e. the subject had to move his/her hand and press a button on a response pad,
- observing a movement, i.e. a video is played where a hand of an actor enters the scene and grasps an object.

Therefore, two kinds of trials were present; trials where a short movie was played for subjects which will be referred to as "observation trials" and trials where the subject had to preform an action which will be referred to as "movement trials". In the movement trials, after 2 seconds from the end of a movement cue, a 'Go' signal was given and the subject was instructed to move his hands whenever he wanted. These trials ended when the subject pressed any button on the response pad. For observation trials four videos were prepared showing a grasping move where the objects grasped were different not to lose the subject's interest. Moreover, the trials were divided into 40 movement trials and 40 observation trials and mixed together randomly to motivate more attention in the subjects.

3.4 BSS Method

An overview of the BSS Algorithm used to detect the RP in segmented single trials is given in Algorithm 1. All 128 channels of the acquired EEG data were used in the analysis. The first step was dividing the continuous EEG data into short segments.

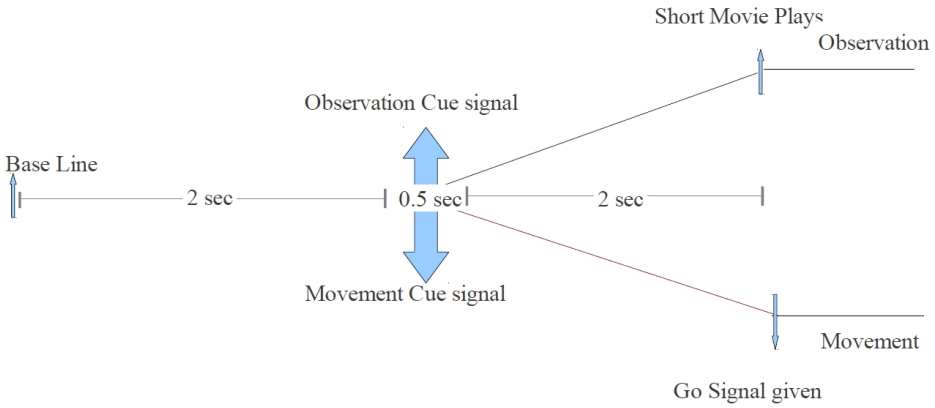

Figure 3.3: The time course of both trials. The up arrows show the cues in observation trials and the down arrows show the cues in movement trials. Note that the first 2 seconds are the same for all trials.

Observation trials were cut based on the start of the short movie. Movement trials were cut based on the beginning of hand movement using HModule markers on EEG data. The length of both trials was the same and equal to 2 seconds before the event occurred. Note that the difference between two kinds of trials was that in one trial the subject was anticipating a movie and in other he was anticipating a go signal to move. Both these trials were used for EEG Analysis and, as shown later in the result section, RP was found in both of them.

3.4.1 Source Extraction using SOBI

After segmenting the signals, SOBI was applied to each trial. By default, the number of separated sources has been set to the number of measurements, i.e. 128. sixteen out of 128 components are shown in Figure 3.4 for one subject's single movement trial. This figure serves to illustrate the output of the SOBI algorithm and to gain better understanding of why the next steps were necessary. All these components were generated for multiple subjects and studied one by one. After careful observation of the components, one source seemed to show features similar to RP (see Figure 3.4

Algorithm 1 BSS-based algorithm for RP detection

Step 1: Segment EEG data to single trials
Step 2: Create the $RP_{template}$ based on $t^2 e^{-t/100}$
Step 3: For each single trial do:

Step 3.1: Apply SOBI with $Source_{num} = m$

Step 3.2: For $i = 1, ..., m$ Calculate

- $VCorr_i = Correlation(RP_{template}, IC_i)$

Step 3.3: Find the $max_{corr} = max(VCorr_i)$

If $max_{corr} > Threshold$ **then**

- RP exists in this trial

end if

top wave on left column). Figure 3.5, shows 20 of the mentioned waves found in 20 movement single trials of one subject. These trials were chosen due to high resemblance of their detected RP to an expected RP waveform with correlation value of more than 0.95. The common features between this wave and RP are the following (also mentioned in Figure 3.5):

- The shape of the wave is similar to the shape of wave in literature, compare Figure 3.5 with Figure 1.5.
- The wave has a very slow rise happening about 160 ms before the beginning of hand movement.
- The peak of the wave occurs around 400 ms to 120 ms before the movement and continues to decrease after the movement.
- Spatial signature of the wave obtained by back projection using electrodes coordinates on scalp, was *motor cortex*, as can be seen in Figure 3.6. In this picture, the scalp maps of the spatial signature of assumed RP extracted from

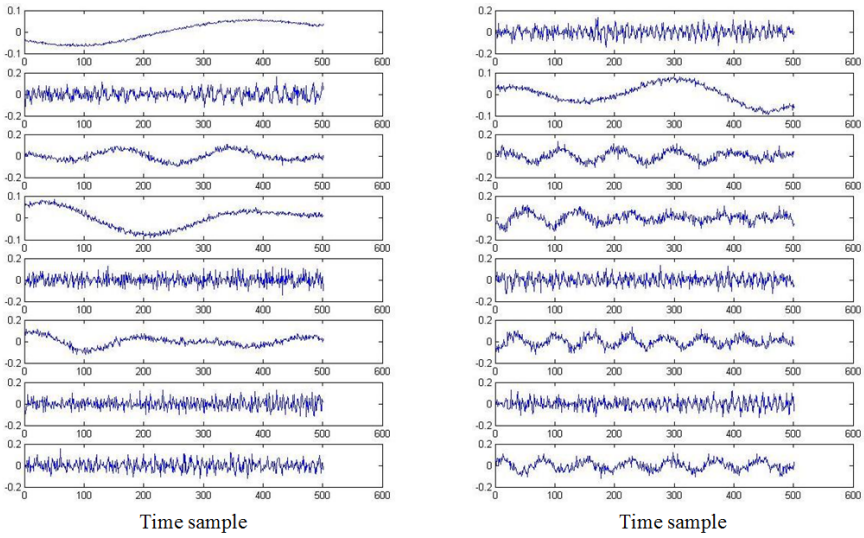

Figure 3.4: 16 out of 128 components generated by SOBI from a single trial of Movement

movement single trials (left), average of scalp maps for 38 out of 40 movement trials (middle) and average of absolute values for the same trials (right) in one subject is given. These 38 trials were chosen based on strong resemblance between the shape of RP found in these trials and the actual RP. In all three images the active part of brain is the motor cortex.

3.4.2 Template Matching

In the next step the goal was to find a way to determine which of the 128 components was to be assumed to be RP. The challenge was the fact that output of SOBI is not completely predictable:

- Sources extracted by SOBI are subjected to scale and sign changes.
- The order of the estimated sources is different in every trial.

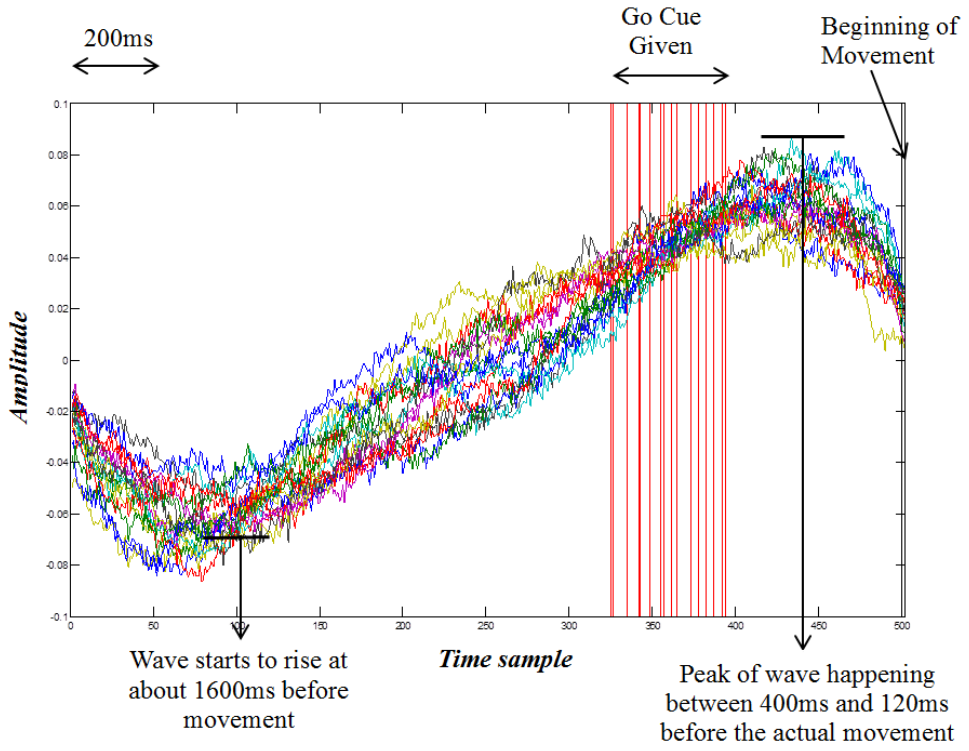

Figure 3.5: 20 waves extracted from 20 trials plotted altogether. Temporal features of the waves similar to RP are marked on image.

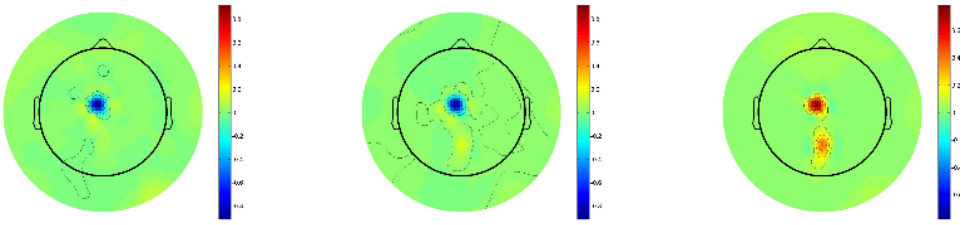

Figure 3.6: Left: Back projection of assumed RP on scalp in one subject. Middle: back projection of average of 38 assumed RP in 38 trials with strong similarity between the shape of detected RP and actual RP in same subject. Right: back projection of the average of the absolute values of the RPs mentioned in middle image.

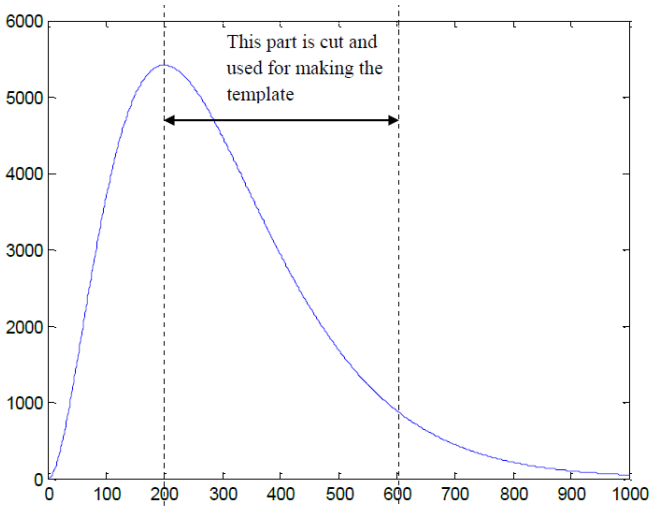

Figure 3.7: Curve gained by plotting modified Gamma function described in Formula 3.4

Therefore, a template matching technique was applied to determine which component is the wanted source. Consequently, a template was developed which simulates the RP waveform. The template was based on Gamma distribution. The original formula of Gamma function is shown in Formula 3.3:

$$f(t;k,\theta) = ct^{k-1}e^{-t/\theta} \tag{3.3}$$

Where $k > 0$ is a shape parameter, $\theta > 0$ is a scale parameter, and c is a normalizing constant. The Gamma curve has a short rise time and a longer tail for small k, and for large k values it is a symmetric waveform. Thus with a small k it is suitable for estimating the shape of actual RP. The Formula 3.3 was modified to simulate the shape of RP, see Formula 3.4. The values of Gamma function parameters and the segment used as template were determined by trial and error.

$$f(t;3,100) = t^2e^{-t/100} \tag{3.4}$$

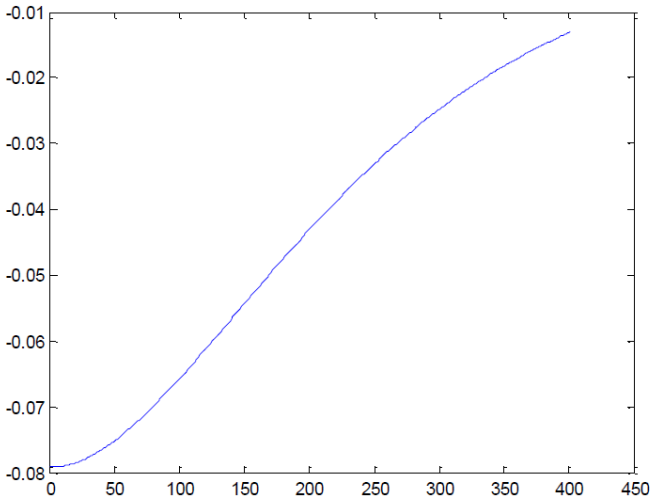

Figure 3.8: Final shape of first template used for automatic detection of RP

The curve obtained by plotting Formula 3.4 is plotted in Figure 3.7. As also marked on Figure 3.7, part of the curve was used and horizontally flipped to generate the first template shown in Figure 3.8. Based on the result gained from first template another template was formed shown in Figure 3.9. As can be seen by comparing Figure 3.8 to Figure 3.9 both templates are very similar, the only difference being the initial points. The result of template matching obtained by both templates is given in the result section. Results show that template 2 generated slightly higher detection rate compared with template 1.

In order to find RP, all 128 components of a single trial was compared with the template and the maximum correlation value for each component was measured. Then the source with highest maximum correlation was extracted. If this source correlation value was greater than a threshold (0.5) then the RP was assumed to be present in that trial.

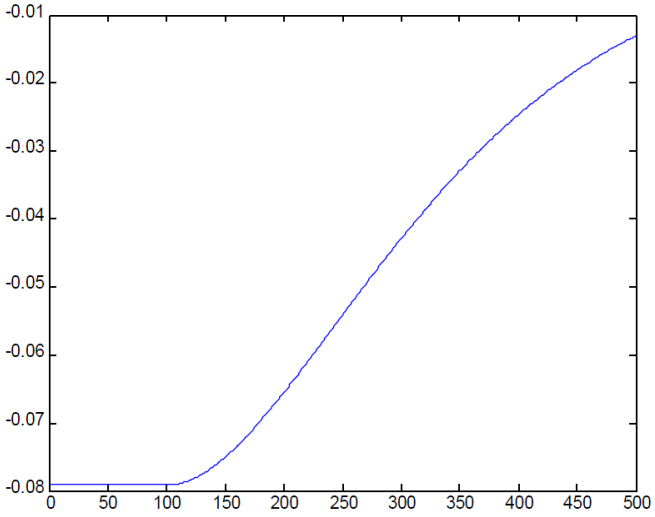

Figure 3.9: Shape of second template used for automatic detection of RP

3.5 Results

The results obtained by applying the method mentioned for detection of RP with template 1 and template 2 for four subjects are shown in Table 3.1 and Table 3.2 respectively.

For each subject 40 trials acquired just before the movement and just before observation of the movement are analyzed. No trial was eliminated for any subject due to any number of reasons such as artifacts. Also, the average of maximum correlation value obtained by comparing the template and the most similar wave to RP in all 40 trials is calculated. Since RP is reported to occur both when movement or observation of movement is about to happen [38, 39], it was expected to detect RP in all the trials analyzed. With this fact in mind, it is obvious from the two tables that template 2 generated better result compared with template 1. Using template 2 for the same objectives the results of RP detection was better for all subjects. However, the improvement varies between 2% to 7% among different subjects.

The method results for detecting the RP wave were promising. The detection rates

was between 82.5% and 95% for the first template and between 82.5% and 100% for the second template.

Table 3.1: Results gained by applying the BSS-method with template 1 to detect RP

Subject		**40 Trials before movement**	**40 Trials before observation**
Subject K	Detected RP Averaged Correlation	87.50% 0.57	90.00% 0.56
Subject R	Detected Averaged Correlation	95.00% 0.55	87.50% 0.54
Subject L	Detected RP Averaged Correlation	82.50% 0.49	82.50% 0.49
Subject P	Detected RP Averaged Correlation	92.50% 0.57	85.00% 0.57

3.6 Discussion

In this chapter a method to detect RP in single trials of EEG data automatically was presented. The most challenging part was to find the RP. To do so, different BSS algorithms such as JADE and FastICA were applied to single trials before the movement but none of the components they produced showed much similarity to the actual RP. However, the results obtained from SOBI had good resemblance to RP. Therefore, the detection method was based on SOBI.

In the application in mind for SOBI or in general ICA, longer segments of EEG data cannot be used. This is because ICA is based on the assumption that EEG signals are short-term stationary [3, 82]. Generally speaking, the sources within different parts of the brain are not always active. They may even move and go deep or be prop-

Table 3.2: Results gained by applying the BSS-method with template 2 to detect RP

Subject		**40 Trials before movement**	**40 Trials before observation**
Subject K	Detected RP Averaged Correlation	90.00% 0.64	95.00% 0.63
Subject R	Detected Averaged Correlation	100.00% 0.66	95.50% 0.57
Subject L	Detected RP Averaged Correlation	82.50% 0.54	85.00% 0.53
Subject P	Detected RP Averaged Correlation	95.00% 0.66	90.00% 0.66

agated to the surface. So, it may not be possible to localize them in a long window. On the other hand, the RP is a locally restricted source [83] or a focal source. As mentioned before, the RP is a local event which is initiated approximately 1.5 seconds before the movement onset. The RP may vanish or be replaced by other brain events. Therefore, choosing long windows for the EEG signals may work for strong and somehow distinct events like eye-blinks or repetitive ERPs but not for a short-duration potential like RP. Moreover, the number of active sources in a short time can be considered fixed. However, in a long segment the number of sources may change and the change in the number of sources within a time segment is not considered by ICA methods. Thus, it is better to use short windows to detect the RP. Consequently, there is a need to divide the EEG data into short segments such as 2 second segments and then apply the algorithms to the result.

3.7 Summary

As it is presented in the results section the shape of template is very important. Even a small change in the shape can result in a better detection rate for all subjects. Improving the curve of the template can have positive effect on detection rate.

In the method used only temporal information of RP was used and compared and the spatial information of wave was checked via back projection to scalp manually after a source was chosen by the method. In order to be more certain that the wave found is the actual RP an extra module could be added to check the spatial location of component automatically. To do so, one idea could be to form the scalp maps and analyze them to see if the source is originated in the motor cortex or not.

Chapter 4

Blind Signal Extraction Technique for Detection of RP

4.1 Introduction

In this chapter, the second attempt to determine whether a RP exists in single trials of the EEG is described. Here, another signal processing technique called Blind Signal Extraction (BSE) is used. In addition, the design of the experimental setup, including the necessary software and hardware to evoke the RP in EEG of the subjects, was modified such that it resembles the real-environment situation. In this experiment, the subjects were asked to move their hands and press a button on the pad whenever they wanted; no specific cues were given and subject had the complete freedom about the movement time. After data acquisition, first, the EEG data was segmented based on the start of hand movement. Then, after minor preprocessing, two algorithms were applied to the single trials. Both algorithms are based on Independent Component Analysis (ICA); the BSS algorithm (see Algorithm 1) was illustrated in the previous chapter and the other will be described in this chapter. However, in the new algorithm, the RP is extracted by applying a proper constraint to the source extraction cost function. As can be seen in the results section, both methods have shown to be resilient across different subjects and had good results on the trials which were expected to

have RP in them (true positive rate).

On the other hand, data included single trials in which the RPs were not present, to evaluate the performance of algorithms against false detection. In this area, the the new algorithm outperforms the traditional BSS which is discussed later on.

The remainder of this chapter is organized as follows; first the basic concepts of the work are presented, which include a review of the ICA problems and solutions. In Section 4.3, the EEG data acquisition is introduced, including the simulation paradigm to obtain two different kinds of trials. In Section 4.4, the overview of the new algorithms used for automatic detection is presented and the steps necessary for automatic detection are illustrated. In the result section the experiments carried out to evaluate the detection algorithms are described. The article ends with the discussion about the results in Section 4.6 and summary in Section 4.7.

4.2 Independent Component Analysis Problem

As mentioned before, EEG signal is assumed to be formed by a number of Independent Components (ICs) or sources. This assumption justifies the use of ICA in EEG signal processing [3]. This concept is depicted in Figure 4.1 One major application of ICA is in two signal separation approaches called Blind Source Separation (BSS) and Blind Signal Extraction (BSE) which are frequently used in biomedical signal analysis and processing such as for EEG or MEG. Both techniques share the common word, blind, referring to the fact that the source signals are unobservable in the mixture signal, no prior information about them exists and the mixing process is unknown. This is in contrast to other techniques such as minimum-norm estimation (MNE) developed by Matti Hämäläinen, [84, 85] that require a prior head model. However, some assumptions are made about the sources or mixing process, such as independency of the sources to make the extraction procedures possible.

In general, in the BSS and BSE methods, the problem is formulated as follows; let's assume $\mathbf{X}(t)$ shows n continues time series from n EEG channels and thus, $\mathbf{x}_i(t)$ shows EEG data recorded by the ith sensor. Since human scalp performs like a conductor, the sources coming from the brain are summed together and any $\mathbf{X}(t)$ can be

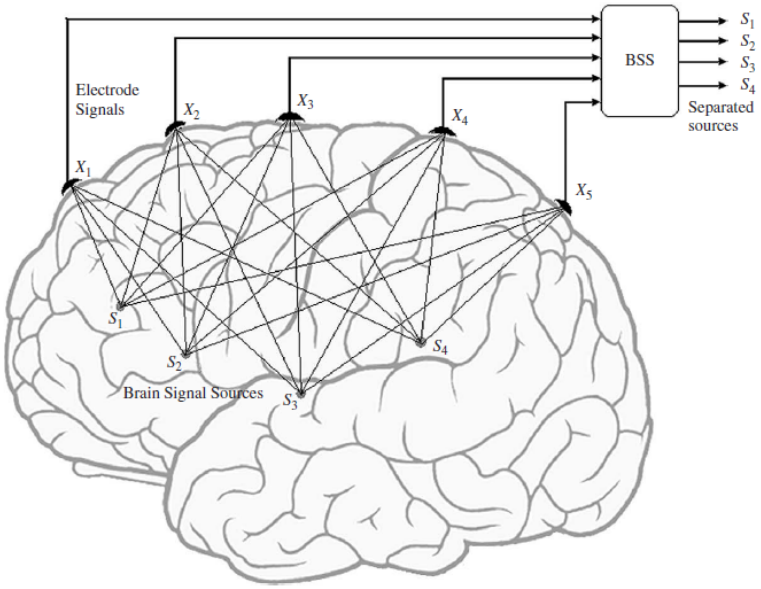

Figure 4.1: The mixing and blind separation of the EEG signals. Taken from [3].

assumed as a linear mixture of m ($n \geq m$) unknown brain sources $\mathbf{s}(t)$ at discrete time t, mixed through unknown $n \times m$ mixing matrix $\mathbf{A}$. That is,

$$\mathbf{x}(t) = \mathbf{A}\mathbf{s}(t) + \mathbf{v}(t) \tag{4.1}$$

where $\mathbf{v}(t)$ is an $n \times 1$ white noise vector independent of the source signals, $\mathbf{X}(t) = [x_1(t), ..., x_n(t)]^T$, $\mathbf{S}(t) = [s_1(t), ..., s_m(t)]^T$ and superscript T represents the transpose operator. Thus, assuming a noiseless environment, one can eliminate $\mathbf{v}(t)$ from the above formula and assume:

$$\mathbf{X}(t) = \mathbf{A}\mathbf{S}(t) \tag{4.2}$$

Now that the similarities between BSE and BSS methods have been addressed, the focus of next part is on their differences on how they tackle the problem of extracting the sources in the next section.

4.2.1 Blind Source Separation techniques

BSS approaches try to recover or estimate all the original sources, $\mathbf{s}_i(t)$, simultaneously from the mixture signals. Different algorithms have been developed for this approach and the challenge is to choose the suitable algorithm based on the application. Since SOBI has shown good results in our previous experiment, it has been used here again to be compared with the BSE results.

4.2.2 Blind Signal Extraction techniques

BSE approaches try to recover or estimate the original sources, $\mathbf{s}_i(t)$, one at a time from the mixture signals. Compared with BSS, BSE has the following advantages:

- By creating some constraints or criteria based on the features of the desired source signals, they can be extracted in a specified order.
- The approach is very flexible and can use different criteria in each step of the extraction, to separate the preferred sources in that step.
- It is possible to extract only the sources of interest and thus, it can save computation time and resources.
- BSE algorithms are simpler than BSS algorithms and can be modified to be applied in a number of different situations.

In this experiment sequential BSE was used with an optimization criterion based on the absolute value of normalized kurtosis. Kurtosis measures the deviation of the extracted source from the normal Gaussian distribution and it is based on the fourth-order central moments of the signal [86]. A Gaussian signal has the kurtosis of zero, for positive values of kurtosis, signal is super-Gaussian or long tailed and for negative values, it is sub-Gaussian or short tailed as demonstrated in Figure 4.2.

According to the Central Limit Theorem, the distribution of the mixture signal is closer to a Gaussian distribution than any of the original sources. Therefore, by maximizing a non-Gaussianity criterion such as the absolute value of kurtosis, one

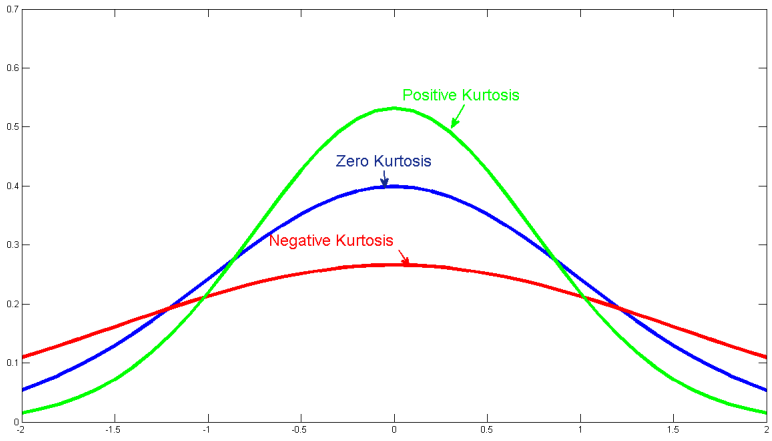

Figure 4.2: Value of kurtosis for different Gaussian distribution compared with normal distribution

can separate the source from the mixture signals. Since the goal is to look for one specific signal, one can formulate the output of the algorithm as:

$$\hat{\mathbf{s}}_\mathbf{i} = \mathbf{y}_i = \mathbf{w}_\mathbf{i}^\mathbf{T}\mathbf{X} \tag{4.3}$$

where $\mathbf{y}_i$ is the $1 \times L$ ith output signal, $\mathbf{w}_i$ is the $1 \times n$ ith row of the unmixing matrix calculated by the algorithm and $\mathbf{X}$ is the $n \times L$ mixture matrix consisting of the electrode signals. L denotes the number of time samples and n is the number of electrodes, as said before. Avoiding index i for simplicity, the goal is to minimize the following cost function:

$$J_m(\mathbf{w}) = -\frac{1}{4}\left|kurt(\mathbf{y})\right| \tag{4.4}$$

where $kurt(\mathbf{y})$ is the normalized kurtosis. Applying the standard gradient descent approach to minimize the cost function in equation (4.4), the following online learning

rule is obtained [86]:

$$\mathbf{w}(k+1) = \mathbf{w}(k) + \eta(k)\varphi(y(k))\mathbf{x}(k) \tag{4.5}$$

where

$$\varphi(y(k)) = b\left(\frac{m_2(y(k))}{m_4(y)(k)}y(k)^3 - y(k)\right)\frac{m_4(y(k))}{m_2^4(y)(k)} \tag{4.6}$$

and the moments m_q can be iteratively estimated in an online application as

$$m_q(k) = (1-\beta)m_q(k-1) + \beta\,|y(k)|^q \tag{4.7}$$

where k is the iteration number and the sample number, m_q is the qth moment and $\beta \in (0,1]$ denotes the adjusting influence of the previous estimate of the moment and the current estimate. The parameter b determines the sign of the kurtosis of the extracted signal which is negative for RP.

Now, in order to form the constraint to extract the RP first, the prior knowledge about the shape and latency of RP in combination to the normalized kurtosis cost function was used. Thus, a reference signal of RP was created to calculate the actual unmixing vector, $\mathbf{w}_{opt}$, which is used to minimize the Euclidean distance between the reference signal and the data with:

$$J_c(\mathbf{w}_{opt}) = \left\|\mathbf{y}_{ref} - \mathbf{w}_{opt}\mathbf{X}\right\|^2 \tag{4.8}$$

where $\|.\|^2$ denotes the Euclidean distance. The solution to this is minimum norm [87]:

$$\mathbf{w}_{opt} = (\mathbf{X}\mathbf{X}^T)^{-1}\mathbf{X}\mathbf{y}_{ref}^T \tag{4.9}$$

Therefore, the distance of the obtained $\mathbf{w}$ from (4.5) and $\mathbf{w}_{opt}$ from (4.9) need to be minimized. So the following should be minimized:

$$d(\mathbf{w}) = \|\mathbf{w}_{opt} - \mathbf{w}\|^2 \tag{4.10}$$

This constrained cost function replaces the original cost function (4.4) and the learning rule becomes:

$$\mathbf{w}(k+1) = \mathbf{w}(k) + \eta(k)\varphi(y(k))\mathbf{x}(k) + K(\mathbf{w}(k) - \mathbf{w}_{opt}) \tag{4.11}$$

where K is the penalty parameter to balance the two cost functions J_m and J_c. If chosen too high, it will overcome the effect of the main cost function while, if chosen too low, it will have a small effect. How to choose K is described in the results section.

In [88], the authors designed a constrained ICA similar to the BSE algorithms to extract the components of brain activation in fMRI data. The cost function designed, is based on both the second-order and the higher-order statistics which uses the prior information about the desired components in the form of a reference signal. The authors in [89] proposed a constraint BSE algorithm which uses the cost function based on fourth-order moment (kurtosis for non-periodic signals, or a new cost function for periodic ones) with a reference signal correlated with the desired source. The algorithm has been reported to be accurate in source extraction from simulated data and also in extraction of the cardiac artifacts from MEG data. In [87] a constrained BSE algorithm based on kurtosis is used to detect the P300 components. They also included a reference signal based on the temporal shape of usual P300 subcomponent in their cost function and were able to correctly extract P3a and P3b signals from the EEG single trials. The CBSE-method developed here uses the same theory described in the Section 4.4.2. Obviously, it resembles the RP.

4.3 EEG Data Acquisition

Both the CBSE-based and the BSS-based methods were tested on two kinds of datasets; the simulated EEG dataset and the real EEG data recorded from normal subjects. This section addresses how these datasets have been formed.

4.3.1 Simulated EEG data

EEG data was simulated using multivariate autoregressive (MVAR) modeling. In this approach a multichannel scheme is assumed. Thus, each signal sample is considered to be related to its previous sample and the previous samples of other channels. Here the methods and parameters are adopted from [90] where the MVAR model uses two time-varying parameters which are a step function and a positive triangle function;

$$\begin{aligned} y_1(n) &= 0.5y_1(n-1) - 0.7y_1(n-2) + c_{12}(n)y_2(n-1) \\ &\quad + v_1(n) \\ y_2(n) &= 0.7y_2(n-1) - 0.5y_2(n-2) + 0.5y_1(n-1) \\ &\quad + c_{21}(n)y_1(n-1) + c_{23}(n)y_3(n-1) + v_2(n) \\ y_3(n) &= 0.8y_3(n-1) + v_3(n) \end{aligned} \tag{4.12}$$

where

$$c_{12}(n) = \begin{cases} 0.5\frac{n}{L} & n \leqslant \frac{L}{2} \\ 0.5(1-\frac{n}{L}) & n > \frac{L}{2} \end{cases} \tag{4.13}$$

and

$$c_{23}(n) = \begin{cases} 0.4 & 0 \leqslant n \leqslant 0.7L \\ 0 & n > 0.7L \end{cases} \tag{4.14}$$

$c_{21}(n)$ is set to 0.2 and L is the number of samples which is set to 2000, same as EEG trials in real data. $v_i(n)$ represents the white noise. For more information on the model and how to set the parameters, please see [90]. To this model, one sinc signal was added which simulated the shape of RP before the movement. The sources are shown in Figure 4.3. These sources, which are referred to as the original sources of the simulated data, were mixed using a randomly generated 5×4 mixing matrix, producing the 5 signals shown in Figure 4.4, which were used in both algorithms for RP extraction. The results of both algorithms on these data are discussed in Section 4.5.

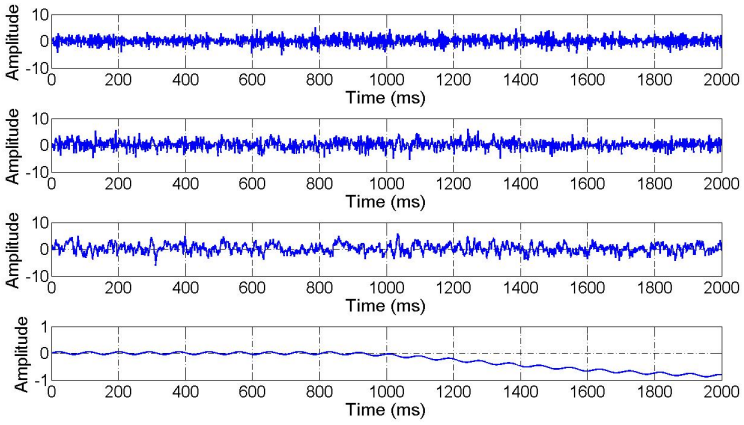

Figure 4.3: The original sources used to create the simulated mixture EEG data. The bottom plot shows the simulated RP.

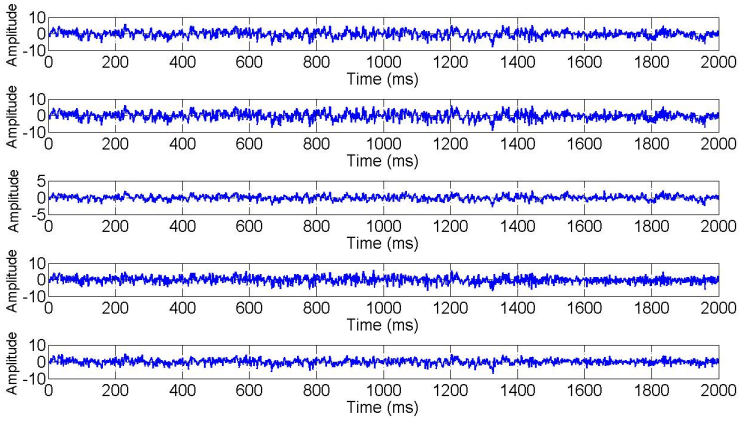

Figure 4.4: The simulated EEG data obtained by mixing the sources of Figure 4.3 using a random mixing matrix. Each plot simulates the data acquired by one EEG electrode.

4.3.2 Real EEG data

Three healthy subjects, 1 male and 2 females, volunteered in conducting the experiment. All subjects were right-handed and aged between 26 and 30 years. None of the subjects had any history of neurological or psychological disorders.

Experiment Hardware and Software Setup

The acquisition framework used E-Prime and EGI's NetStation software to acquire EEG data from a 128-channel Sensor Net (Electrical Geodesic, Eugene, USA) helmet. The E-Prime software was used for experimental paradigm and stimuli delivery as described in Section 3.3.1. A HModule was also attached to the hand of subjects to mark the beginning of hand movement.

The whole experiment had a duration between 10 and 11 minutes (the time variation is due to the fact that the subjects were free to move their hand whenever they wanted) and contained two parts, each lasting about 5 minutes. Preparing each subject and adjusting the sensor net on his/her head took approximately between 25 and 30 minutes. Therefore, the whole experiment time did not take longer than 45 minutes per subject. The EEG data was recorded with the sampling frequency of 1000 Hz.

Experiment Paradigm Simulation

As mentioned above, the EEG data recording paradigm included two parts, each with different instructions:

- Part 1: Steady; the subject was asked to remain calm, breath normally with open eyes and try not to think of anything or move.
- Part 2: Hand movements; the subject was asked to move his/her hand whenever he/she wanted at the speed he/she wanted (self-paced movement).

The instruction of what was asked in the experiment was given to subjects both orally and in writing at the beginning of the experiment. At the start of each part, a

cue was shown on a monitor to inform the subject of what task they should perform. Other than these two cues, no other cues were given to subjects for two reasons:

- First, this was necessary to simulate the real-world situation as accurately as possible.

- Second, giving a cue to the subjects might evoke potentials which are uncalled for such as CNV described in Section 2.2.3, which is a slow negative wave that develops in the interval between a "warning" and a "go" stimulus and reflects preparation for *signaled* movements.

In part 2, the EEG data to be analyzed started 2 seconds before the movements. Since no cue was given in the trials of this part, the HModule resting time was set to 5 seconds. This means the time duration between two sequential hand movements had to be at least 5 seconds. Otherwise, the HModule would not send any signal to E-Prime and the trial had to be repeated by the subject. As for the results, it was assured that 40 valid trials were obtained for each subject.

4.4 Comparison of CBSE-Based Algorithm with BSS-Based Algorithm

Algorithm 1 shows the pseudocode of the BSS-based algorithm and Algorithm 2 shows the pseudocode of the CBSE-based algorithm used for detecting the RP is single trials. All 128 channels acquired EEG data were used in our analysis. The EEG data was divided into two categories; pre-movement and steady trials. Pre-movement trials were obtained by cutting the EEG data based on HModule markers to 2 seconds before the beginning of the hand movements. Since there were 40 hand movements, 40 trials were obtained in this category. The steady trials were obtained by cutting the first 5 minutes of the steady data to 2 seconds long non-overlapping segments. Thus, there were 150 trials in the steady category. Both categories, pre-movement and steady trials, were used in the evaluation of the algorithms.

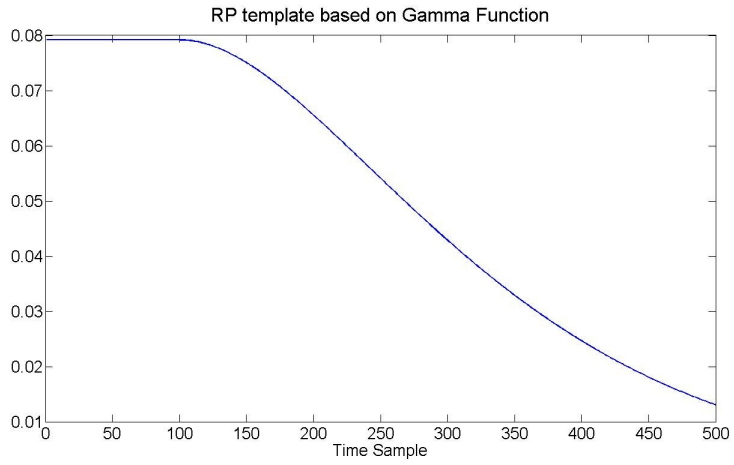

Figure 4.5: The final shape of the template based on Gamma function

4.4.1 BSS-Based Algorithm

In this algorithm (see Algorithm 1), after applying SOBI to each single trials of EEG data, a number of ICs are obtained which show the original sources that were active in the mixture signal. Unfortunately, the output of SOBI is not predictable. The sources extracted by SOBI are subjected to scale and sign change. Moreover, the order of the extracted sources in different trials varied. To determine which one of the sources was similar to RP, a template matching technique was used. The shape of RP was simulated with the help of Gamma function $f(t;k,\theta) = \frac{1}{\Gamma(k)} t^{k-1} e^{-t/\theta}$ with $k = 3$ and $\theta = 100$ and a small adjustment was added to that. Figure 4.5 shows the final shape of the template used in the BSS-based algorithm. Then, the correlation between each ICs in the output of SOBI with this template was calculated. When the value of correlation exceeded a *Threshold* it was assumed that RP was present in that trial. For more information please refer to Section 3.4.

4.4.2 CBSE-Based Algorithm

In this algorithm (see Algorithm 2), first, the EEG data was filtered in the range from 0.1 to 70Hz. The filtering was such that the CBSE algorithm can be in line with [87]. After that, the RP reference signal, $\mathbf{y}_{ref}$, was created. Both the Gamma wave (see Figure 4.5) and an average over 40 trials containing RP (see Figure 4.6) have been used as reference signal. Then, the $\mathbf{w}_{opt}$ was calculated with equation (4.9). The actual unmixing vector, $\mathbf{w}$, was initialized with random values. In each iteration the new $\mathbf{w}$ was computed using equation (4.11) and after each iteration of the algorithm it was compared with $\mathbf{w}_{opt}$. If, after some iterations, the Euclidean distance between $\mathbf{w}_{opt}$ and $\mathbf{w}$ were less than the $Threshold$ for a trial, it was assumed that an RP existed in that trials. Otherwise it was assumed that there was no RP in that trial.

Algorithm 2 CBSE-based algorithm for RP detection

Step 1: Segment EEG data to single trials
Step 2: Create $\mathbf{y}_{ref}$
Step 3: For each single trial do:

Step 3.1: Filter the data between 0.5 Hz and 70 Hz

Step 3.2: Form $\mathbf{w}_{opt}$, based on $\mathbf{y}_{ref}$ with equation (4.9)

Step 3.3: Initialize $\mathbf{w}$ randomly

Step 3.4: Minimize the cost function in equation (4.10)

if $d(\mathbf{w}) < Threshold$ **then**

- RP exists in this trial

end if

4.5 Results

Both methods were applied to two datasets, the simulated data and real data. In simulated data, the goal was to extract the RP source as close as to the actual source

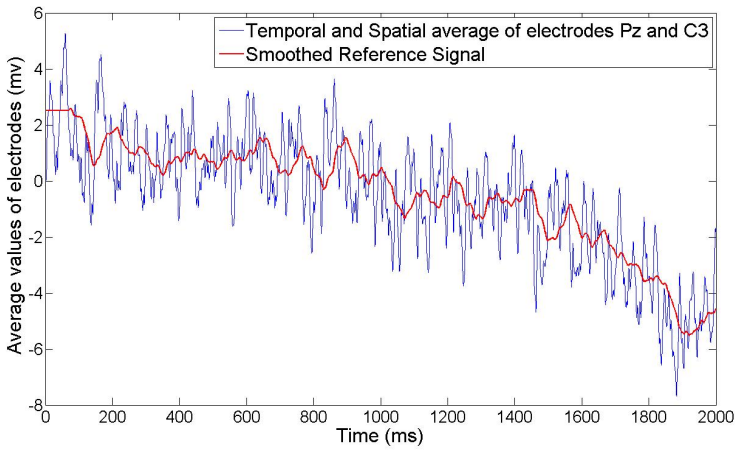

Figure 4.6: The shape of signals used for creating the reference signal

as possible. In real data, both categories of trials were used to evaluate the detection rate of the algorithms. The trials where RP was expected to be found, meaning pre-movement trials, were used for true positive rate evaluation and the trials for which RP was not expected to be found, meaning steady trials, were used to obtain the false positive rate of the algorithms.

The parameter K in the CBSE algorithm has been set by trial and error. If the parameter K in the CBSE is set to zero, the algorithm will be unconstrained and the output would be considered not RP. To set this parameter, small values for K (10^{-5}) were considered and the extracted RP was observed. At this small value, the results were not satisfactory. therefore, the value of K was increased slowly until a practical value (10^{-4}) was reached where the extracted RP was good and similar to its documented shape depicted in Figure 1.5. The β parameter in (4.7) was set to 0.5. The learning rate, $\eta(k)$ in (4.11), was set to 10^{-3} at the beginning of the algorithm and was reduced by 1% in every iteration. These values were the same for simulated and real EEG data and were not changed across the subjects or different categories of trials.

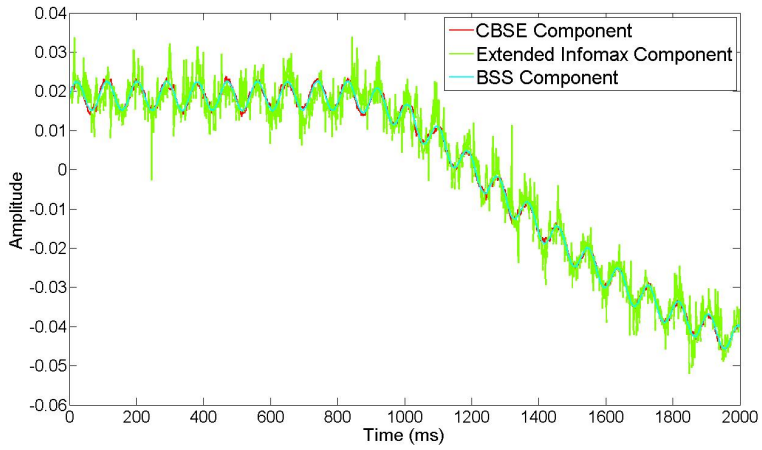

Figure 4.7: The extracted RP in simulated data: the result of SOBI and CBSE method overlap while the result of Extended Infomax is noisy.

4.5.1 Simulated Data

For this experiment, the simulated EEG data shown in Figure 4.4 were used. The goal was to extract the source with the RP shape simulated, shown in Figure 4.3, bottom plot. The SOBI and Extended Infomax algorithm described in [91] were applied to the data as well as the constrained BSE-algorithm. Extended Infomax uses a learning algorithm for a feed-forward neural network that blindly separates the linear mixtures of independent sources with different distributions using information maximization theory. The results of the extracted sources are showed in Figure 4.7. Comparing the three extracted signals with the original source, it is visually comprehensible that the CBSE-based method has a good performance.

Moreover, the performances of three algorithms on the simulated data were measured with respect to Mean Square Error (MSE) and Signal to Noise Ratio (SNR):

$$MSE = 10\log\frac{1}{N}\sum_{i=1}^{N}(s(i)-\hat{s}(i))^2 \tag{4.15}$$

$$SNR = 10\log\left(\frac{\sum_{i=1}^{N}(s(i))^2}{\sum_{i=1}^{N}(s(i)-\hat{s}(i))^2}\right) \tag{4.16}$$

where N is the number of time samples, $s(i)$ shows the original source and $\hat{s}(i)$ is the extracted source. In order to calculate the error for the three algorithms, the original source was used as the reference. Since SOBI output components are subjected to scale change, the extracted sources and the original source were normalized before calculation of the errors. The results are shown in Table 4.1. As can be seen in this table, SOBI and CBSE have similar results while Extended Infomax results on this data are noisy (lower SNR and higher MSE).

Here, it was assumed that the number of independent sources is less than or equal to the number of EEG channels. Otherwise, none of the components driven from SOBI or Infomax algorithm would have any similarities to the simulated RP.

Table 4.1: MSE and SNR of three blind algorithms for simulated data

	Extended Infomax with template matching	**SOBI with template matching**	**CBSE**
MSE	-42.6112	-45.6082	-45.6062
SNR	6.7727	10.2771	10.2751

4.5.2 Real Data

For the second experiment the real data recorded from human brain with the features described in EEG data acquisition were used. Here, Receiver Operating Characteristic (ROC) curves are plotted to describe the performance of the binary classifier at different values of the *Threshold* for both methods. To have a better view of the algorithms preformance, the output of the algorithm for one *Threshold* is shown in Table 4.2 and Table 4.3, where the value of the *Threshold* is 0.5 and 10^{-5} respectively.

In order for BSS-based algorithms to be applicable, the number of sources active in the brain should be less than the number of electrodes. Thus, the very robust and well known algorithm developed in [92] was implemented to obtain the number of independent sources from EEG data. The number of independent sources obtained by this algorithm in a randomly chosen 10-second segment of data was no more than 52. Since all 128 electrode channels were used and the EEG segments were 2 seconds long, it is possible to apply both algorithms to the data.

Figure 4.8 shows the BSS-based algorithm detection rate and Figure 4.9 shows the CBSE-algorithm detection rate. For the BSS-based method, since the value of correlation ranges from 0 to 1, the $Threshold$ was changed between 0.1 and 0.9, increased by 0.1 in each step, and the values of false positive rate and true positive rate were calculated accordingly. As can be seen in Figure 4.8, the change of $Threshold$ affects both rates similarly. This means that both false positive rate and true positive rate increase or decrease simultaneously with the change of $Threshold$. The curves shows the poor performances of this method for all three subjects.

For the CBSE method, the $Threshold$ was changed between 10^{-8} and 1. In every step the value of threshold was multiplied by 10. The ROC curves for the three subjects are shown in Figure 4.9; for each subject the results for two different $\mathbf{y}_{ref}$, one based on the average and another based on the Gamma function are plotted. As can be seen, in this method the true positive rate and false positive rate are independent from each other. The performance of binary classifier was acceptable in the range of $10^{-7} < Threshold < 10^{-4}$. However, lower values of $Threshold$ imply a larger number of iterations in the optimization process and thus require more computation time. A practicable value for $Threshold$ can be 10^{-5}, which produces good results with acceptable computation time (0.26 s for each single trial on average using an Intel CoreTM i5-1199M CPU @ 2.40GHz with 3.00 GB of RAM and MATLAB as programming language). An example of the algorithm performance for this value for three subjects can be viewed in Table 4.3.

As can be seen in Figure 4.8 and Figure 4.9, both algorithms can produce good re-

Table 4.2: BSS-algorithm detection results on real data ($Threshold = 0.5$).

Subjects	**True Positive (in 40 single trials)**	**False Positive (in 150 single trials)**
Subject F	40	118
Subject L	40	110
Subject P	40	112
Mean	40	113.3

Table 4.3: CBSE-algorithm detection results on real data ($Threshold = 10^{-5}$).

	average $\mathbf{y}_{ref}$		Gamma-based $\mathbf{y}_{ref}$	
Subjects	**True Positive (in 40 single trials)**	**False Positive (in 150 single trials)**	**True Positive (in 40 single trials)**	**False Positive (in 150 single trials)**
Subject F	39	22	39	28
Subject L	38	3	38	4
Subject P	40	0	39	8
Mean	39	8.3	38.7	12.3

sults in case of correct classification. However as regards to false detections, meaning detection of RP in the trials with no RP, the CBSE-based algorithm had a much better performance. This is due to the fact that the BSS-based algorithm, all the sources are extracted, which are usually many, and some of them pass the criterion to be misclassified as RP.

The time of extraction in both cases also differs significantly. Average extraction time of RP in one trial via the CBSE-based algorithm was 0.26s ($Threshold = 10^{-5}$) while for BSS-based algorithm it was 51.90s using Intel CoreTM i5-1199M CPU @ 2.40GHz with 3.00 GB of RAM and MATLAB as programming language. Again, this is due to simultaneous extraction of all sources by SOBI.

Figure 4.10 and Figure 4.11 show 20 extracted RPs in 20 single trials from pre-

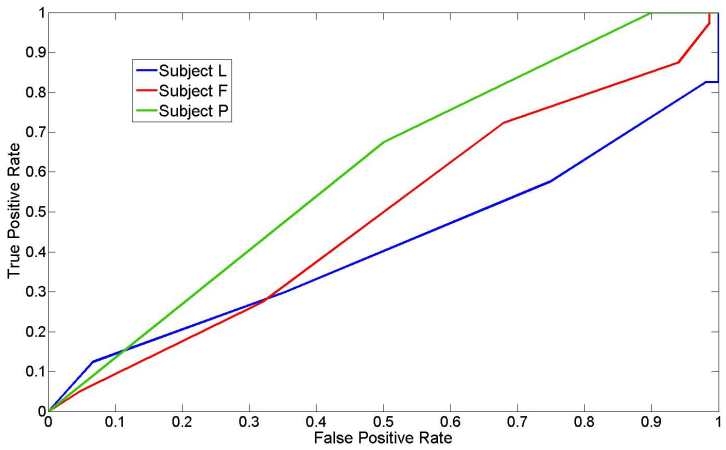

Figure 4.8: ROC curves of the BSS method for 3 subjects. As can be seen the change of $Threshold$ affects true positive and false positive rate similarly.

movement category by the BSS-based algorithm and by the CBSE-based algorithm in the second experiment where the cues were eliminated.

4.6 Discussion

The shape of the RP signal extracted by both algorithms is different (compare Figure 4.11 with Figure 4.10). This is because in CBSE-based algorithm the reference signal, $\mathbf{y}_{ref}$, was designed as the trade-off between having maximum true positive rate and minimum false positive rate. Thus, all the values of $\mathbf{y}_{ref}$ except the last 400 was set to zero. Setting fewer values to zero gives us a more similar shape to Figure 4.10 or Figure 1.5, but also increases the false positive rate.

The changes for the values of Kurtosis of the extracted signal in every iteration are shown in Figure 4.12 ($Threshold = 10^{-5}$). This figure shows the convergence of the CBSE-based algorithm after only 23 iterations, when the method meets its stopping criterion, when the value of Kurtosis is at its maximum.

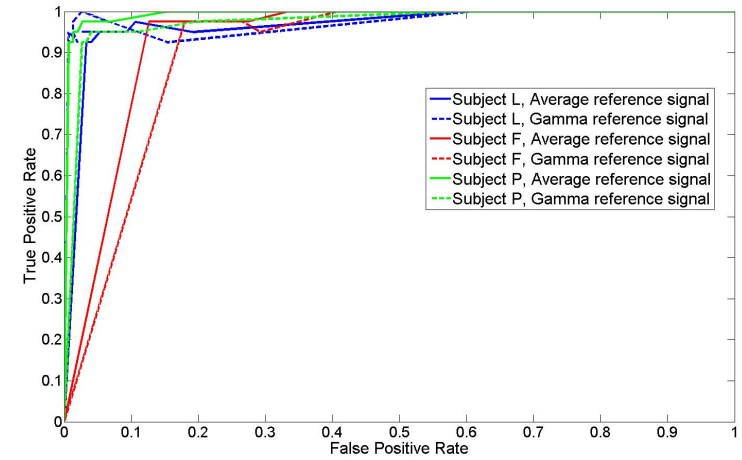

Figure 4.9: ROC curves of the BSE method for 3 subject using two different $\mathbf{y}_{ref}$: the average signal and the general Gamma function. As can be seen the change of *Threshold* affects the true positive and false positive rate independent from each other.

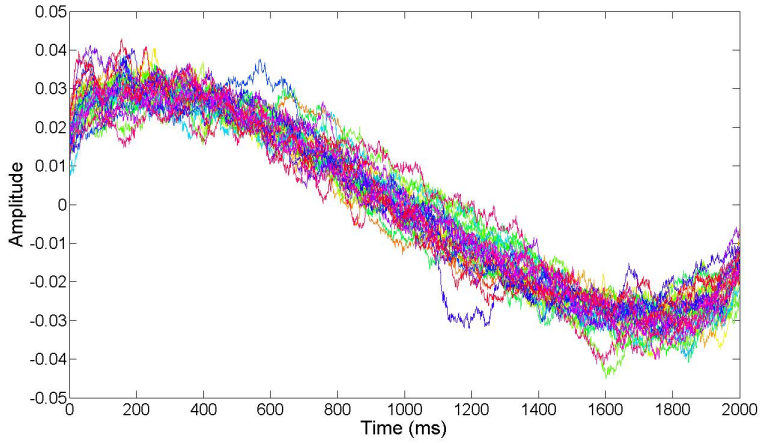

Figure 4.10: 20 RPs extracted in 20 single trials by the BSS-based algorithm

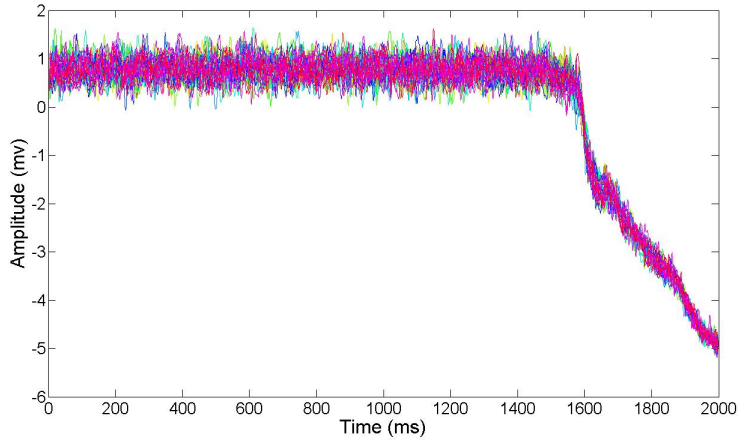

Figure 4.11: 20 RPs extracted in 20 single trials by the CBSE-based algorithm

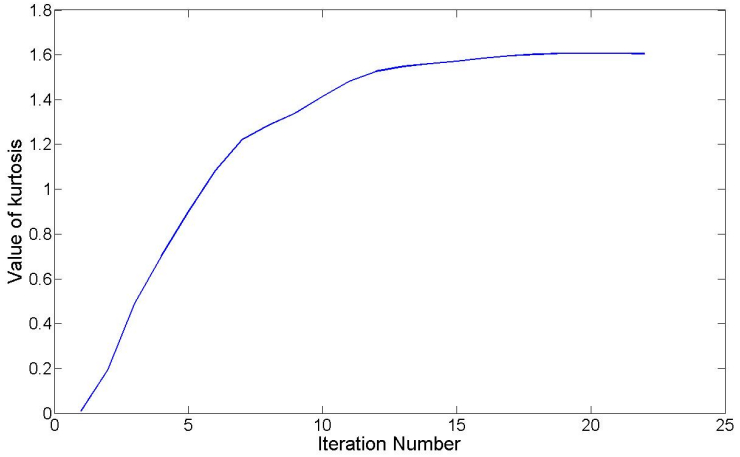

Figure 4.12: Convergence of the CBSE-algorithm in one single trial: the value of Kurtosis is increasing in every iteration with respect to the new learning rule described in (4.11).

4.7 Summary

The main idea of this chapter was to demonstrate the superiority of CBSE-based algorithm in detection of brain potential compared with BSS-based algorithm. To sum up, in BSS-based algorithm, first all the possible sources in the EEG single trial are extracted and then the source that is of interest is looked for. CBSE-based algorithm performs differently by adding some constraint to the cost function, only the sources of interest are extracted and the other active potentials or noise are ignored from the very beginning.

Chapter 5

Analysis of a new paradigm for P300 speller

The chief function of the body
is to carry the brain around.

– Thomas A. Edison

5.1 Introduction

In this chapter, a new P300 Speller paradigm is evaluated from both a subjective and an objective point of view. The probabilistic classifier used in this paradigm can be updated based on new incoming information, using Bayes' rule. In the traditional classifier the decision is based on determining the row or column of interest and marking their intersection as the letter of interest. However, in the new paradigm, each letter has a probability of being the letter of interest, which is updated with each flash. This change of manner from row or column to letter gives the subjects the flexibility to tune the Brain-Computer Interface (BCI) with their own pace, i.e., spend more time on the letters which are harder for them to communicate and less on

the easier letter. Here, we describe the experiments designed to evaluate the subjects' preferences and comfort with the new paradigm compared with the old one. As can be seen in the result section, the new improved paradigm is ranked higher from both a subjective and an objective point of view.

5.2 Brain-Computer Interface (BCI)

Millions of people suffer from sever neuro-muscular disorders and disabilities such as amyotrophic lateral sclerosis (ALS), brainstem stroke, etc. Many of them cannot communicate with others through the usual neuromuscular pathways and must rely instead on alternative means of communication that use the remaining muscle function, such as eye-gaze shifting, EMG activity or respiration. Some of them which are severely affected may even lose all voluntary muscle control, including eye movements and respiration, and may be completely locked-in to their bodies, unable to communicate in any kind of way. Moreover, the keyboard and mouse provide the users with reliable, but unnatural forms of input, being primitive transducer of muscular movement. If they are replaced with BCIs, the users are capable of direct communication with the computer [4, 33].

BCI research tries to design new communication paradigms and systems which translate human intentions, reflected in brain signals, to control signals. This concept is depicted in Figure 5.1. According to the definition put forth at the first international meeting for BCI technology in 1999, a BCI was defined as "a communication system in which messages or commands that an individual sends to the external world do not pass through the brain's normal output pathways of peripheral nerves and muscles"[62, 93].

Thus, BCIs rely on brain activity to generate user-intended action. An ultimate goal of BCI research is to allow patients with severe motor disabilities to send commands to computers, only by means of brain activity. However, recently, the human-computer interaction community developed a great interest towards the application of BCI for larger groups of users that are not dependent on BCIs as their only means of communication, e.g. healthy subjects. This development holds great potential for

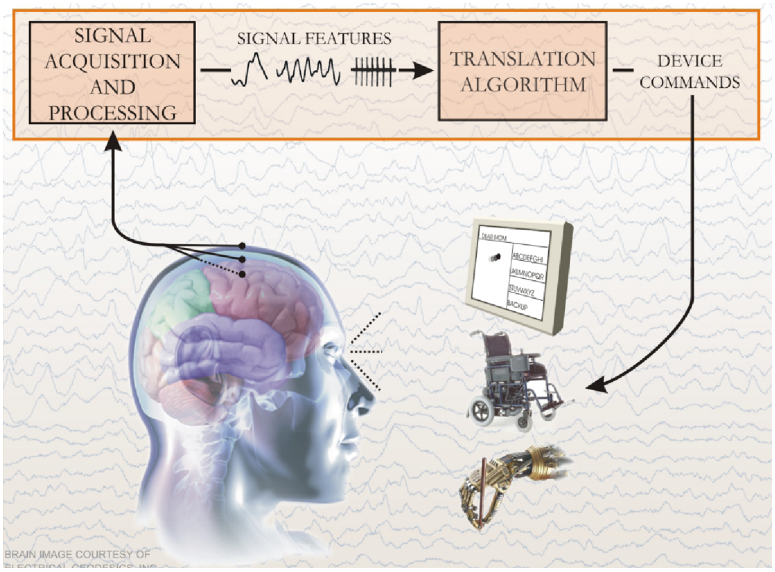

Figure 5.1: The schematic of a general BCI system: The neurophysiological signal is recorded from the user and the relevant features which are informative about user intent or state are extracted. Then, they are translated into the control parameters that are used by the application to respond to the user's state or intent. Taken from [33].

the further development of BCI devices, algorithms, and approaches, which is also necessary for its advancement for patients [93].

5.3 P300 Speller

As mentioned in Section 1.2.2, P300 potential is a positive deflection in the EEG signal that occurs approximately 300 ms after stimulus onset and is typically recorded via centro-parietal electrodes. P300 potential is evoked by subject's attention towards rare stimuli in a random series of stimulus events also called oddball paradigm, which is depicted in Figure 5.2. Based on this phenomenon, the P300 speller (see Figure 5.3) was developed, which is a BCI paradigm that allows the selection of characters on a virtual keyboard and thus allows communication via brain only. In the P300 speller,

the characters are flashed in groups and the users' task is to focus their attention on the character they want to communicate (character of interest). Therefore, the flashes of the group containing the character of interest present the stimuli and are relatively rare, consequently, they evoke a P300 potential. The task of the paradigm is to identify the groups of interest and find their intersection as the character of interest.

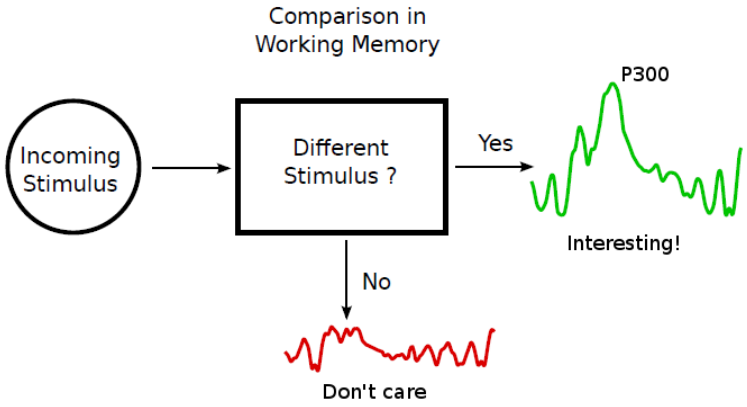

Figure 5.2: The fundamentals of the oddball paradigm: the P300 potential is evoked by the subject's attention towards a rare stimuli in a random series of stimulus events. Taken from [33].

5.3.1 Row-column paradigm (RCP)

In the traditional approach or RCP, the items are displayed in matrix form and are flashed in rows and columns of that matrix successively, as shown in Figure 5.3. The algorithm tries to detect the item of interest the single item belonging to the interaction of the row and the column which showed the largest P300-like response. Since the amplitude of ERPs such as P300 in single trial EEGs are small (see Section 1.2), it is often necessary to repeat stimulations in order to obtain averaged signals that can be classified correctly. A *repetition* is then defined by flashing of all the rows and columns of the matrix once. A *trial* to spell a specific letter is formed of many

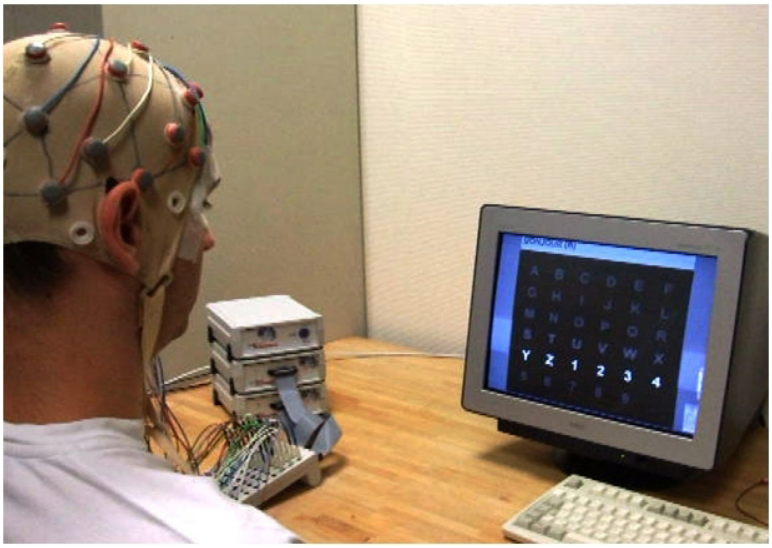

Figure 5.3: The P300 Speller is a BCI paradigm that allows the selection of characters on a virtual keyboard and thus communication via brain only. Taken from http://www.inserm.fr.

repetitions (traditionally between 3 and 15). Thus, a trial is defined as the succession of stimulations and observations that are needed to select one item (see Figure 5.4)

5.3.2 Improving the RCP paradigm - State of the art

There have been many different attempts to improve the efficiency of communication in RPC:

- different stimulus features such as inter-stimulus interval (ISI) also known as stimulus onset asynchrony (SOA) [94, 95, 96, 97, 98]
- different signal processing approaches [99, 100, 101, 102]
- different numbers of repetitions in a trial [98, 100, 102, 103]
- various physical appearances such as background/foreground colors [104, 105], matrix size [96, 97] or item size and distance between the items [104].

- use of motion in rows and columns [106, 107]
- random flash of a single item in the matrix also known as "single cell paradigm" (SCP) [108, 109]
- replacing the row or column of items with famous face images at the flash time to produce a larger P300 potential [110].
- multi-flash of the row or columns in a repetition to reduce the final number of flashes in a trial [111]
- flashing in groups of non-adjacent items instead of rows and columns [103, 112].

An interesting improvement called the "splotch" stimulus presentation was reported in [112]. In this flashing schema, items are flashed in pre-defined groups instead of rows and columns. The splotch flashing schema was developed to prevent adjacency-distraction errors (i.e. attention and response to stimuli in adjacent row or column) and double-flash errors (i.e. one item flashed twice in a row consecutively causing no or overlapping P300 responses) which happens in the RPC [94, 113]. Authors in [103] used this method to develop their visual paradigm, also referred to as the "checkerboard paradigm" (CBP). CBP includes a 8×9 matrix of items virtually superimposed on a checkerboard. Items in black and white boxes make two virtual 6×6 matrices. Before each trial, the items in each smaller matrix is randomized and each row and column in the virtual matrices is flashed similar to RCP. Thus the subjects see 6 random boxes flashing at a time. The study reported an increase of 15% in performance and more satisfaction from the subjects' feedback.

5.4 Method

The main aim of this experiment was to compare two modes against each other. The *default mode* which tried to simulate the traditional RCP paradigm and the *advanced mode* which included the improved paradigm. The features of both paradigms and the improvements done are mentioned bellow.

5.4.1 The flashing schema

Default Mode

In the default mode the items of the matrix were flashed in rows and columns randomly to simulate the traditional RCP paradigm.

Advance Mode

The flashing of the items was similar to what reported in [103] and [112], i.e., the splotch stimulus presentation. In each repetition 12 pre-defined *groups* flashed. Each group consists of 6 non-adjacent items. Each item belongs to two groups only and these two groups have only this particular item in common (see Figure 5.4). To avoid double-flashing error, the groups were divided into two sets; one resembling the six raw of RCP and another resembling the six columns. The machine was forced to flash all the six groups of the first set before starting to flash the groups of second set to minimize the risk of the subject missing one flash of the item. Furthermore, the order in which the 12 groups flashed in one repetition was kept the same in the trial regarding the spelling of one item, also referred to as static random stimulation (SRS). The mode is called "random" since items seem to have been grouped in a random manner.

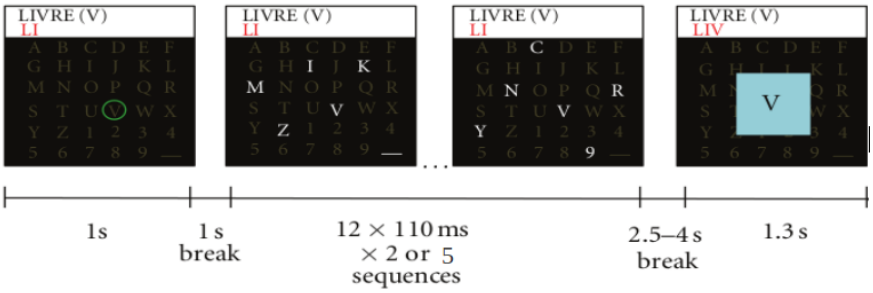

Figure 5.4: The target letter is indicated by a green circle, for 1 second. Letters are flashed by groups of 6 letters. After a delay, the letter chosen by the P300 classifier is displayed for 1.3 seconds.

5.4.2 Feature extraction

Feature extraction was same for both modes and based on the following principle. The raw data was down-sampled to 100 Hz and then bandpass filtered between 1 and 20 Hz. Extracting features was done by applying a linear spatial filtering approach named xDAWN [114] which results in orthogonal linear spatial filters learned from the subject's training data. Using these filters reduces the dimension of the data and maximizes the distinction between two class of targets where P300 potential is evoked and non-target. Five spatial filters was used to be in line with [98, 115] and were applied to time intervals of 0 to 600 ms after flash onset. The evoked potentials in this interval include P300 and early visual response [98, 116].

5.4.3 Classification

Default Mode

In the default mode, the number of repetition in each trial were fixed. The two-class Naive Bayes classifier was applied. The training data was used to learn the spatial filters and classifier parameters. Then, the data in each trial was averaged and, using the classifier, the row and column containing the item of interest was determined. Their intersection was the BCI decision and was showed to the subject as feedback.

Advance Mode: Adaptive accuracy-based algorithm stopping at the flash level

For classification, two multivariate-Gaussian models were used in the classifier (one Gaussian distribution per class, i.e., target and non-target). The classifiers parameters (the mean and variance of each Gaussian) were learned from the training data. For simplicity, it was assumed that there is a conditional independence between features over time and space [98, 115]. This assumption provides a fast update of the BCI's posterior belief with each new observation.

Using Markovian approach, the posterior probability associated with each item of the matrix was computed by applying Bayes rule after each new flash and considering

the posterior belief as the prior for the next observation. That is, at the time t,

$$P(L|Y_t,\theta,g_t) \propto P(Y_t|\theta,L,g_t)\cdot P(\theta,L,g_t) \tag{5.1}$$

where Y_t indicates the new vector of observed features, $\theta = \{\mu_1,\mu_0,\Sigma_1,\Sigma_0\}$ refers to all the classifier parameters which are the means and variances of the two Gaussian distributions, index 1 refering to the target and index 0 to the non-target class, respectively, L is a N-long vector full of zeros with 1 at the target position and g_t is a N-long vector full of zeros with 1 at each location corresponding to the six items that where flashed at time t. $N = 36$ denotes the number of items in the matrix. Since θ is learned from the training session and g_t is known, the Equation 5.1 simplifies to:

$$P(L|Y_t,\theta,g_t) \propto P(Y_t|\theta,L,g_t)\cdot P_t(L) \tag{5.2}$$

The prior distribution over L is indexed by time. This reflects the sequential nature of the observation process and the fact that the prosterior belief at time $t-1$ becomes the prior belief at time t, that is:

$$P_t(L) = P(L|Y_{t-1},\theta,g_{t-1}) \tag{5.3}$$

At the given time t, this prior probability follows a multinomial distribution:

$$P_t(L) = \prod_{k=1}^{N} \lambda_{t-1,k}^{L_k} \tag{5.4}$$

Where $L_k$is a N-long vector full of zeros but one 1 at position k (assuming item k is the target), and $\lambda_{t-1,k}$ shows the posterior probability of item k being the target. The likelihood is given by the mixture model which is:

$$P(Y_t|\theta,L,g_t) = \prod [N(Y_t;\mu_1,\Sigma_1)]^{g_{t,k}\cdot L_k} . [N(Y_t;\mu_0,\Sigma_0)]^{g_{t,k}\cdot(1-L_k)} \tag{5.5}$$

As a result, the posterior distribution will also correspond to a multinomial distribution (so-called conjugate priors) whose update boils down to applying the following rules for each item, under the normalization constraint in equation 5.6:

$$log(\lambda_{t,k}) = log(\lambda_{t-1,k}) + \frac{1}{2}(Y_t - \mu_0)^T . \overset{-1}{\underset{0}{\sum}}(Y_t - \mu_0) - \frac{1}{2}(Y_t - \mu_1)^T . \overset{-1}{\underset{1}{\sum}}(Y_t - \mu_1) + \frac{1}{2} log(\frac{|\Sigma_0|}{|\Sigma_1|}) + cste \quad (5.6)$$

if item k has been flashed at time t (where $cste$ denotes the constant). Otherwise:

$$log(\lambda_{t,k}) = log(\lambda_{t-1,k}) \quad (5.7)$$

Finally, based on the above updates, the adaptive decision relies on a natural information theoretic measure of uncertainty, namely the Shannon's entropy of the posterior distribution, meaning at the time t:

$$H_t = -\sum_{k=1}^{N} P_t(L_k) \cdot log(P_t(L_k)) = -\sum_{k=1}^{N} \lambda_{t,k} \cdot log(\lambda_{t,k}) \quad (5.8)$$

Entropy is always positive but decreases as information is accumulated or uncertainty decreases. In other words, it gets closer to zero as the posterior distribution gets closer to an ideal distribution with full probability weight associated with a single item, meaning that the BCI is sure about which item is the target. In practice, the threshold of a specific subject is learned from the training set. In the test phase, a decision is made, as soon as the entropy falls below the threshold. If the threshold is never reached, a decision is made after a ten repetitions. Note that, the higher the threshold, the lower the accuracy required to make the decision and the faster but more risky the spelling.

5.5 Data Acquisition

Twenty-one healthy subjects (5 male, 16 female, age range: 18-36 years; mean age: 22.71 ± 4.9 years) volunteered in conducting the experiment. All subjects signed an informed consent approved by the local Ethical Committee and received monetary compensation for their participation. All subjects reported normal vision and had no previous experience with the P300-Speller or with any other BCI paradigm.

The data acquisition consisted of four main steps:

1. Preparation and instructions: The subjects read about the experiment. Then, they were asked to sign the consent forms and answer some questions about their health. Later, the subjects were informed of the experiment tasks during the fixation of electrode net on their head and other device configurations.

2. Training sessions 1 and 2: In the first training session participants were asked to spell 30 letters, one after the other. No feedback were provided. Fifteen items were flashed with the advanced mode and another fifteen items were flashed using the default mode. These data were used to tune each mode with the subjects' EEG. In the second session the subjects were asked to spell 6 five-character words in advanced mode with the feedback. In the short break after the training session, the BCI parameters for subsequent online feature extraction and classification were updated with each individual's results.

3. Test sessions 1 to 4: After training, the subjects went through four true spelling sessions, lasting approximately 12 minutes each. Every session was made of 5 sentences. Subjects received feedback after each character. The delay between two sequential character was 4.7 seconds Within a session, letters were spelled using the same number of repetitions (either 2 or 5) and the same stimulation mode (default or advanced).

4. Debrief: After recording, participants were asked to fill-in a questionnaire about the test sessions. Rating between 1 and 10, they answered to questions about their perception of task difficulty and of the performance of the machine. The results of debriefing is summarized in Table 5.3.

5.5.1 EEG Hardware and Software Setup

EEG was recorded using the Acticap system with Ag/AgCl electrodes (Brain Products, Germany) using 12 electrodes. The Electrodes were placed at F_z, C_z, P_7, P_3, P_z, P_4, P_8, PO_{10}, PO_9, O_1, O_2 and O_z in the 10-20 Conventional System. All electrodes were referenced to an electrode placed on the nose and their impedences were kept

below 10 $k\Omega$. Analog signals were amplified by the BrainAmp amplifier, powered with a rechargeable battery (PowerPack), digitized at a rate of 1000 Hz and filtered through a 0.1-150 Hz bandpass using Brain Vision Recorder software (Brain Products, Germany).

Stimulation was handled by a C++/SDL software on a dedicated computer. EEG data was recorded according to the procedure implemented in Openvibe.

5.5.2 Experimental Paradigm Simulation

The 6×6 matrix used in the current study was made of the 26 letters (A-Z), 9 digits (1-9) and one symbol (_). The angular dimension of the matrix was $8.67°H \times 11.33°W$. Each symbol subtended $0.48°H \times 0.48°W$ of visual angle and the distance between each character was $1.24°H \times 1.62°W$. Moreover, symbols were larger (font size + 5) while intensified and subtended $0.62°H \times 0.62°W$ of visual angle, to yield larger P300 amplitudes [117].

In the training session, the number of repetitions was set to six, while the test sessions had four different conditions: a fast, more error-prone mode, made of short (2-repetition long) trials and a slow, less risky mode made of five-repetition long trials, in each mode letters were flashed using either default or advanced paradigm flashing schema (RCP or SRS). Flash duration was set to 60 ms and stimulus onset asynchrony (SOA) to 110 ms.

The place of each character to be spelled was shown with a green circle at the beginning of the trial in training and test sessions. Then, throughout the trial, the character of interest was shown in brackets at the top of the screen.

5.6 Analysis and Results

5.6.1 Objective Study 1: Accuracy and Bit rate

Table 5.1 and Table 5.2 show the results of the experiments in the fast and slow mode for both paradigms. Spelling accuracy and transfer rates (bits/minute) with and without the interval between selections for each participant is described in these tables for

each subjects. Spelling accuracy correspond to number of items that where correctly spelled in one condition divided by the number items in one mode. It should be noted that the sentences in one mode (slow with 5 repetitions or fast with 2 repetitions) were the same for both paradigms. Information Transfer Rate (ITR) or bit rate is common but imperfect measure of BCI performance. Transfer rate in bits/minute, was calculated from B, the average number of bits transmitted per decision [118, 119]:

$$B = log_2(M) + (1-p).log_2(\frac{1-p}{M-1}) \tag{5.9}$$

where M is the number of classes (which is 36 since a 6×6 matrix of items was used) and p is the accuracy of the P300 speller achieved by a specific subject. Then, the B was used to calculate the transfer rates which is reported in bits per minute and combines the spelling accuracy and the number of flashes per letter;

$$ITR = \frac{B}{T} \tag{5.10}$$

where T is the average duration of a letter decision in minutes. Many studies have ignored the inter-selection time when reporting transfer rates and thus used (5.10), while others report both transfer rates, with (in this case the inter-selection time is added to denominator in (5.10)) and without inter-selection time. For an easy comparison of this work with all studies, both types of transfer rates was reported in Table 5.1 and Table 5.2. Thus,

Moreover, to assess the statistical significance of differences in performance, the spelling accuracies, averaged numbers of flashes and transfer rates were compared with Wilcoxon tests (to compare paired-groups of proportions for real data) using the Rcmdr software which will be described below.

In the slow or safe mode with SRS flashing schema, the online spelling accuracy was $89.58\% \pm 9.74(SD)$, for an average of $63.66 \pm 7.91(SD)$ flashes, which corresponds to 21.76 bits/min. In the safe mode with default flashing schema (RCP), accuracy was $78.9\% \pm 13.73(SD)$, which corresponds to 18.18 bits/minute. In the risky mode with advanced condition (SRS), the spelling accuracy was $58.51\% \pm 19.01(SD)$, for an average of $26.34 \pm 2.02(SD)$ flashes, which corresponds to 17.06

bits/minute. In the risky mode with default condition (RCP) the spelling accuracy was $57.37\% \pm 15.38(SD)$, which corresponds to 16.91 bits/minute (Figure 5.5).

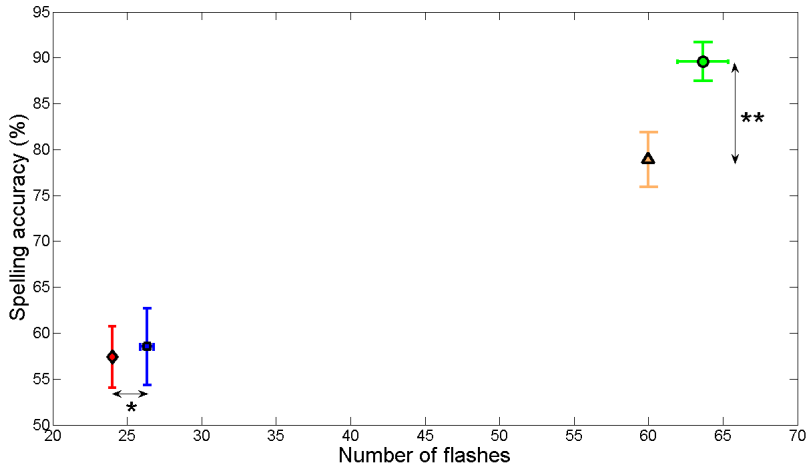

Figure 5.5: Online spelling accuracy as a function of the averaged number of flashes for each four condition: fast SRS (blue square), fast RCP (red diamond), slow SRS (green circle) and slow RCP (orange triangle). Error bars indicate the standard error of the mean. p-value: * p<0.001 , ** p<0.001.

Wilcoxon test reveals that the transfer rates were higher for the advanced mode than for the default mode, in five repetitions, with and without considering the time between selections (p-value < 0.01 and p-value < 0.01 respectively). Even though the number of flashes was not much different between these two conditions (p-value = 0.07). It was higher on average in the advanced mode. However, in two repetitions, the superiority of the advanced mode cannot be inferred, as there is no difference between advanced and default mode in transfer rate without considering the time between selections (p-value = 0.37). Moreover, the transfer rate was slightly higher on average in the default mode. This happened because in 2 repetitions it was very hard to determine the letter of interest. Thus, for most subjects the algorithm needed more flashes to make a decision which is reflected in Table 5.1, meaning, the number of

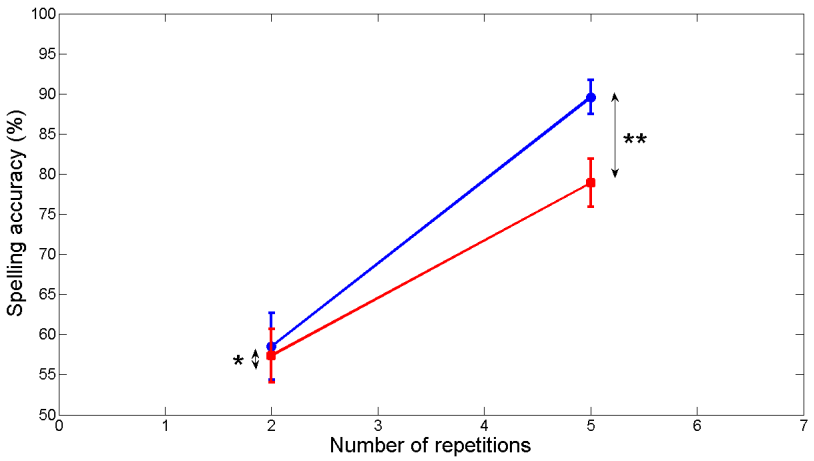

Figure 5.6: Spelling accuracy as a function of the number of repetitions (2 or 5), obtained with advanced (blue circle) and default (red square) paradigms, respectively. Error bars indicate the standard error of the mean. p-values: * p = 0.59; ** p < 0.001.

flashes in advanced mode (with SRS flashing schema) was higher (p-value < 0.001); 26.34 in average in advanced mode versus the fix number of 24 flashes in the default mode (with RCP flashing schema). The higher the number of flashes, the more time needed to determine the letter of interest and therefore the lower the transfer rate. Considering the time between selections, the data does not show any significant difference between default and advanced paradigm in fast mode (p-value = 0.92). It can also be seen that their average values were close to each other.

Figure 5.6 shows the online results of the experiment as a function of the number of repetitions, comparing the performance of the P300-Speller for the four conditions classified according to difficulty (2 or 5 repetitions) and paradigms (with RCP or SRS flashing schema). Performance are significantly better with 5 compared to 2 repetitions in advanced mode (p-value < 0.001) and default mode (p-value < 0.001). Post-hoc analysis confirmed that the effect of improved stimulation was significant with 5 repetitions (p-value <0.001) but not much different in case of only 2 repetitions (p-value = 0.59).

Table 5.1: Accuracy and transfer rates for the fast mode (Number of repetition: 2)

		Advance Paradigm (AM2)				**Default Paradigm (DM2)**		
Subject Code	Number of Letters	Accuracy (%)	Mean Flashes	Transfer rates excluding the time between selections	Transfer rates including the time between selections	Accuracy (%)	Transfer rates excluding the time between selections	Transfer rates including the time between selections
1	87	71.26	26.41	58.46	22.33	82.76	82.33	29.61
2	90	68.89	32.33	45.21	19.47	50	36.48	13.12
3	78	66.67	24.6	56.35	20.59	67.95	59.57	21.42
4	83	83.13	26.02	76.5	28.96	85.54	87.1	31.33
5	91	28.57	25.35	13.84	5.15	45.05	30.88	11.11
6	76	46.05	26.39	29.08	11.11	56.58	44.44	15.98
7	83	38.55	24.88	23.16	8.52	40.96	26.49	9.53
8	80	75	25.84	64.94	24.47	61.25	50.44	18.14
9	87	44.83	25.05	29.35	10.85	42.53	28.14	10.12
10	86	73.26	25.74	62.72	23.58	65.12	55.63	20.01
11	76	93.42	28.82	84.85	34.17	82.89	82.56	29.69
12	88	43.18	24.35	28.42	10.32	61.36	50.59	18.19
13	68	61.76	25.72	47.7	17.92	50	36.48	13.12
14	72	65.28	27.06	49.54	19.21	59.72	48.44	17.42
15	77	40.26	26.77	23.09	8.89	50.65	37.24	13.4
16	76	68.42	24.91	58.04	21.37	56.58	44.44	15.98
17	75	74.67	29.64	56.2	23.02	56	43.71	15.72
18	75	70.67	26.89	56.63	21.88	65.33	55.93	20.11
19	69	31.88	27.86	15.14	5.97	31.88	17.57	6.32
20	79	25.32	23.39	12.19	4.31	27.85	13.99	5.03
21	85	57.65	25.05	43.87	16.21	64.71	55.07	19.81
Means	80.05	**58.51**	**26.34**	44.54	**17.06**	57.37	**47.02**	16.91
SD	6.72	19.01	2.02	20.89	8.21	15.39	19.82	7.13

Table 5.2: Accuracy and transfer rates for the slow mode (Number of repetition: 5)

		Advance Paradigm (AM5)				**Default Paradigm (DM5)**		
Subject Code	Number of Letters	Accuracy (%)	Mean Flashes	Transfer rates excluding the time between selections	Transfer rates including the time between selections	Accuracy (%)	Transfer rates excluding the time between selections	Transfer rates including the time between selections
1	81	96.3	61.01	42.48	24.98	88.89	37.24	21.75
2	76	75	69.47	24.15	14.96	48.68	13.98	8.17
3	89	83.15	81.29	24.5	16.06	84.27	33.96	19.83
4	84	100	53.08	53.12	29.43	92.86	40.29	23.53
5	79	77.22	53.71	32.77	18.25	73.42	27.01	15.78
6	91	95.6	67.97	37.59	23.08	75.82	28.47	16.63
7	86	86.05	72.64	29.07	18.3	67.44	23.54	13.75
8	88	97.73	66.66	40.07	24.42	70.45	25.26	14.75
9	82	90.24	61.4	37.38	22.04	75.61	28.34	16.55
10	80	98.75	63.34	43.14	25.76	86.25	35.34	20.64
11	88	100	51.95	54.28	29.78	97.73	44.52	26
12	81	81.48	57.89	33.25	19.13	83.95	33.74	19.71
13	83	92.77	62.49	38.62	22.94	63.86	21.56	12.6
14	79	98.73	75.77	36.04	23.05	94.94	42.01	24.54
15	74	90.54	67.92	34	20.87	81.08	31.82	18.58
16	79	91.14	61.49	38	22.42	74.68	27.77	16.22
17	75	100	63.04	44.73	26.66	96	42.93	25.08
18	77	81.82	56.03	34.59	19.63	79.22	30.61	17.88
19	80	82.5	65.91	29.82	18.09	83.75	33.6	19.63
20	72	65.28	52.82	25.38	14.03	48.61	13.95	8.15
21	66	96.97	71.03	37	23.1	89.39	37.62	21.97
Means	80.48	**89.58**	**63.66**	**36.67**	**21.76**	78.9	31.12	18.18
SD	6.09	9.74	7.91	8.11	4.34	13.73	8.53	4.98

5.6.2 Objective Study 2: Electrophysiology Analysis

The aim of this study was to investigate the EEG data in each condition to see if subjects showed more motivation in one condition in comparison with the other conditions during the given task. Here, more motivation refers to generation of better ERPs. Thus, the ERPs had to be extracted and compared in each condition. With this goal in mind, the data had to be cleaned of artifacts such as eye blinks first. Before the experiment, the subjects were asked to try to stay as calm and motionless as possible and not to blink during the flashing of items. This warning reduced the number of sunwanted artifacts such as blinking but did not eliminate them in total. Therefore, an artifact correction procedure based on ICA was applied to all subjects' recorded EEG data. The core of this procedure was the Matlab implemented function for ICA called *runica* which is a function for automated infomax ICA decomposition with several enhancements[120]. The artifact removal procedure followed the steps below:

- The raw EEG data of the subjects was fed to *runica* function. The output of the function is the ICA weight matrix and a data matrix which can be used to calculate the independent components, the mixing and unmixing matrices.

- Using the obtained information, the temporal and spatial distributions of all extracted component was plotted on two different graphs.

- The eye blink artifact has a specific temporal and spatial distribution that makes it distinguishable from other components. In the temporal domain, it has a repetitive spiky shape and in the spatial domain it has one main component in the front of the head. Considering these two features, the eye blink component was identified and removed. Figure 5.7 and Figure 5.8 show temporal and spatial distributions of extracted components for subject 1 in fast SRS condition, respectively. As can be seen, one of the main extracted components represents the eye blink artifact as is also pointed out in the figure caption.

- Using the mixing matrix, all other components were mixed together to form the cleaned EEG data.

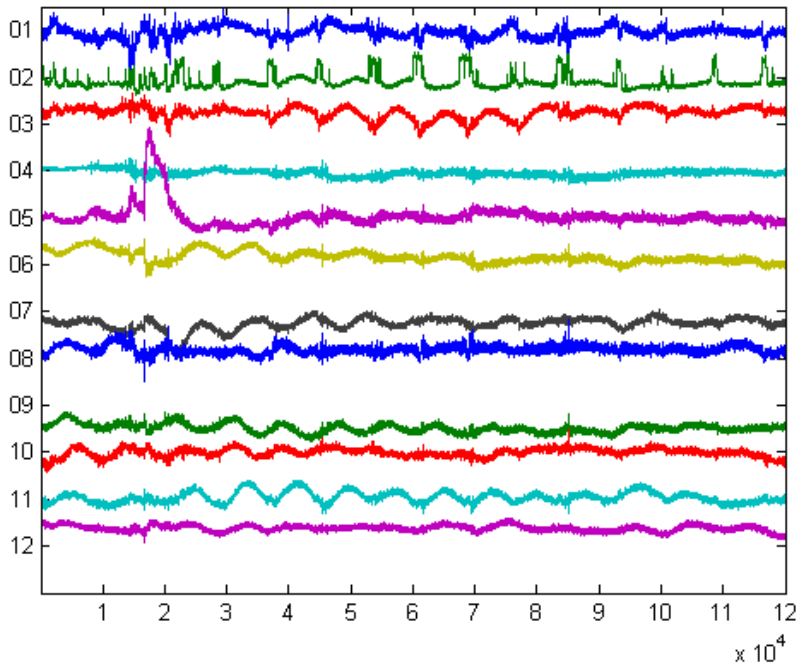

Figure 5.7: Temporal distribution of all extracted components using *runica*. The second component from the top of the figure shows typical repetitive spiky features seen in a eye blink artifact.

It should be noted that in this procedure the raw EEG data with a high sampling frequency of 1000 Hz was used since most ICA algorithms perform more accurately with higher frequency data.

Then the amplitudes of P300 and N1 was computed to see in which condition amplitude of P300 was increased among subjects. To do so, for each subject the following procedure was performed on their artifact-free EEG data:

- The EEG data was segmented from -200 ms to 1000 ms (zero corresponds to flash onset).
- The segments were divided into two groups of target and non-target, depending

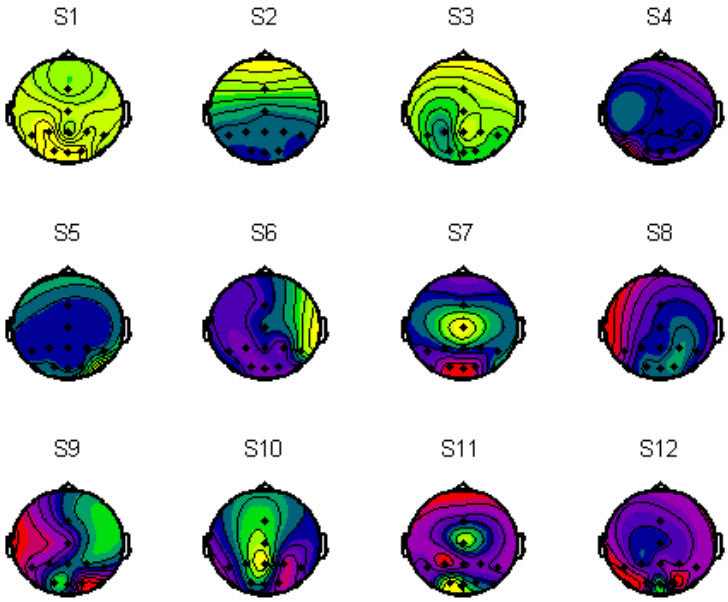

Figure 5.8: Spatial distribution of all extracted components using *runica*. The second component in the figure, marked by *S2*, has the typical spatial signature of an eye blink artifact.

whether or no not the flashed items contained the letter of interest.

- The segments were averaged for each groups for one subject.
- The averaged segments were low-pass filtered with cutoff frequency of 20 Hz.
- Baseline correction were performed for each averaged segments by subtracting the average of before flash onset data (from -200 ms to 0 ms) from the filtered data (-200 ms to 1000 ms).
- The difference between target trials and non-target trials were calculated.

- One channel, P_7, was selected to be in line with [118]. Other channels, such as C_z, P_8, F_z or P_z failed to produce better results.

- The average amplitude and latency of P300 and N1 (N1 or N100 is a negative ERP with short latency which represents the brain response to a rapid visual stimulus [3]) was determined for each subject. P300 corresponds to the maximum value in interval of 250 ms to 500 ms and N1 corresponds to the minimum value in the interval 150 ms to 270 ms.

Then to form the grand average for each condition, the baseline corrected averaged EEGs of all 21 subjects in one condition were averaged again. Thus, at the end, for each condition two grand averages corresponding to target flash segments and non-target flash segments were computed and their difference was also calculated and plotted. Moreover, the grand average of latency and amplitude of P300 and N1 was determined. The topographies of the scalp at the latencies of the peaks of N1 and P300 for each condition were also computed. Figure 5.9 and Figure 5.10 show the results of the electrophysiological study for advanced fast condition (AM2). In the top plot of Figure 5.9, the grand average of the ERPs with their standard deviation (in the interval -200 to 1000 ms with zero corresponding to flash onset on channel P_7) are shown for the correct trials with a black line and for the incorrect trials with a red line. The standard deviation is shown in the form of a halo covering the solid lines. In the bottom plot, N1 and P300 are marked and their amplitudes and latencies are mentioned. For those latencies, the topographies of the head is plotted in Figure 5.10. In this figure, the average distribution of currents on scalp can be seen for the correct (top), incorrect trials (bottom) and their difference, at the peak latency of the P300 (446.19 ms ±53.40 (SD)) and N1 (222.57 ms ±25.23 (SD)).

Figure 5.11 and Figure 5.12 show the results of the electrophysiological study for the default fast condition (DM2) following the same description and notion. In the Figure 5.12, topographies are shown at the peak latency of the P300 (448.81 ms ±48.42 (SD)) and N1 (228 ms ±18.97 (SD)) for this mode. Here, the average amplitude of P300 was 0.99 ±0.82 (SD). The average amplitude of N1 was -3.09 ±1.19 (SD).

Figure 5.13 and Figure 5.14 show the results of the electrophysiological study for the advanced slow condition (AM5). In the Figure 5.14, topographies are shown at the peak latency of the P300 (435.81 ±63.76 (SD)) and N1 (217.33 ±22.49 (SD)) for this mode. Here, the average amplitude of P300 was 0.76 ±0.54 (SD). The average amplitude of N1 was -2.07 ±0.97 (SD).

Figure 5.15 and Figure 5.16 show the results of the electrophysiological study for the default slow condition (DM2). In the Figure 5.16, topographies are shown at the peak latency of the P300 (460.95 ±48.32 (SD)) and N1 (240.81 ±21.61 (SD)) for this mode. Here, the average amplitude of P300 was 0.59 ±0.68 (SD). The average amplitude of N1 was -2.76 ±1.46 (SD).

There is a strong relation between the amplitude of N1 and the spelling performance of each subject (p-value < 0.05) in each condition. However, with the analysis described no relation between amplitude of P300 and spelling performance were found. Using the results obtained, there is no evident difference on the EEG signals with respect to different modes (default mode vs. advanced mode). Even though better results are obtained regarding the spelling accuracy and transfer rates in advanced mode (see Section 5.6.1), unfortunately, applying the analysis above this improvement can not be explained from point of view of the changes in ERPs and EEG signals.

5.6.3 Subjective Study 1: Subjects' Evaluation forms

Questions and average ratings are reported in Table 5.3. In general, participants were highly motivated in all four conditions: they scored their motivation on a 1-to-10 scale at least $7.71 \pm 2.19(SD)$, being mostly motivate in slow advanced condition (AM5), $8.33 \pm 1.53(SD)$. Moreover, their answers towards other questions are also more in favor of slow advanced mode. The subjects stated that this mode could be better controlled, was less difficult and less boring. In addition, in slow advanced mode, they had stronger feeling that the number of flashes was directly related to their level of concentration and performance.

Regarding individual preferences:

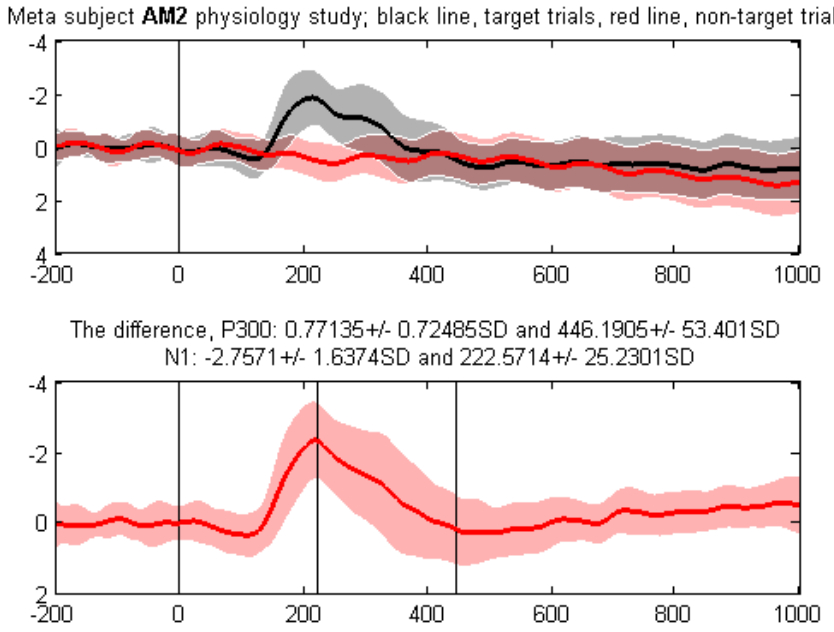

Figure 5.9: Top: grand average and standard deviation of event-related potentials (-200 ms to 1000 ms, channel P7) in advanced fast condition (AM2) associated with responses to target flashes (black line) and responses to non-target flashes (red line). Bottom: The difference between the two grand averages; the second vertical line from left shows the N1 latency and the third one corresponds to the latency of P300. Zero time corresponds to flash onset.

- 61% of the subjects preferred the safe dynamic mode (slow advanced condition (AM5)) because it required less concentration and was more accurate.
- 9.5% of the subjects preferred the risky dynamic mode (fast advanced condition (AM2)) and 14.2% preferred the risky fixed mode (fast default condition (DM2)) as they were faster and, thus, more challenging.
- 14.2% of the subjects preferred the safe fixed mode (slow default condition

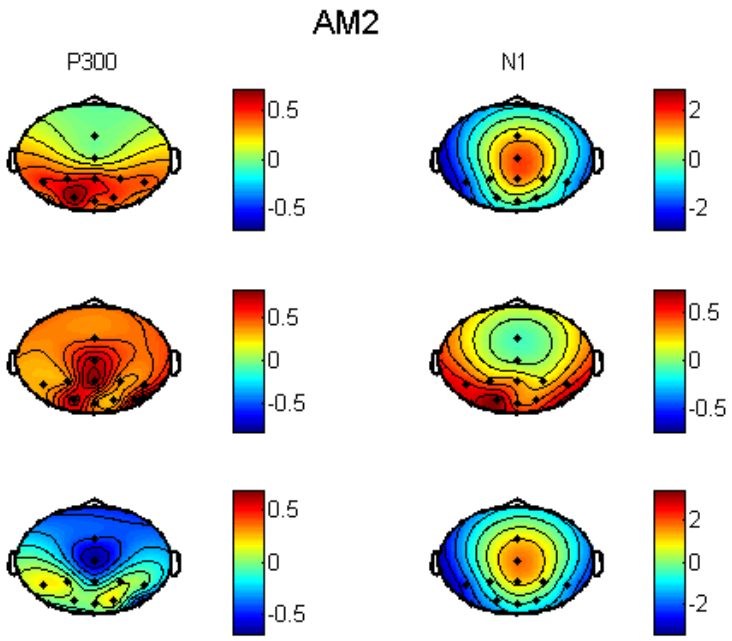

Figure 5.10: Topographies in advanced fast condition (AM2) for target (top), non-target (middle) and their difference corresponding to the latencies of the peaks of the N1 and P300.

(DM5)) because the number of flashes is known and the machine gives the impression of being more reliable.

Interestingly, 66.7% of the participants preferred the condition in which they obtained the highest accuracy.

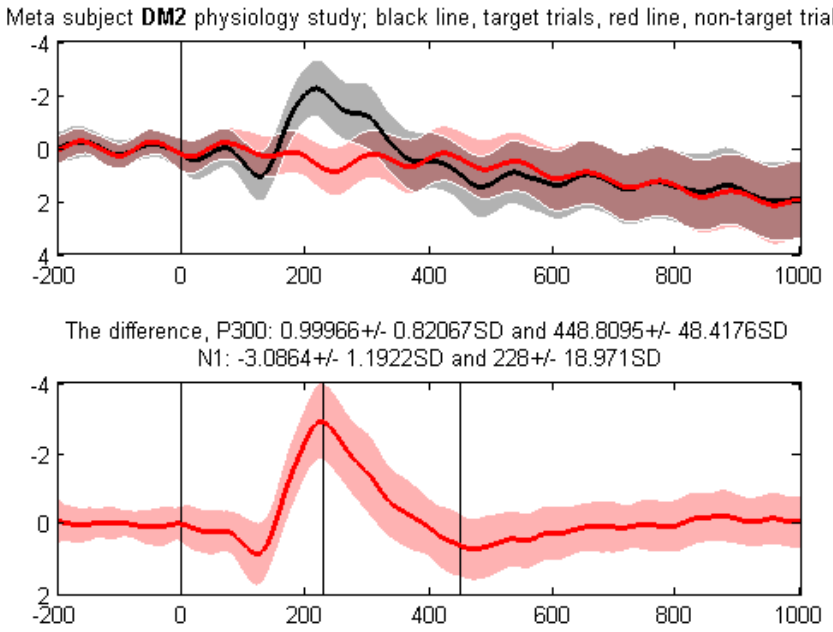

Figure 5.11: Top: grand average and standard deviation of event-related potentials (-200 ms to 1000 ms, channel P7) in default fast condition (DM2) associated with responses to target flashes (black line) and responses to non-target flashes (red line). Bottom: The difference between the two grand averages; the second vertical line from left shows the N1 latency and the third one corresponds to the latency of P300. Zero time corresponds to flash onset.

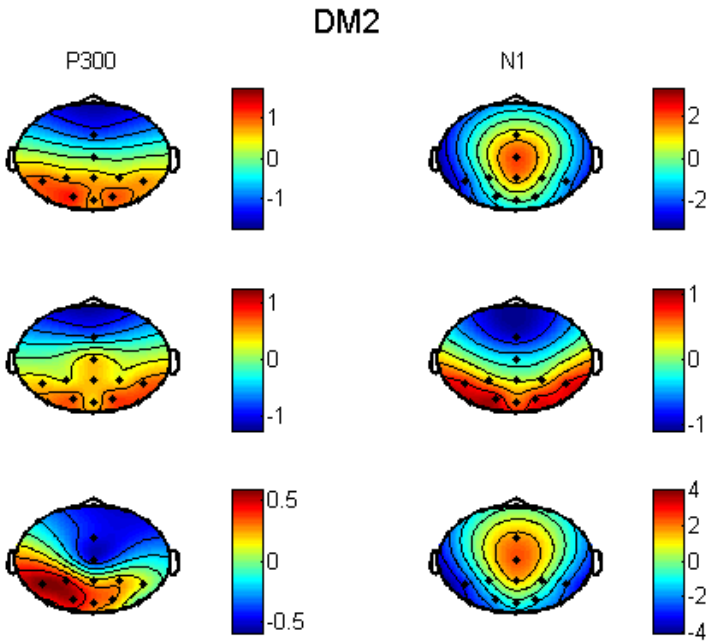

Figure 5.12: Topographies in default fast condition (DM2) for target (top), non-target (middle) and their difference corresponding to the latencies of the peaks of the N1 and P300.

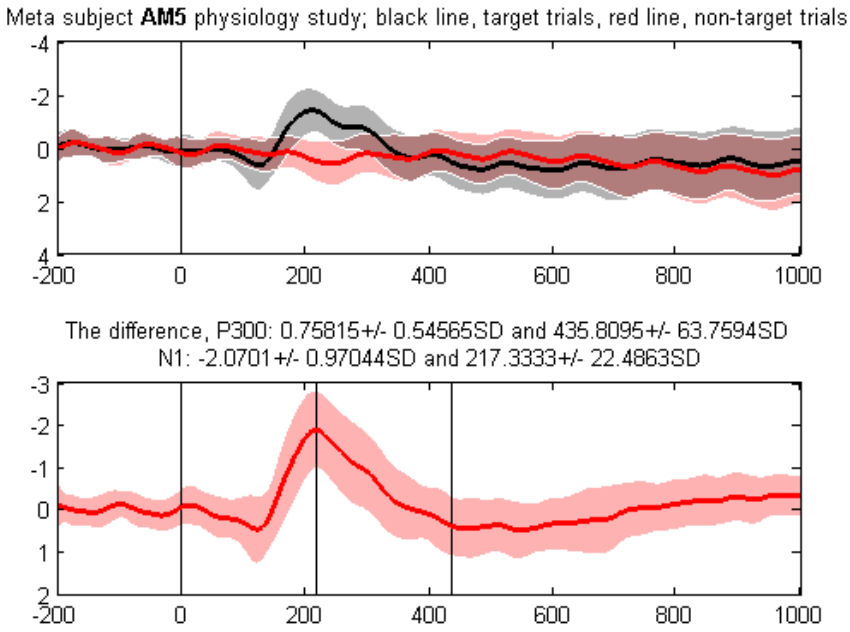

Figure 5.13: Top: grand average and standard deviation of event-related potentials (-200 ms to 1000 ms, channel P7) in advanced slow condition (AM5) associated with responses to target flashes (black line) and responses to non-target flashes (red line). Bottom: The difference between the two grand averages; the second vertical line from left shows the N1 latency and the third one corresponds to the latency of P300. Zero time corresponds to flash onset.

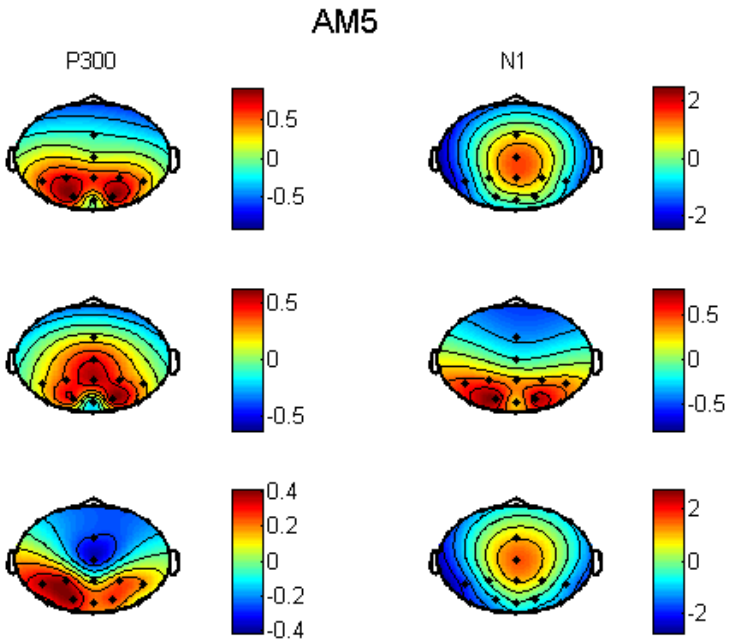

Figure 5.14: Topographies in advanced slow condition (AM2) for target (top), non-target (middle) and their difference corresponding to the latencies of the peaks of the N1 and P300.

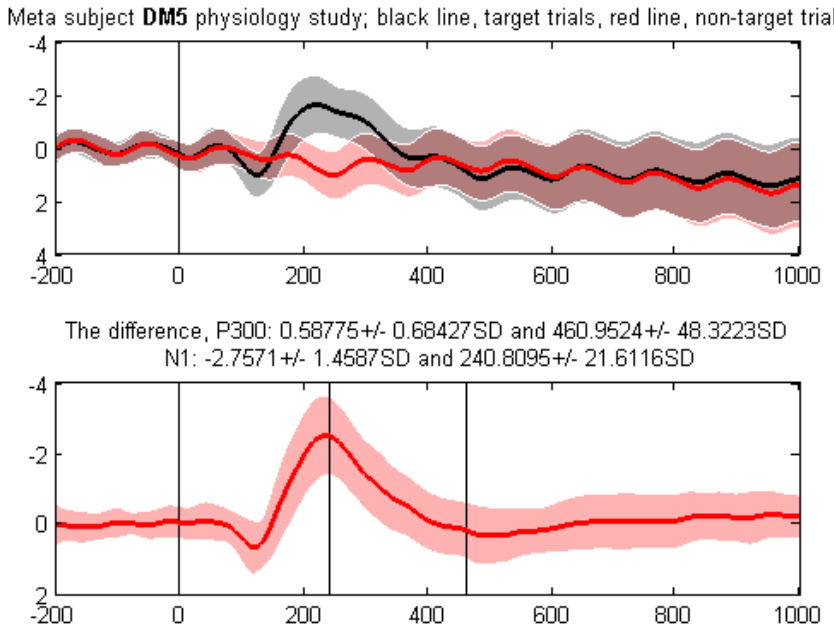

Figure 5.15: Top: grand average and standard deviation of event-related potentials (-200 ms to 1000 ms, channel P7) in default slow condition (DM2) associated with responses to target flashes (black line) and responses to non-target flashes (red line). Bottom: The difference between the two grand averages; the second vertical line from left shows the N1 latency and the third one corresponds to the latency of P300. Zero time corresponds to flash onset.

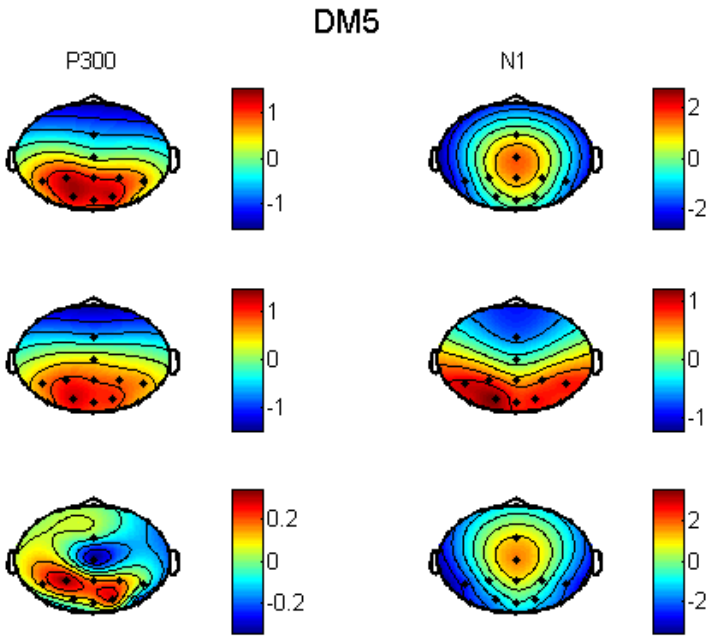

Figure 5.16: Topographies in default slow condition (DM5) for target (top), non-target (middle) and their difference corresponding to the latencies of the peaks of the N1 and P300.

Table 5.3: Questionnaire and averaged ratings over the whole group (N = 21). Ratings ranged between 1 (most negative response) and 10 (most positive response).

Questions	**AM2**	**DM2**	**AM5**	**DM5**
Q1. How well did you control the machine?	4.52 ± 2.16	4.52 ± 2.84	**7.62**$\pm$1.86	6.90 ± 2.53
Q2. Did the machine perform well?	5.43 ± 2.78	5.33 ± 2.65	**7.95**$\pm$1.99	7.38 ± 1.8
Q3. How difficult did you found the mode?	6.62 ± 2.67	7.05 ± 2.92	**4.23**$\pm$2.64	5 ± 3.05
Q4. Was the task boring?	6.52 ± 2.8	6.38 ± 2.69	**4.71**$\pm$2.49	5.05 ± 2.52
Q5. Was the task motivating?	7.95 ± 2.42	7.95 ± 1.99	**8.33**$\pm$1.53	7.71 ± 2.19
Q6. Just before the feedback, did you sense it was going to be a mistake?	4.95 ± 2.58	**6.19**$\pm$2.65	4.43 ± 2.98	5.28 ± 2.92
Q7. How much did errors upset you?	**6.81**$\pm$2.93	**6.81**$\pm$2.73	6.19 ± 3.04	6.19 ± 3.19
Q8. Did you sense that the number of flashes was related to your level of concentration?	3.95 ± 3.01	3.05 ± 2.48	**5.43**$\pm$3.8	3.95 ± 3.37

5.7 Discussion

In the current study, the performance of the new paradigm for P300 speller, also referred to as the advanced paradigm, was compared with the default row/column paradigm. To have better understanding of the effect of each paradigm (advanced vs. default), the following questions where kept in mind during the processing of data:

- Which paradigm creates a better performance, with respect to spelling accuracy and transfer rates?
- Which paradigm results in improved generation of which ERPs? How can the better result in one paradigm be rationalized with respect to ERPs and EEG signals?
- Which paradigm was more user-friendly, easier to control and comfortable from the subjects' point of view?

To answer each question, a study was designed and performed on the data of all subjects. The final results show that the performance is fairly improved in advanced paradigm specially with the higher number of repetitions depicted in Figure 5.6. The results of subjects' transfer rates and accuracy are both increased in the advanced paradigm even when the number of repetition is low.

Although the improvement is evident in terms of transfer rates and accuracy, the analysis of EEG signals did not indicate a clear difference in terms of ERPs. Further analysis or different approaches to the electrophysiological study towards extraction of ERPs might be needed in order to answer which ERPs were stronger in which paradigm and how the better performance of subjects in advanced paradigm can be rationalized with respect to their EEG signals.

Looking at the subjects' opinion reflected in their questionnaires, it is obvious that the subjects preferred the advanced paradigm with a higher number of repetitions, as this paradigm could be better controlled, was less difficult and boring and was felt related to their level of concentrations.

5.8 Summary

The main idea and priority in this chapter was to understand and work with a brain computer interfacing application in action. P300 speller is one of the oldest and best-defined BCIs that ease the communication between patients with others in form of writing. Different studies try to modify this paradigm and therefore improve the communication process by increasing the transfer rate or spelling accuracy. In this chapter one of the proposed ideas to improve the paradigm which includes the flashing schema and the classification algorithm was studies and compared with the default paradigm. The results of different tests conducted on the EEG data gathered with each paradigm were in favor of the newly proposed paradigm.

Conclusion

Pre-movement neuronal activity refers to the patterns by which neurons fire before a subject performs a movement. Through experiments with different animals including monkeys and also human subjects, it has been shown that several regions of the brain are active and involved in initiation and preparation of the movement.

Prior to any movement, a negative cortical potential called, Readiness Potential (RP), starts to develop as a part of movement planning and movement preparation. This potential and its features have been well documented by neuroscientists. Moreover, over the past decade, there has been a number of studies in EEG signal processing which used pre-movement or pre-imaginary EEG data to extract information about the movement yet to come for applications such as Brain Computer Interfacing. Although, in these studies, the RP has been evoked and its features have been used in single-trial analysis, none of these studies focuses on the extraction of this potential.

In the traditional methods, EEG data corresponding to movement preparation is averaged over a number of trials and the average RP is used to evaluate changes in the RP signal before or during movement. However, averaging results in a loss of information related to the inter-trial variability of RP. The inter-trial variability of RP can change in different circumstances, such as fatigue states. Therefore, there is an essential need to apply the single trial-based method for estimating RP. Detection and extraction of this potential can benefit researchers in clinical neurosciences in the rehabilitation of malfunctioning brains and those working on brain computer interfacing in the developments of a suitable mechanism to detect the intention of movement.

The first part of this study was devoted to a review of the features that characterize the pre-movements and pre-motor imageries (before imagining the movement) EEG data in humans from both Neuroscientists' and Engineers' points of view. The brain status before a voluntary movement was described and it was also discussed, how it has been used in practical applications such as BCIs. Usually, in BCI applications, the focus of the study is on the after-movement or motor imagery potentials. However, Chapter 2 shows that it is possible to develop BCIs based on the before-movement or motor imagery potentials such as the RP. Using the pre-movement or pre-motor imagery potentials, one can correctly predict the onset of the upcoming movement, its direction and even the limb that is engaged in the performance. This information can help in designing a more efficient rehabilitation tool as well as BCIs with a shorter response time which appear more natural to the users. The main aim of this chapter is to show that the pre-movements and pre-motor imageries interval, even in non-invasive EEG, has showed to have significant prediction potentials.

A considerable fraction of the study was devoted to introducting two algorithms for the extraction of RP in single trials of EEG data, described in Chapter 3 and Chapter 4. Both algorithms are based on the ICA approaches. One algorithm is based on the BSS technique and the other on the constraint BSE technique. To summarize, in BSS-based algorithms, first all the possible sources in the EEG single trial are extracted and then the one that is of interest is looked for. Constraint BSE-based algorithms perform differently, that is, by adding some constraint to the cost function, only the sources of interest are extracted and the other active potentials or noise are ignored from the very beginning. Although the main idea of developing these algorithms was *extraction* of RP in single trials of EEG in which RP is evoked, they both have been also tested for the concept of *detection* in Chapter 4. Both algorithm showed good results in extracting RP but in detecting the RP, especially considering the false positive rate, constraint BSE algorithm showed to be superior in comparison with BSS algorithm. The two algorithms were also compared in terms of time and true positive rate. Their extraction efficiency was compared on simulated EEG data with respect to subjective and objective evaluation meaning MSE and SNR. The extracted RP from real EEG single trials in both methods was also described for

subjective evaluation.

On-line analysis of EEG single trials for BCI applications has been investigated in Chapter 5 with the famous P300 Speller paradigm. In this chapter the traditional P300 speller, i.e. RCP, is compared with the improved version. The new version of the P300 Speller improves the RCP paradigm in two points; firstly, changing the flashing schema to reduce the double-flashing and adjacency-distraction errors and, secondly using an adaptive learning and decision making algorithm to stop the trial when a certain threshold is reached and the item of interest can be determined with a certain accuracy. This change of precision from row or column (groups of item in general) to the item gives the subjects the flexibility to tune the BCI to their own pace, meaning, spend more time on the specific items that are harder for them to communicate and less on the easier items. The experiments designed to evaluate the subjects' preferences and comfort with the new paradigm, compared with the old one, are also described. As can be seen in Chapter 5, the new improved mode is ranked higher from both a subjective and an objective point of view.

Perspectives and Future Works

In this research two algorithms for brain signal processing have been developed which can be further expanded. Some remarks on Chapter 3 and Chapter 4 are as follows:

- The SOBI algorithm in the BSS method gives the corresponding scalp projections of the extracted sources as well as the correspondence temporal time course of the signal. Some of the extracted sources which are mistaken with RP shapes are transmitted from other regions of the brain than the motor cortex. This information can be used in the BSS-based algorithm to reduce the false detection rate. However, this modification would increase the computation time.

- Right now the constraint BSE algorithm is applicable for short segments of single trials. In order to use the method for the whole continuous EEG, a prepro-

cessing model should be generated to extract small segments with a windowing method. In this case the length of the window and the length of window movement can highly affect the detection success rates. This modification will make the method applicable to continuous long-term EEG.

- Both BSS and constraint BSE algorithm use no or little pre-processing for EEG single trials. Adding the right kind of pre-processing can further improve their results.

- By detecting RP in various trials one can correctly infer that the intention of the subject is rising and anticipate an upcoming movement or movement imagination and be prepared for it. Finding RP can be the first step in predicting the subject's next behavior. By predicting the human movement, it is possible to evaluate the next motor task before it happens and, if necessary, stop it to prevent any problem. This feature could have a useful application on platforms where human error may have fatal consequences, such as in driving a car or a plane. Moreover, detecting the upcoming movement can have benefits in rehabilitation systems that want to alarm other applications like monitoring the patient's posture.

- In addition, automatic detection of RP in single trials can benefit neuroscientist and help them better understand the human perception since this is the first stage of brain activation against an intention. A robotic arm controlled by the brain can be nicely initialized for a smooth take off if this component is correctly detected. Also, for people with physical challenges, this will be the main clue of having the intention to move.

The P300 Speller is a well-known and well-investigated brain computer interfacing paradigm. There have been many suggestions in literature to improve its efficiency with focus on speed or accuracy. Some remarks on Chapter 5, which deals with P300 Speller, are the following:

- The idea used for the P300 Speller to have adaptive trials with various timing (different number of repetitions) and stopping criterion based on the accuracy

and measure of satisfaction of the task done, can also be used in other applications of brain computer interfacing including games.

- Of course, improving the flashing schema, feature extraction or classification algorithms for EEG single trials, can improve the P300 accuracy. However, if one wants to think outside of the box, use of the natural language processing techniques in this paradigm can also be advantageous. In the end, the aim of the paradigm is to allow subjects to communicate with the outside world in form of *writing*. Fusion of the P300 Speller with natural language processing methods such as automatic spelling correction or automatic word completion can make the BCI seem more intelligent and thus more appealing to the users.

Publications

Journal Papers

[2] **Pouya Ahmadian**, Saeid Sanei, Luca Ascari, Lara González-Villanueva and M. Alessandra Umiltà, "Constrained Blind Source Extraction of Readiness Potentials from EEG", *IEEE Transactions on Neural Systems and Rehabilitation Engineering* (IF: 3.436), vol. 21, no. 4, pp. 567-575, 2013 (Digital Object Identifier: 10.1109/TNSRE.2012.2227278) (currently online).

[4] **Pouya Ahmadian**, Stefano Cagnoni and Luca Ascari, "How capable is non-invasive EEG data of predicting the next movement? A mini review", *Frontiers in Human Neuroscience* (IF: 2.9), vol 7, pp. 124, 2013 (Digital Object Identifier: 10.3389/fnhum.2013.00124) (currently online)

Conference Papers

[1] **Pouya Ahmadian**, Saeid Sanei, Luca Mussi, Luca Ascari, and M. Alessandra Umiltà, "Automatic Detection of Readiness Potential", *Proceedings of the 9th IASTED International Conference on Biomedical Engineering (BioMed 2012), Feb 15-17, 2012, Innsbruck, Austria*, (ERA Ranking: A)

[3] **Pouya Ahmadian**, Saeid Sanei, Lara González-Villanueva, M. Alessandra Umiltà

and Luca Ascari“A Framework for detection of Readiness Potentials in Single trials of EEG”, *MIBISOC2013, May 15-17, 2013, Brussels, Belgium*.

Bibliography

[1] S. P. Wise, "The primate premotor cortex: past, present, and preparatory," *Annual Review of Neuroscience*, vol. 8, no. 1, pp. 1–19, 1985.

[2] D. A. Rosenbaum, "Human movement initiation: specification of arm, direction, and extent," *Journal of experimental psychology. General*, vol. 109, pp. 444–474, Dec. 1980.

[3] S. Sanei and J. A. Chambers, *EEG Signal Processing*. John Wiley & Sons Ltd, 2007.

[4] K. Nazarpour, *Brain Signal Analysis in Space-Time-Frequency Domain; An Application to Brain Computer Interfacing*. PhD thesis, University of Cardiff, 2008.

[5] S. Baillet, J. C. Mosher, and R. M. Leahy, "Electromagnetic brain mapping," *IEEE Signal Processing Magazine*, vol. 18, no. 6, pp. 14–30, 2001.

[6] T. Ball, M. Kern, I. Mutschler, A. Aertsen, and A. Schulze-Bonhage, "Signal quality of simultaneously recorded invasive and non-invasive EEG," *NeuroImage*, vol. 46, no. 3, pp. 708–716, 2009.

[7] A. K. Engel, C. K. E. Moll, I. Fried, and G. A. Ojemann, "Invasive recordings from the human brain: Clinical insights and beyond," *Nature Reviews Neuroscience*, vol. 6, no. 1, pp. 35–47, 2005.

[8] J. R. Wolpaw and D. J. McFarland, "Control of a two-dimensional movement signal by a noninvasive brain-computer interface in humans," in *Proceedings of the National Academy of Sciences of the United States of America*, vol. 101, pp. 17849–17854, 2004.

[9] K.-R. Müller and B. Blankertz, "Towards non-invasive brain-computer interfaces," *IEEE Signal Process Magazine*, vol. 23, no. 5, pp. 125–128, 2006.

[10] L. Citi, R. Poli, C. Cinel, and F. Sepulveda, "P300-based BCI mouse with genetically-optimized analogue control," *IEEE Transactions on Neural Systems and Rehabilitation Engineering*, vol. 16, no. 1, pp. 51–61, 2008.

[11] S. Makeig, A. J. Bell, T. P. Jung, and T. J. Sejnowski, "Independent component analysis of electroencephalographic data," *Advances in Neural Information Processing Systems*, vol. 8, no. 1, pp. 45–151, 1996.

[12] J. W. Belliveau, D. N. Kennedy, R. C. McKinstry, B. R. Buchbinder, R. M. Weisskoff, M. S. Cohen, J. M. Vevea, T. J. Brady, and B. R. Rosen., "Functional mapping of the human visual cortex by magnetic resonance imaging," *Science*, vol. 254, pp. 716–719, 1991.

[13] M. M. Ter-Pogossian, M. E. Phelps, E. J. Hoffman, and N. A. Mullani, "A positron-emission transaxial tomograph for nuclear imaging (PET)," *Radiology*, vol. 114, no. 1, pp. 89–98, 1975.

[14] A. Salek-Haddadi, M. Merschhemke, L. Lemieux, and D. R. Fish, "Simultaneous EEG-correlated ictal fMRI," *NeuroImage*, vol. 16, pp. 32–40, 2002.

[15] H. Laufs, A. Kleinschmidt, A. Beyerle, E. Eger, A. Salek-Haddadi, C. Preibisch, and K. Krakow, "EEG-correlated fMRI of human alpha activity," *Neuroimage*, vol. 19, no. 4, pp. 1463–1476, 2003.

[16] J. Clarke and A. I. Braginski, *The SQUID Handbook*, vol. 1. Wiley-Vch, 2004.

[17] H. Yoshinaga, T. Nakahori, Y. Ohtsuka, E. Oka, Y. Kitamura, H. Kiriyama, K. Kinugasa, K. Miyamoto, and T. Hoshida, "Benefit of simultaneous recording of EEG and MEG in dipole localization," *Epilepsia*, vol. 43, no. 8, pp. 924–928, 2002.

[18] W. G. Walter and M. A. Camb, "The location of cerebral tumours by electro-encephalography," *Lancet*, vol. 228, pp. 305–308, 1936.

[19] W. G. Walter and V. J. Dovey, "Electro-encephalography in cases of subcortical tumour," *Journal of Neurology & Psychiatry*, vol. 7, pp. 57–65, 1944.

[20] E. Kirmizi-Alsan, Z. Bayraktaroglu, H. Gurvit, Y. H. Keskin, M. Emre, and T. Demiralp., "Comparative analysis of event-related potentials during go/nogo and CPT: decomposition of electrophysiological markers of response inhibition and sustained attention," *Brain Research*, vol. 1104, no. 1, pp. 114–128, 2006.

[21] E. Niedermeyer and F. L. da Silva, *Electroencephalography: Basic Principles, Clinical Applications, and Related Fields*. Lippincott Williams & Wilkins, 5th ed., Nov. 2004.

[22] T. Ishihara and N. Yoshii, "Multivariate analytic study of EEG and mental activity in juvenile delinquents," *Electroencephalography and Clinical Neurophysiology*, vol. 33, no. 1, pp. 71–80, 1972.

[23] Y. Mizuki, M. Tanaka, H. Isozaki, H. Nishijima, and K. Inanaga, "Periodic appearance of theta rhythm in the frontal midline area during performance of a mental task," *Electroencephalography and Clinical Neurophysiology*, vol. 49, no. 3-4, pp. 345–351, 1980.

[24] Y. Mizuki, "Frontal lobe: mental functions and EEG," *The American journal of EEG technology*, vol. 27, pp. 91–101, 1987.

[25] G. E. Chatrian, L. Bergamini, and M. Dondey, "A glossary of terms most commonly used by clinical electroencephalographers," *Electroencephalography and Clinical Neurophysiology*, vol. 37, no. 5, pp. 538–548, 1974.

[26] E. Niedermeyer, G. L. Krauss, and C. E. Peyser, "The electroencephalogram and mental activation," *Clinical Electroencephalography*, vol. 20, no. 4, pp. 215–227, 1989.

[27] G. E. Chatrian, M. C. Petersen, and J. A. Lazarte., "The blocking of the rolandic wicket rhythm and some central changes related to movement," *Electroencephalography and Clinical Neurophysiology*, vol. 11, no. 3, pp. 497–510, 1959.

[28] D. Klass and R. Bickford, "Observations on the rolandic arceau rhythm," *Electroencephalography and Clinical Neurophysiology*, vol. 9, p. 570, 1957.

[29] S. Arroyo, R. P. Lesser, B. Gordon, S. Uematsu, D. Jackson, and R. Webber, "Functional significance of the mu rhythm of human cortex: an electrophysiologic study with subdural electrodes," *Electroencephalography and Clinical Neurophysiology*, vol. 87, no. 3, pp. 76–87, 1993.

[30] G. Pfurtscheller and C. Neuper, "Simultaneous EEG 10 Hz desynchronization and 40 hz synchronization during finger movements," *NeuroReport*, vol. 3, no. 12, pp. 1057–1060, 1992.

[31] G. Pfurtscheller and C. Neuper, "Movement and ERD/ERS," in *The Bereitschaftspotential: Movement-related cortical potentials* (M. Jahanshahi and M. Hallett, eds.), pp. 1–17, New York: Kluver Academic/Plenum, 2003.

[32] G. Pfurtscheller, D. Flotzinger, and C. Neuper, "Differentiation between finger, toe and tongue movement in man based on 40 Hz EEG," *Electroencephalography and Clinical Neurophysiology*, vol. 90, no. 6, pp. 456–460, 1994.

[33] R. Poli, "Brain signals + evolutionary computation = human competitive brain computer interfaces." Lecture Notes in MIBISOC Second Technical Course, 2012.

[34] P. W. Ferrez and J. del R. Millan, "Error-related EEG potentials generated during simulated brain-computer interaction," *IEEE Transactions on Biomedical Engineering*, vol. 55, no. 3, pp. 923–929, 2008.

[35] H. Shibasaki and M. Hallett, "What is the bereitschaftspotential?," *Clinical Neurophysiology*, vol. 117, pp. 2341–2356, 2006.

[36] L. Deecke and H. H. Kornhuber, "Human freedom, reasoned will, and the brain: The bereitschaftspotential story," in *The Bereitschaftspotential: Movement-related cortical potentials*, New York: Kluver Academic/Plenum, 2003.

[37] M. Jahanshahi and M. Hallett, "The bereitschaftspotential: What does it measure and where does it come from," in *The Bereitschaftspotential: Movement-related cortical potentials* (M. Jahanshahi and M. Hallett, eds.), pp. 1–17, New York: Kluver Academic/Plenum, 2003.

[38] J. A. Pineda, B. Z. Allison, and A. Vankov, "The effects of self-movement, observation, and imagination on mu rhythms and readiness potentials (RP's): toward a brain-computer interface (BCI),," *IEEE Trans. on Rehabilitation Engineering*, vol. 8(2), pp. 219–222, 2000.

[39] J. M. Kilner, C. Vargas, S. Duval, and S.-J. Blakemore, "Motor activation prior to observation of predicted movement," *Nature Neuroscience*, vol. 7, pp. 1299–1301, 2004.

[40] J. Polich, "Updating P300: an integrative theory of P3a and P3b," *Clinical Neurophysiology*, vol. 118, no. 10, pp. 2128–2148, 2007.

[41] R. Johnson, "On the neural generators of the P300 component of the event related potential," *Psychophysiology*, vol. 30, pp. 90–97, 1993.

[42] G. Plourde and T. Picton, "Long-latency auditory evoked potentials during general anesthesia: N1 and P3 components," *Anesthesia and Analgesia*, vol. 72, pp. 342–350, 1991.

[43] U. Hoffmann, J. M. Vesin, T. Ebrahimi, and K. Diserens, "An efficient P300-based brain-computer interface for disabled subjects," *Journal of Neuroscience Methods*, vol. 167, no. 1, pp. 115–125, 2008.

[44] S. J. Blakemore, S. J. Goodbody, and D. M. Wolpert, "Predicting the consequences of our own actions: The role of sensorimotor context estimation," *Journal of Neuroscience*, vol. 18, no. 18, pp. 7511–7518, 1998.

[45] D. M. Wolpert and J. R. Flanagan, "Motor prediction," *Current Biology*, vol. 11, no. 18, pp. R729–R732, 2001.

[46] D. J. Crammond and J. F. Kalaska, "Prior information in motor and premotor cortex: Activity during the delay period and effect on pre-movement activity," *Journal of Neurophysiology*, vol. 84, no. 2, pp. 1645–1655, 2000.

[47] I. Toni and R. E. Passingham, "Movement preparation: neuroimaging studies," in *The Bereitschaftspotential: Movement-related cortical potentials* (M. Jahanshahi and M. Hallett, eds.), pp. 1–17, New York: Kluwer Academic/Plenum, 2003.

[48] J. M. Kilner, C. Vargas, S. Duval, S.-J. Blakemore, and A. Sirigu, "Motor activation prior to observation of a predicted movement," *Nature Neuroscience*, vol. 7, no. 12, pp. 1299–1301, 2004.

[49] G. Pfurtscheller and C. Neuper, "Motor imagery and direct brain- computer communication.," *Proceedings of the IEEE*, vol. 89, no. 7, pp. 1123–1134, 2001.

[50] J. W. Rohrbaugh, K. Syndulko, and D. B. Lindsley, "Brain wave components of the contingent negative variation in humans," *Science*, vol. 191, no. 4231, pp. 1055–1057, 1976.

[51] C. H. M. Brunia, "CNV and SPN: Indices of anticipatory behavior," in *The Bereitschaftspotential: Movement-related cortical potentials* (M. Jahanshahi and M. Hallett, eds.), pp. 283–320, New York: Kluwer Academic/Plenum, 2003.

[52] G. Alpay, M. Goerke, and B. Sturmer, "Precueing imminent conflict does not override sequence-dependent interference adaptation.," *Psychological research*, vol. 73, Nov. 2009.

[53] C. Haw, D. Lowne, and S. Roberts, "User specific template matching for event detection using single channel," in *Graz 2006 conference on Brain Computer Interface*, 2006.

[54] O. Bai, V. Rathi, P. Lin, D. Huang, H. Battapady, D.-Y. Fei, L. Schneider, E. Houdayer, X. Chen, and M. Hallett, "Prediction of human voluntary movement before it occurs," *Clinical Neurophysiology*, vol. 122, pp. 364–372, 2011.

[55] I. K. Niazi, N. Jiang, O. Tiberghien, J. F. Nielsen, K. Dremstrup, and D. Farina, "Detection of movement intention from single-trial movement-related cortical potentials," *Journal of Neural Engineering*, vol. 8, no. 6, p. 066009, 2011.

[56] E. Lew, R. Chavarriaga, S. Silvoni, and J. R. Millan, "Detection of self-paced reaching movement intention from EEG signals," *Frontiers in Neuroengineering*, vol. 5, p. 13, 2012.

[57] H. Lakany and B. Conway, "Understanding intention of movement from electroencephalograms," *Expert Systems*, vol. 24, pp. 295–s304, 2007.

[58] P. S. Hammon, S. Makeig, H. Poizner, E. Todorov, and V. R. de Sa, "Predicting reaching targets from human EEG," *IEEE Signal Processing Magazine*, vol. 25, no. 1, pp. 69–77, 2008.

[59] Y. Wang and S. Makeig, "Predicting intended movement direction using EEG from human posterior parietal cortex," in *Foundations of augmented cognition: Neuroergonomics and operational neuroscience (HCII 2009)* (D. D. Schmorrow, I. V. Estabrooke, and M. Grootjen, eds.), pp. 437–446, Berlin: Springer, 2009.

[60] B. Blankertz, G. Curio, and K.-R. Müller, "Classifying single trial EEG: Towards brain computer interfacing," in *Neural Information Processing Systems: Natural and Synthetic (NIPS 2001)* (T. G. Dietterich, S. Becker, and Z. Ghahramani, eds.), pp. 157–164, MIT Press, 2001.

[61] B. Blankertz, "Data set self-paced 1s," *BCI Competition 2003*, n.d. Retrieved 5 March 2013. from http://www.bbci.de/competition/ii/berlin_desc.html.

[62] B. Blankertz, K.-R. Müller, G. Curio, T. M. Vaughan, G. Schalk, J. R. Wolpaw, A. Schlögl, C. Neuper, G. Pfurtscheller, T. Hinterberger, M. Schröder, and N. Birbaumer, "The BCI competition 2003: Progress and perspectives in detection and discrimination of EEG single trials," *IEEE Transactions on Biomedical Engineering*, vol. 51, no. 6, pp. 1044–1051, 2004.

[63] Z. Zhang, Y. Wang, Y. Li, and X. Gao, "BCI competiton 2003 - data set IV," *IEEE Transactions on Biomedical Engineering*, vol. 51, no. 6, pp. 1081–1086, 2004.

[64] M. Congedo, F. Lotte, and A. Lecuyer, "Classification of movement intention by spatially filtered electromagnetic inverse solutions," *Physics in Medicine and Biology*, vol. 51, no. 8, pp. 1971–1989, 2006.

[65] B. Blankertz, G. Dornhege, C. Schäfer, R. Krepki, J. Kohlmorgen, K.-R. Müller, V. Kunzmann, F. Losch, and G. Curio, "Boosting bit rates and error detection for the classification of fast-paced motor commands based on single-trial EEG analysis," *IEEE Transactions on Neural Systems and Rehabilitation Engineering*, vol. 11, no. 2, pp. 100–104, 2003.

[66] V. Morash, O. Bai, S. Furlani, P. Lin, and M. Hallettd, "Classifying EEG signals preceding right hand, left hand, tongue, and right foot movements and motor imageries," *Clinical Neurophysiology*, vol. 119, no. 11, pp. 2570–2578, 2008.

[67] S. Haufe, M. S. Treder, M. F. Gugler, M. Sagebaum, G. Curio, and B. Blankertz, "EEG potentials predict upcoming emergency brakings during simulated driving," *Journal of Neural Engineering*, vol. 8, no. 5, p. 056001, 2011.

[68] J. Ontona, M. Westerfieldb, and J. T. S. Makeig, "Imaging human EEG dynamics using independent component analysis," *Neuroscience and Biobehavioral Reviews*, vol. 30, pp. 808–822, 2006.

[69] S. Choi, A. Cichocki, and A. Beloucharni, "Second order nonstationary source separation," *Journal of VLSI Signal Processing*, vol. 32, no. 1-2, pp. 93–104, 2002.

[70] J. F. Cardoso and A. Souloumiac, "Blind beamforming for nongaussian signals," *IEEE Trans. Signal Processing*, vol. 140, no. 6, pp. 362–370, 1993.

[71] A. Hyvärinen and E. Oja, "A fast fixed-point algorithm for independent component analysis," *Neural Computation*, vol. 9, no. 7, pp. 1483–1492, 1996.

[72] A. Belouchrani, K. Abed-Meraim, J.-F. cois Cardoso, and E. Moulines, "A blind source separation technique using second order statistics," *IEEE Trans. on Signal Processing*, vol. 45(2), pp. 434–444, 1997.

[73] A. C. Tang, B. A. Pearlmutter, N. A. Malaszenko, and D. B. Phung, "Independent components of magnetoencephalography: single-trial response onset times," *Neuroimage*, vol. 17, pp. 1773–1789, 2002.

[74] A. C. Tang, B. A. Pearlmutter, N. A. Malaszenko, D. B. Phung, and B. C. Reeb, "Independent components of magnetoencephalography: localization," *Neural Computation*, vol. 14, pp. 1827–1858, 2002.

[75] A. C. Tang, J. Y. Liu, and M. T. Sutherland, "Recovery of correlated neuronal sources from EEG: The good and bad ways of using SOBI," *NeuroImage*, vol. 28, pp. 507–519, 2005.

[76] J. Escudero, R. Hornero, D. Abásolo, and A. Fernández, "Comparison of blind source separation preprocessings applied to magnetoencephalogram recordings to improve the classification of alzheimer's disease patients," *International Journal of Bioelectromagnetism*, vol. 12, no. 4, pp. 183–189, 2010.

[77] C. A. Joyce, I. F. Gorodnitsky, and M. Kutas, "Automatic removal of eye movement and blink artifacts from EEG data using blind component separation," *Psychophysiology*, vol. 41, pp. 2317–2321, 2004.

[78] A. C. Tang, M. T. Sutherland, and C. J. McKinney, "Validation of SOBI components from high density EEG," *NeuroImage*, vol. 25, pp. 539–553, 2005.

[79] Y. Wang, M. T. Sutherland, L. L. Sanfratello, and A. C. Tang, "Single-trial classification of ERPs using second order blind identification (SOBI)," in *Proc. of the Third International Conference on Machine Learning and Cybernetics*, vol. 7, (Shanghai, China), pp. 4246–4251, 2004.

[80] "Henesis WiModule." [Online]. Available: http://www.henesis.eu/prod-wimodule-eng.htm. Last visit: [26 April 2012].

[81] L. González-Villanueva, L. Chiesi, and L. Mussi, "Wireless human motion acquisition system for rehabilitation assessment," in *Proc. of the 25th IEEE Int. Symposium on Computer-Based Medical Systems*, 2012.

[82] S. Makeig, A. J. Bell, T.-P. Jung, and T. J. Sejnowski, "Independent component analysis of electroencephalographic data," *Advances in Neural Information Processing Systems*, vol. 8, pp. 145–151, 1996.

[83] I. Rektor, "Scalp-recorded bereitschaftspotential is the result of the activity of cortical and subcortical generators: a hypothesis," *Clinical Neurophysiology*, vol. 113, pp. 1998–2005, 2002.

[84] C. M. Michela, M. M. Murraya, G. Lantza, S. Gonzaleza, L. Spinellib, and R. G. de Peraltaa, "EEG source imaging," *Clinical Neurophysiology*, vol. 115, no. 10, pp. 2195–2222, 2004.

[85] F.-H. Lin, T. Witzel, S. P. Ahlfors, S. M. Stufflebeam, J. W. Belliveau, and M. S. Hämäläinen, "Assessing and improving the spatial accuracy in meg source localization by depth-weighted minimum-norm estimates," *Neuroimage*, vol. 31, pp. 160–171, 2006.

[86] A. Cichocki and S. I. Amari, *Adaptive Blind Signal and Image Processing, Learning Algorithms and Applications*. New York, NY, USA: John Wiley & Sons, Inc., 2002.

[87] L. Spyrou and S. Sanei, "A robust constrained method for extraction of p300 subcomponents," in *Proc. of IEEE ICASSP, 2006*, vol. 2, 2006.

[88] W. Lu and J. C. Rajapakse, "Approach and applications of constrained ICA," *IEEE Trans. on Neural Networks*, vol. 16, pp. 203–212, Jan 2005.

[89] A. K. Barros, R. Vigário, V. Jousmäki, and N. Ohnishi, "Extraction of event-related signals from multichannel bioelectrical measurements," *IEEE Trans. on Biomedical Engineering*, vol. 47, pp. 583–588, May 2000.

[90] A. Omidvarnia, M. Mesbah, J. M. OToole, P. Colditz, and B. Boashash, "Analysis of the time-varying cortical neural connectivity in the newborn EEG: A time-frequency approach," in *7th International Workshop on Systems, Signal Processing and their Applications (WoSSPA 2011)*, pp. 179–182, 2011.

[91] T.-W. Lee, M. Girolami, and T. J. Sejnowski, "Independent component analysis using an extended infomax algorithm for mixed subgaussian and supergaussian sources," *Neural Computation*, vol. 11, pp. 417–441, 1999.

[92] X. Bai and B. He, "Estimation of Number of independent brain electric sources from the scalp EEGs," *IEEE Trans. on Biomedical Engineering*, vol. 53, no. 10, pp. 1883–1892, 2006.

[93] C. Mühl, *Toward affective brain-computer interfaces : exploring the neurophysiology of affect during human media interaction*. Phd thesis, Univ. of Twente, June 2012.

[94] J. Lu, W. Speier, X. Hu, and N. Pouratian, "The effects of stimulus timing features on p300 speller performance," *Clinical Neurophysiology*, vol. 124, pp. 306–314, 2013.

[95] L. Farwell and E. Donchin, "Talking off the top of your head: Toward a mental prosthesis utilizing event-related brain potentials," *Electroencephalography and Clinical Neurophysiology*, vol. 70, pp. 510–23, 1988.

[96] B. Allison and J. Pineda, "ERPs evoked by different matrix sizes: Implications for a brain computer interface (BCI) system," *IEEE Transactions on Neural Systems and Rehabilitation Engineering*, vol. 11, pp. 110–113, 2003.

[97] E. Sellers, D. Krusienski, D. McFarland, T. Vaughan, and J. Wolpaw, "A P300 event-related potential brain-computer interface (BCI): The effects of matrix size and inter stimulus interval on performance," *Biological Psychology*, vol. 73, pp. 242–52, 2006.

[98] E. Maby, G. Gibert, P. E. Aguera, M. Perrin, O. Bertrand, and J. Mattout, "The OpenViBE P300-speller scenario: a thorough online evaluation," in *Human Brain Mapping Conference*, (Barcelona, Spain), 2010.

[99] M. Kaper and H. Ritter, "Generalizing to new subjects in brain-computer interfacing," in *Engineering in Medicine and Biology Society, 2004. IEMBS '04. 26th Annual International Conference of the IEEE*, vol. 2, pp. 4363–4366, 2004.

[100] H. Serby, E. Yom-Tov, and G. Inbar, "An improved P300-based brain-computer interface," *IEEE Transactions on Neural Systems and Rehabilitation Engineering*, vol. 13, pp. 89–98, 2005.

[101] D. Krusienski, E. Sellers, F. Cabestaing, S. Bayoudh, D. McFarland, T. Vaughan, and J. Wolpaw, "A comparison of classification techniques for the p300 speller," *Journal of Neural Engineering*, vol. 3, pp. 299–305, 2006.

[102] A. Lenhardt, M. Kaper, and H. Ritter, "An adaptive P300-based online brain-computer interface," *IEEE Transactions on Neural Systems and Rehabilitation Engineering*, vol. 16, pp. 121–30, 2008.

[103] G. Townsend, B. LaPallo, C. Boulay, D. Krusienski, G. Frye, C. Hauser, N. Schwartz, T. Vaughan, J. Wolpaw, and E. Sellers, "A novel P300-based brain-computer interface stimulus presentation paradigm: Moving beyond rows and columns," *Clinical Neurophysiology*, vol. 121, pp. 1109–1120, 2010.

[104] M. Salvaris and F. Sepulveda, "Visual modifications on the P300 speller BCI paradigm," *Journal of Neural Engineering*, vol. 6, p. 046011, 2009.

[105] K. Takano, T. Komatsu, N. Hata, Y. Nakajima, and K. Kansaku, "Visual stimuli for the P300 brain-computer interface: A comparison of white/gray and green/blue flicker matrices," *Clinical Neurophysiology*, vol. 120, pp. 1562–1566, 2009.

[106] B. Hong, F. Guo, T. Liu, X. Gao, and S. Gao, "N200-speller using motion-onset visual response," *Clinical Neurophysiology*, vol. 120, pp. 1658–1666, 2009.

[107] S. Martens, N. Hill, J. Farquhar, and B. Scholkopf, "Overlap and refractory effects in a brain-computer interface speller based on the visual P300 event-related potential.," *Journal of Neural Engineering*, vol. 6, p. 026003, 2009.

[108] C. Guan, M. Thulasidas, and J. Wu, "High performance P300 speller for brain-computer interface," in *IEEE Int. Workshop on Biomedical Circuits Systems*, 2004.

[109] C. Guger, S. Daban, E. Sellers, C. Holzner, G. Krausz, R. Carabalona, F. Gramatica, and G. Edlinger, "How many people are able to control a P300-based brain-computer interface (BCI)?," *Neuroscience Letters*, vol. 462, pp. 94–98, 2009.

[110] T. Kaufmann, S. M. Schulz, C. Grünzinger, and A. K. übler, "Flashing characters with famous faces improves ERP-based brain-computer interface performance," *Journal of Neural Engineering*, vol. 8, p. 056016, 2011.

[111] G. Pires, U. Nunes, and M. Castelo-Branco, "Comparison of a row-column speller vs. a novel lateral single-character speller: Assessment of BCI for severe motor disabled patients," *Clinical Neurophysiology*, vol. 123, pp. 1168–1181, 2012.

[112] B. Allison, *P3 or not P3: Toward a better P300 BCI*. PhD thesis, University of California, USA, 2003.

[113] J. Lu, "Characterizing P300 speller performance: The effects of stimulus timing features and search for a physiological biomarker," Master's thesis, University of California, Los Angeles, USA, 2012.

[114] B. Rivet, A. Souloumiac, V. Attina, and G. Gibert, "xDAWN algorithm to enhance evoked potentials: application to brain-computer interface," *IEEE Transactions on Biomedical Engineering*, vol. 56, no. 8, pp. 2035–2043, 2009.

[115] M. Perrin, E. Maby, R. Bouet, O. Bertrand, and J. Mattout, "Detecting and interpreting responses to feedback in BCI," in *5th International Brain-Computer Interface Workshop & Training Course*, (Graz, Austria), 2011.

[116] M. Treder and B. Blankertz, "(c)overt attention and visual speller design in an ERP-based brain-computer interface.," *Behavioral and Brain Functions*, vol. 6, no. 28, 2010.

[117] G. Gibert, V. Attina, J. Mattout, E. Maby, and O. Bertrand, "Size enhancement coupled with intensification of symbols improves p300 speller accuracy," in *Proc. 4th International BCI Interface Workshop and Training Course*, pp. 250–255, 2008.

[118] M. Perrin, E. Maby, S. Daligault, B. Bertrand, and J. Mattout, "Objective and subjective evaluation of online error correction during p300-based spelling," *Advances in Human-Computer Interaction*, vol. 2012, p. 578295, 2012.

[119] S. Chennu, A. Alsufyani, M. Filetti, A. M. Owen, and H. Bowman, "The cost of space independence in p300-bci spellers," *Journal of NeuroEngineering and Rehabilitation*, vol. 10, p. 82, 2013.

[120] A. Delorme and S. Makeig, "EEGLAB: an open source toolbox for analysis of single-trial EEG dynamics including independent component analysis," *Journal of Neuroscience Methods*, vol. 134, pp. 9–21, 2004.

Acknowledgements

I would like to express my appreciation to all those who provided me the possibility to complete this thesis.

I wish to thank, first and foremost the European Commission for the financial support as, this work has been funded by the European Commission under the MIBISOC project (Grant Agreement: 238819), within the action Marie Curie Initial Training Network of the 7FP. In addition, the coordinator, Dr. Oscar Cordon and other projects managers and staff such as Carmen Pena showed me a warm and welcoming attitude every time I faced a bureaucratic challenge or problem. Their open mildness and flexibility to bend the rules in my favor as much as possible helped me make the most out of the opportunities I came cross during my time in the network.

I would like to thank Dr. Luca ascari for recruiting me in the MIBISOC network. It gives me great pleasure in acknowledging the support and help of Professor Stefano Cagnoni. Working with him and being able to benefit from his vast knowledge of soft computing was one of the highlights of my PhD. I would like to thank him specially for his constructive comments on my ideas and work and furthermore, for his generosity and patient attitude towards me.

I would also like to thank Dr. M. Alessandra Umiltà and Dr. Vittorio Gallese for trusting me with there high-level EEG data acquisition system and their guidance on how to record EEG data. In addition, I would like to thank all the people participated in my EEG recording experiments.

As a part of MIBISOC project, I had to spend at least two secondment in other institutes across Europe. Although this was a obligatory term of my contract, it proved

to be the most beneficiary one in my case. I used this criteria to visit two of the best facilities and get families with the work of experts in the field. I am indebted to Professor Saeid Sanei from university of Surrey, UK, who guided me into the right approach towards understanding the EEG signal analysis. Moreover, I consider it an honor to have worked with Dr. Jeremie Mattout and Dr. Emmanuel Maby from Lyon Neuroscience Research Center, France. My time there was spend working with their brain computer interface paradigm and the experience gained during those two month in Lyon is priceless.

This thesis is dedicated to my parents who have given me their love and devotion throughout my life. Spacial thanks to my father, Dr. Moussa Ahmadian, for English proofreading two of my articles and his comments on my writing.

Last but not least, I would like to express my deepest gratitude to my husband, Hamid Hassannejad. Looking back, I faced many ups and downs during these three years. He always tried to support and encourage me in any way he could. Personally, I am certain that, finishing this dissertation would not have been possible without him by my side.